NUREG/CR-4348 Vol. I
ANL-85-42 Vol. I

NUREG/CR-4348 Vol. I
ANL-85-42 Vol. I

COMMIX-1B: A THREE-DIMENSIONAL TRANSIENT SINGLE-PHASE COMPUTER PROGRAM FOR THERMAL HYDRAULIC ANALYSIS OF SINGLE AND MULTICOMPONENT SYSTEMS

VOLUME I: EQUATIONS AND NUMERICS

ARGONNE NATIONAL LABORATORY, ARGONNE, ILLINOIS
Operated by THE UNIVERSITY OF CHICAGO

Prepared for the Office of Nuclear Regulatory Research
U. S. NUCLEAR REGULATORY COMMISSION
under Interagency Agreement DOE 40-550-75

Available from

Superintendent of Documents
U. S. Government Printing Office
Post Office Box 37082
Washington, D.C. 20013-7982

and

National Technical Information Service
Springfield, VA 22161

NUREG/CR-4348 Vol. I
ANL-85-42 Vol. 1

(Distribution
Code: R7)

ARGONNE NATIONAL LABORATORY
9700 South Cass Avenue
Argonne, Illinois 60439

COMMIX-1B: A THREE-DIMENSIONAL TRANSIENT SINGLE-PHASE COMPUTER PROGRAM FOR THERMAL HYDRAULIC ANALYSIS OF SINGLE AND MULTICOMPONENT SYSTEMS

VOLUME I: EQUATIONS AND NUMERICS

Analytical Thermal Hydraulic Research Program
Components Technology Division

September 1985

Prepared for the

U. S. Nuclear Regulatory Commission
Office of Nuclear Regulatory Research
Washington, D.C. 20555

under Interagency Agreement DOE 40-550-75

NRC FIN No. A2045

LIST OF CONTRIBUTORS

A large number of people have contributed to the development of the COMMIX code and to the preparation of this report. Since it was a team effort, there was considerable overlap in the areas of responsibility and contribution. The participants are listed below according to their area of primary activity.

Report compilation and project control	:	V. L. Shah
COMMIX-1A base	:	H. M. Domanus, R. C. Schmitt, W. T. Sha and V. L. Shah
Code architecture and methods	:	H. M. Domanus, R. C. Schmitt, and F. F. Chen
Turbulence modeling		F. F. Chen
Skew-upwind differencing option	:	C. C. Miao and F. F. Chen
Code development and programming	:	H. M. Domanus, R. C. Schmitt, F. F. Chen, and C. C. Miao
Overall project direction and management	:	W. T. Sha

COMMIX-1B:
A THREE-DIMENSIONAL TRANSIENT SINGLE-PHASE COMPUTER PROGRAM FOR THERMAL HYDRAULIC ANALYSIS OF SINGLE AND MULTICOMPONENT SYSTEMS

VOLUME I: EQUATIONS AND NUMERICS

ABSTRACT

The COMMIX-1B computer program is an extended version of COMMIX-1A with three major additions: (1) three more turbulence-model options for the computation of turbulent diffusivities, (2) a volume-weighted skew-upwind difference scheme to reduce numerical diffusion, and (3) a single formulation to combine semi-implicit and fully-implicit solution procedures.

COMMIX-1B solves the conservation equations of mass, momentum, and energy, and transport equations of turbulence parameters. It is designed to perform steady-state/transient, single-phase, three-dimensional analysis of fluid flow with heat transfer in a single-component or a multicomponent system. The program is developed for the analysis of heat transfer and fluid flow processes in a nuclear reactor system. However, it is designed in a generalized fashion such that with no or minimal modification, it can be used to analyze processes in any engineering equipment, or in any system.

The following are unique features of the COMMIX code.

- **New Porous-Medium Formulation**: COMMIX uses a new porous-medium formulation with the parameters volume porosity, directional surface porosity, distributed resistance, and distributed heat source or sink. With this formulation, the COMMIX code has the capability to model an anisotropic flow domain with stationary structures. The porous-medium formulation with the additional parameter directional surface porosity represents a unified approach to thermal-hydraulic analysis. Because of this feature, it is now possible to perform a multidimensional thermal-hydraulic simulation of either a single component, such as a rod bundle, reactor plenum, piping system, heat exchanger, etc., or a multicomponent system that is a combination of these components.

- **Two Solution Procedures**: In COMMIX, two solution procedures, semi-implicit and fully implicit, are available as a user's option. The semi-implicit procedure, a modification of the ICE technique, is designed for fast transient analysis, where our interest is to examine flow phenomenon in the time period of the order of Courant time step size. The fully implicit procedure, named SIMPLEST-ANL and

similar to the SIMPLE/ SIMPLER algorithms, is designed for normal and slow transients, where our interest is to examine phenomena at times that are larger than Courant time step size.

- **Geometrical Package**: A special geometrical package has been developed and implemented that permits modeling of any complex geometry in the most storage-efficient way.

- **Skew-Upwind Difference Scheme**: A new volume-weighted skew-upwind difference scheme has been developed and implemented that reduces numerical diffusion observed in simulations of flow inclined to grid lines. The scheme also eliminates temperature over/undershoots that are found to occur when simulations are performed with normal skew-upwind differencing schemes.

Volume I (Equations and Numerics) of this report describes in detail the basic equations, formulations, solution procedures, rebalancing scheme, and models to describe the auxiliary phenomena. Volume II (User's Manual) contains the input instruction, sample problems, flow charts, and description of available options and boundary conditions.

CONTENTS

CONTENTS (Contd.)

CONTENTS (Contd.)

FIGURES

FIGURES (Contd.)

FIGURES (Contd.)

TABLES

TABLES (Contd.)

EXECUTIVE SUMMARY

The COMMIX (**COM**ponent **Mix**ing) codes are designed for analyzing heat transfer and fluid flow. The COMMIX-1B computer program--an extended version of COMMIX-1A--is designed to analyze steady-state/transient, single-phase, three-dimensional compressible/incompressible flow with heat transfer in a reactor component/multicomponent system.

The three major changes that have been implemented in COMMIX-1A to develop COMMIX-1B are

- Addition of three turbulence models to provide more options in the computation of turbulent diffusivities,
- Addition of a new volume-weighted skew-upwind difference scheme to reduce numerical diffusion, and
- Combination of semi-implicit and fully implicit solution procedures into one single formulation.

One of the major unique features of COMMIX is its porous-medium formulation, which has been rigorously derived through local volume averaging. In the new formulation, we use volume porosity, directional surface porosity* (directional because surface porosity is an anisotropic vector quantity), distributed resistance, and distributed heat source or sink. We refer to the formulation as new because **the concept of adding a parameter directional surface porosity is new.** In the conventional porous-medium formulation, only the volume porosity, distributed resistance, and distributed heat source are used. Volume porosity is the ratio of the volume occupied by fluid in a control volume to the total control volume. Surface porosity is similarly defined as the ratio of fluid flow area through a control surface to the total control surface area.

In any numerical analysis of an engineering system, modeling must include distributed resistance (friction factor) because, in general, it is not a precisely known quantity. Thus, with the conventional porous-medium formulation, the flow distribution that we obtain completely depends on how accurately we model the distributed resistance. However, in the case of the new porous-medium formulation, due to the introduction of directional surface porosity (a geometrical quantity that can be prescribed accurately), the dependence of the velocity field on resistance modeling is reduced. Hence, we obtain improved resolution and accuracy in the modeling of velocity and temperature fields. The new porous-medium formulation thus represents the **first unified approach** to thermal-hydraulic analysis. The conventional porous-medium formulation can be considered a subset of this new porous-medium formulation.

The COMMIX code provides detailed local velocity and temperature fields for the problems under consideration. The conservation equations of mass, momentum, and energy, and transport equations of turbulence parameters are solved as a boundary value problem in space and an initial value problem in

---

*In previous publications, we have used the term surface permeability.

time. The discretization equations are obtained by integrating the conservation equations over a control volume.

The code has a wide range of applicability. It is capable of solving thermal-hydraulic problems involving either a single component, such as a rod bundle, reactor plenum, piping system, heat exchanger, etc., or a multicomponent system that is a combination of these components.

COMMIX has two alternative solution schemes. One is semi-implicit and is a modification of the ICE technique. The other, a fully implicit scheme called SIMPLEST-ANL, is a modification of the numerical procedure known as SIMPLER. The option for solution schemes is implemented in such a way that a user can switch from one solution scheme to another at any time during the transient simulation of a problem.

The code has a modular structure and permits analysis using either Cartesian or cylindrical coordinate systems. It has two thermal-hydraulic property packages, one for liquid sodium and one for water. Besides these two packages, an option is available for users to input simplified thermal physical property correlations that are valid in the desired range of applications.

Another unique feature of the COMMIX code is its geometrical package. The basic concept is to use computational cells (either in Cartesian or cylindrical coordinates) as building blocks that are stacked up to approximate the shape of the physical systems under consideration. Then volume porosity and directional surface porosity are used to account for the differences between the geometry used in computation and the actual configuration. This feature permits the COMMIX code to model any irregular and complex geometry encountered in a real engineering system. Furthermore, the computer storage requirement of the COMMIX code is optimized; only the computational cells used in calculations are counted.

Volume I (Equations and Numerics) of this report describes in detail the basic equations, formulation, volume-weighted skew-upwind difference scheme, and the solution procedures. It also describes models used for the following phenomena:

- Momentum interaction between fluid and stationary solid structures,
- Thermal interaction between fluid and stationary solid structures,
- Turbulence, and
- Effects of wire wrap for fuel assembly applications.

In Volume II (User's Manual), we provide flow charts, description of subroutines, geometry modeling, initialization procedures, input instructions, etc. Two sample problems are also included so that readers who plan to use COMMIX-1B can become familiar with the input/output structures of the code.

1. INTRODUCTION

COMMIX is a computer code for heat transfer and fluid flow analysis. Since the development of COMMIX-1 in 1976, many features have been added to augment the code's applicability. Consequently, COMMIX has become a very general-purpose computer code with a very wide range of applications. Although developed for nuclear reactor applications, with no or minimal modifications, COMMIX can be used to analyze processes in engineering systems.

Many industries and organizations involved in design or analysis of nuclear reactors are already using COMMIX. However, due to the code's generality of formulation and its wide range of applications, people from other disciplines have also found COMMIX a very useful tool. We therefore expect the number of COMMIX users to increase in the future. Prospective users of COMMIX can benefit from a comprehensive description of the code. The purpose of the present report is to meet this need.

In describing COMMIX-1B, we have two distinct aims. One is to convey to the reader the capabilities of COMMIX, what equations are solved, and how they are solved, which we have done here (Volume I). The second aim is to present a step-by-step procedure on how to use COMMIX. To achieve this, we must describe the procedure with sufficient detail that a reader has no or minimum difficulty in attempting to use COMMIX. This, of course, is very difficult, but we are attempting it in the second part of this report, Volume II.

This volume describes the basic equations, formulations of discretization equations, auxiliary models, solution procedures, etc. Volume II, the User's Manual, describes all the information needed by the user, e.g., input description, flow chart, sample problems, and user options.

1.1 OVERVIEW OF COMMIX-1B

The COMMIX-1B code is a generalized computer code for heat transfer and fluid flow analysis. Although it has been designed specifically for reactor component/multicomponent applications, it has been developed in a way that make it applicable to any other complex engineering system. Its capability includes steady-state/transient, three-dimensional, and single-phase analysis of nuclear reactor systems under normal and off-normal operating conditions.

In general, a computer code developed for numerical simulation of an engineering process can be classified as either a system code or a component code.

- A system code generally deals with many interlinking components; it accounts for component interactions to provide an overall analysis of a whole system without detailed analysis of all the components of a system.

- A component code, in contrast, deals with only one component of interest and provides a detailed numerical simulation of a single component.

COMMIX-1B can be described as both a system code and a component code because it is capable of providing detailed information about a single component or analyzing a multicomponent system in sufficient detail. Because of this broad capability, COMMIX-1B can also provide detailed information about component interactions.

COMMIX-1B is an extended version of the COMMIX-1A code[1] that was released in 1983. COMMIX-1B has retained all flexibilities, formulations, and solution techniques of its predecessor, but now contains three more features. These are:

1. Three additional turbulence models to provide more user-desired options for computation of turbulent diffusivities. The models implemented are
   - Zero-equation mixing length model,
   - One-equation (k) model, and
   - Two-equation (k-ϵ) model.

   Here k is the turbulence kinetic energy and ϵ is the rate of dissipation of k.

2. A new volume-weighted skew-upwind difference scheme to reduce numerical diffusion observed specifically in the analysis of flow inclined to numerical grid lines.

3. A single formulation combining both semi-implicit and fully implicit solution schemes.

COMMIX-1B solves the conservation equations of mass, momentum, and energy, and transport equations of turbulence parameters, as a boundary-value problem in space and an initial-value problem in time. The staggered grid system is used, which considers the field variables as located at the center of a cell and flow variables as located at the surface of a cell.

COMMIX-1B is a well tested computer code. Already, a large number of computations[2-37] for complex situations have been performed. The structure of the code is modular. It has many unique features and these are described in the following section.

1.2 UNIQUE FEATURES OF COMMIX SERIES

1.2.1 New Porous Media Formulation

As do all the codes in the COMMIX series, COMMIX-1B employs conservation equations that are based on a new porous-medium formulation based on local volume-averaging[38-44]*. It uses four parameters--volume porosity, directional surface porosity, distributed resistance, and distributed heat source (sink)--to model the effects of internal solid structures. In the conventional porous-medium formulation, only three parameters--volume porosity, distributed

*Recently, the new porous-medium formulations have been further refined via time-volume averaging.

resistance, and distributed heat source--are used. The addition of a fourth parameter, directional surface porosity[38-47], is a new concept.

The parameter volume porosity is defined as the ratio of the volume occupied by fluid in a control volume to the total control volume. The directional surface porosity is similarly defined as the ratio of area allowed for fluid flow through a control surface to the total control surface area. We use the adjective "directional" because surface porosity is an anisotropic vector quantity.

Implementing the fourth parameter, directional surface porosity, has the following advantages. In any thermal-hydraulic analysis, flow resistance due to internal structures and/or irregular geometry (friction factor) generally is not precisely known for most engineering applications, and must be modeled as a distributed resistance. In the conventional porous-medium formulation, the accuracy of numerical prediction therefore depends primarily on how well the resistanceis modeled. In the case of the new porous-medium formulation, two parameters, distributed resistance and directional surface porosity, are available for modeling of velocity and temperature fields in anisotropic media. Incidently, the directional surface porosity is a geometrical parameter and can be calculated precisely. By the introduction of directional surface porosity in the new porous-medium formulation, we reduce the dependence of numerical prediction on the modeling of distributed resistance (an empirical parameter not precisely known). Thus, the concept of adding directional surface porosity greatly facilitates modeling of velocity and temperature fields in anisotropic media and, in general, improves resolution, and accuracy.

If we set directional surface porosity equal to one, the new formulation reduces to the conventional porous-medium formulation. We can therefore consider the conventional porous-medium formulation as a subset of the new porous-medium formulation. Furthermore, if we set the volume porosity equal to one and distributed resistance and heat source to zero, the porous-medium formulation reduces to a continuum-medium formulation. Thus, the new porous-medium formulation can be considered a most general and unified approach to thermal-hydraulic analysis.

1.2.2 Two-Solution Algorithms

In COMMIX-1B, we have maintained two solution algorithms as user's options:

- A semi-implicit algorithm derived from the Los Alamos ICE Technique[48-50]. This algorithem is ideally suited for analyzing fast transients, where we are interested in details at small time intervals (on the order of Courant time step size).

- A fully implicit algorithm named SIMPLEST-ANL. This algorithm is a modification of the Patankar-Spalding numerical procedure[51] known as SIMPLE/SIMPLER. It is particularly suitable for the analysis of slow and normal transients.

We have combined these two solution procedures into one formulation, but implemented such so that a user can switch from one solution scheme to another at any time during a transient simulation of the same problem.

1.2.3 Geometry Package

The geometry package developed and implemented in COMMIX-1A is also retained in COMMIX-1B. This package is capable of approximating any irregular geometry. It uses basic computational cells as building blocks to model the geometry under consideration. Then both volume porosities and directional surface porosities are used to account for the differences between the approximated and actual configuration.

To save computer storage, a computational cell is defined by a number rather than its conventional (i, j, k) location, where i, j, and k are the computational cell indices in the three principal axes (e.g., x, y, and z in the Cartesian coordinate system). With this approach, the storage requirement depends only on the total number of computational cells and not on the dimensional values of (IMAX * JMAX * KMAX), where IMAX, JMAX, and KMAX denote the maximum values of computational cell indices in the three corresponding principal axes.

A normal three-dimensional computational cell has six surfaces. But to facilitate true and proper modeling of a complex irregular geometry (most geometries in engineering systems are complex and irregular), we have provided flexibility so that a user can specify an additional seventh surface, called an irregular surface, to a computational cell.

1.3 OTHER FEATURES OF COMMIX-1B

Other features of COMMIX-1B are described below.

- The following four turbulence model options are provided to give COMMIX-1B a wide range of applications:
  - Constant turbulent diffusivity model
  - Zero-equation mixing length model
  - One-equation (k) model
  - Two-equation (k-ϵ) model
- A volume-weighted skew-upwind difference scheme has been developed and implemented to reduce numerical diffusion, specifically for the case of flow inclined to grid lines.
- The discretization equations are formulated by integrating the conservation equations and transport equations over a control volume surrounding a grid point. Thus, the derivation process and resulting equations have direct physical meaning, and the consequent solution satisfies conservation principles.
- The final form of all of the sets of discretization equations is

$$a_0^{\phi}\phi_0 - \sum_{\ell=1}^{6} a_\ell^{\phi}\phi_\ell - b_0^{\phi}, = 0 \ ,$$

where ϕ is a dependent variable and the subscript ℓ stands for neighboring points. This general form of the discretization equation lends itself to various solution schemes, e.g., cell by cell, line by line, plane by plane, block iterative, direct matrix inversion.

- The program has a decoupled-transient-simulation option that permits solution of
  - mass-momentum equations only, or
  - energy equation only, or
  - coupled mass-momentum and energy equations,

  at any given time step.

- The code has an option that allows use of either Cartesian or cylindrical coordinates.

- The COMMIX-1B code has a modular structure, which permits rapid implementation of the latest available drag models, heat-transfer models, etc.

- COMMIX-1B has built-in properties for liquid sodium and water, with an option permitting use of simplified property correlations for any fluid.

- The code also contains:
  - A generalized resistance model to permit specification of resistance due to internal structures (fuel rods, wire wrap, baffles, grid spacers, etc.).
  - A generalized thermal structure formulation to model thermal interaction between structures (fuel rods, wire wraps, duct wall, baffles, etc.) and surrounding fluid.
  - Options for mass rebalancing schemes, either in a primary or user-specified direction, for improving the mass convergence rate.

- Heat source/sink and boundary conditions can be functions of time.

- The COMMIX-1B code is structured to permit solution of 1D, 2D, or 3D calculations.

1.4 ORGANIZATION OF THE REPORT

This volume describes the formulations of the governing equations for three-dimensional, single-phase, steady/transient flow with heat transfer. The description starts with differential equations and deals with numerical methods incorporated into the COMMIX-1B program. Section 2 is devoted to the general form of governing conservation equations for a quasi-continuum domain. This generalization facilitates unified development of the numerical method and the construction of the computer program.

The quasi-continuum domain is defined as a medium that contains finite, dispersed, stationary heat-generating (or absorbing) solid structures. The effects of solid structures in a medium are accounted for by introducing volume porosity, directional surface porosity, distributed resistance, and distributed heat sources.

Section 3 describes the staggered grid arrangement and the conventions used in COMMIX-1B to define the location of a control volume. Section 4 assembles the finite-difference equations. The finite-difference formulation of the general equation is presented in Sec. 4.5. Because a staggered grid system is used, the control volumes for momentum equations are different and require special consideration. The special features of the finite-difference equations for momentum are discussed in Sec. 4.6.

The pressure appearing in the momentum equation must be such that the velocity distribution obtained satisfies the continuity equation. The derivation of the pressure equation (derived by combining the momentum and continuity equations) is presented in Sec. 5.

Currently, there are four turbulence models to account for turbulence effects.

- Constant Turbulent Diffusivity: This model is very simple; the turbulent viscosity and turbulent thermal conductivity are assumed constant. No transport equation is solved.

- 0-Equation: In this model the turbulent viscosity is assumed to be a function of mixing length and velocity gradient. No transport equation is solved.

- One-Equation: In the one-equation turbulence model, the partial differential equation for turbulence kinetic energy (k) is solved and the turbulence quantities are evaluated.

- Two-Equation: We solve the transport equations of turbulence kinetic energy k and dissipation rate of turbulent kinetic energy ε to evaluate turbulent quantities.

All these models are described in Sec. 6.

General practice in the formulation of convective terms is to use pure-upwind differencing rather than central differencing. This is because the pure-upwind scheme prevents instability at high Peclet numbers. However, it has been found that with pure-upwind differencing the false (numerical) diffusion can be large if the flow is inclined to grid lines. To minimize the numerical diffusion, we have implemented two additional options in COMMIX-1B--skew-upwind differencing as suggested by Rahiby[52], and a volume-weighted skew-upwind difference scheme developed at ANL[36]. Both these difference schemes are described in Sec. 7. The Von Newmann stability analysis of the volume-weighted skew-upwind differencing scheme is presented in Appendix A.

In the initial period of development, emphasis was on the analysis of hexagonal fuel assemblies. Consequently, several options have been maintained in COMMIX-1B that facilitate the analysis of hexagonal fuel assemblies. These options are described in Sec. 8.

Section 9 describes several of the models that have been maintained in the COMMIX-1B computer program, including a generalized-force model, and a generalized thermal-structure model. The force model computes distributed resistance to account for the friction between fluid and submerged solids. The thermal-structure model is designed for computing the distributed heat source (fluid and submerged solids) and the thermal inertia of submerged solids.

In COMMIX-1B, there are several boundary condition options for momentum, energy, and continuity equations. These options are described in Sec. 10.

To speed-up convergence, we have developed a mass rebalancing scheme, described in Sec. 11. In the current version, two alternative formulations leading to two alternative solution procedures are available--the semi-implicit modified ICE-type solution scheme and the fully implicit solution scheme SIMPLEST-ANL, an extension of the numerical procedures known as SIMPLE/SIMPLER. Section 12 presents an overall flow chart and describes in detail the semi-implicit and fully implicit solution sequences. In Sec. 13, we highlight the major differences between the semi-implicit and fully implicit solution schemes and between the fully implicit scheme (SIMPLEST-ANL) and SIMPLER algorithms.

The thermodynamic and transport properties of liquid sodium and water are given in Appendix B.

Volume II of this report is written specifically for COMMIX-1B users. It describes steady-state and transient calculation and various procedures in the preparation of load modules, input data, reading and writing of restart files, etc. Two sample problems, along with their description, input, and output, are presented to provide a sound introduction to the capabilities of COMMIX-1B. The code input description is also included in Volume II.

2. GENERAL FORM OF CONSERVATION EQUATIONS

The conservation equations of mass, momentum, and energy possess a common form. If we denote the general dependent variable as ϕ, the corresponding conservation equations have the following form in the Cartesian coordinate system.

In Continuum Domain:

$$\underbrace{\frac{\partial}{\partial t}(\rho\phi)}_{\text{(Unsteady)}} + \underbrace{\frac{\partial}{\partial x}(\rho u\phi) + \frac{\partial}{\partial y}(\rho v\phi) + \frac{\partial}{\partial z}(\rho w\phi)}_{\text{(Convection)}}$$

$$= \underbrace{\frac{\partial}{\partial x}\left(\Gamma_\phi \frac{\partial\phi}{\partial x}\right) + \frac{\partial}{\partial y}\left(\Gamma_\phi \frac{\partial\phi}{\partial y}\right) + \frac{\partial}{\partial z}\left(\Gamma_\phi \frac{\partial\phi}{\partial z}\right)}_{\text{(Diffusion)}} + \underbrace{S_\phi}_{\text{(Source)}} \qquad (2.1a)$$

In Quasicontinuum Domain[41]:

$$\underbrace{\frac{\partial}{\partial t}(\gamma_v \rho\phi)}_{\text{(Unsteady)}} + \underbrace{\frac{\Delta(\gamma_x \rho u\phi)}{\Delta x} + \frac{\Delta(\gamma_y \rho v\phi)}{\Delta y} + \frac{\Delta(\gamma_z \rho w\phi)}{\Delta t}}_{\text{(Convection)}}$$

$$= \underbrace{\frac{\Delta\left(\gamma_x \Gamma_\phi \frac{\partial\phi}{\partial x}\right)}{\Delta x} + \frac{\Delta\left(\gamma_y \Gamma_\phi \frac{\partial\phi}{\partial y}\right)}{\Delta y} + \frac{\Delta\left(\gamma_z \Gamma_\phi \frac{\partial\phi}{\partial z}\right)}{\Delta z}}_{\text{(Diffusion)}} + \underbrace{\gamma_v S_\phi}_{\text{(Source)}} . \qquad (2.1b)$$

Here u, v, and w are the velocities in the x, y, and z directions, respectively; γ_v is the volume porosity (fraction of the volume occupied by the fluid) and γ_x, γ_y, and γ_z are the directional surface porosities (fraction of the surface area that is unobstructed to fluid flow) in the x, y, and z directions, respectively. The convective and diffusive terms $\Delta(\psi)/\Delta x_i$ in Eq. 2.1b are defined as

$$\frac{\Delta(\psi)}{\Delta x_i} = \frac{\psi(x_i + \Delta x_i/2) - \psi(x_i - \Delta x_i/2)}{\Delta x_i} , \qquad (2.2)$$

in which x_i stands for the x, y, or z coordinate. The diffusion coefficient Γ_ϕ and the source term S_ϕ are specific to each meaning of ϕ. The sources for all conservation equations are given in Tables 2.1 and 2.2.

The conservation equations in the cylindrical coordinate system also have the same general form (Eq. 2.1) when we place the centrifugal and Coriolis force terms in the source term S_ϕ. We can, therefore, apply all formulations

Table 2.1 Source Terms in the Cartesian Coordinate System

Equation	Variable (ϕ)	Direction	Diffusion Coefficient (Γ_ϕ)	Source Term (S_ϕ)
Continuity	1	Scalar	0	0
Momentum				
(i)	u	x direction	μ	$\rho g_x + V_x - R_x - \left(\frac{\partial p}{\partial x}\right)$
(ii)	v	y direction	μ	$\rho g_y + V_y - R_y - \left(\frac{\partial p}{\partial y}\right)$
(iii)	w	z direction	μ	$\rho g_z + V_z - R_z - \left(\frac{\partial p}{\partial z}\right)$
Energy	h	Scalar	k	$\frac{dp}{dt} + \dot{Q}_{rb} + \dot{Q} + \Phi$

V_x, V_y, V_z : Balance of the viscous diffusion terms

R_x, R_y, R_z : Distributed resistances due to solid structures in a momentum control volume

$\dot{Q}_{rb}$: Rate of heat liberated from solid structures per unit fluid volume

$\dot{Q}$: Rate of internal heat generation per unit fluid volume

Φ : Dissipation function

Table 2.2 Source Terms in the Cylindrical Coordinate System

Equation	Variable (ϕ)	Direction	Diffusion Coefficient (Γ_ϕ)	Source Term (S_ϕ)
Continuity	1	Scalar	0	0
Momentum (i)	v_r	r direction	μ	$\rho \frac{v_\theta^{2*}}{r} + \rho g_r + V_r - R_r - \frac{1}{r}\frac{\partial}{\partial r}(rp)$
(ii)	v_θ	θ direction	μ	$-\frac{\rho v_r v_\theta^{**}}{r} + \rho g_\theta + V_\theta - R_\theta - \frac{1}{r}\frac{\partial}{\partial \theta}(p)$
(iii)	v_z	z direction	μ	$\rho g_z + V_z - R_z - \frac{\partial}{\partial z}(p)$
Energy	h	Scalar	k	$\frac{dp}{dt} + \dot{Q}_{rb} + \dot{Q} + \Phi$

* : Centrifugal force term

** : Coriolis force term

V_r, V_θ, V_z : Balance of the viscous diffusion terms

R_r, R_θ, R_z : Distributed resistance due to solid structures in a momentum control volume

$\dot{Q}_{rb}$ Rate of heat liberated from solid structures per unit fluid volume

$\dot{Q}$: Rate of internal heat generation per unit fluid volume

Φ : Dissipation function

for the Cartesian coordinates to cylindrical coordinates with the simple transformations shown in Table 2.3.

Table 2.3 Transformations for Cartesian and Cylindrical Coordinate Systems

Cartesian Coordinates	Cylindrical Coordinates
x	r
y	θ
z	z
Δx	Δr
Δy	$r\Delta\theta$
Δz	Δz
u	v_r
v	v_θ
w	v_z

Equation 2.1b can be considered very general, because it reduces to the conservation equation for a continuum regime (Eq. 2.1a) when we make volume porosities and directional surface porosities = 1 ($\gamma_v = \gamma_x = \gamma_y = \gamma_z = 1.0$), distributed resistances $R_x = R_y = R_z = 0$ (or $R_r = R_\theta = R_z = 0$ in a cylindrical coordinate system), and heat source $\dot{Q}_{rb} = 0$.

For turbulent flow, all quantities in Eq. 2.1 are considered time-averaged values and diffusion coefficient Γ is interpreted as the effective (laminar and turbulent) diffusion coefficient, i.e.,

$$\Gamma_\phi = \Gamma_{\phi,\text{laminar}} + \Gamma_{\phi,\text{turbulent}}. \tag{2.3}$$

We can also express the effective diffusion coefficient as the ratio of effective viscosity to the corresponding Prandtl number, i.e.,

$$\Gamma_\phi = \frac{\mu_{\text{laminar}} + \mu_{\text{turbulent}}}{\sigma_\phi}. \tag{2.4}$$

Here, σ_ϕ is the Prandtl number based on the diffusivity of variable ϕ.

The transport equations of turbulence parameters k and ε for computation of the turbulent diffusion coefficient also have the same general form as Eq. 2.1; however, for clarity of presentation, they are included in Sec. 6.

3. CONTROL VOLUME

3.1 CONSTRUCTION OF A COMPUTATIONAL CELL

The computational cells around a grid point can be defined in a number of ways. In COMMIX-1B, the computational cell is defined by the locations of cell volume faces, and a grid point is placed in the geometrical center of each cell volume. Cell sizes can be nonuniform. This type of construction is shown in Fig. 3.1. The convention used in COMMIX-1B for defining the neighboring cells and cell faces is given in Table 3.1.

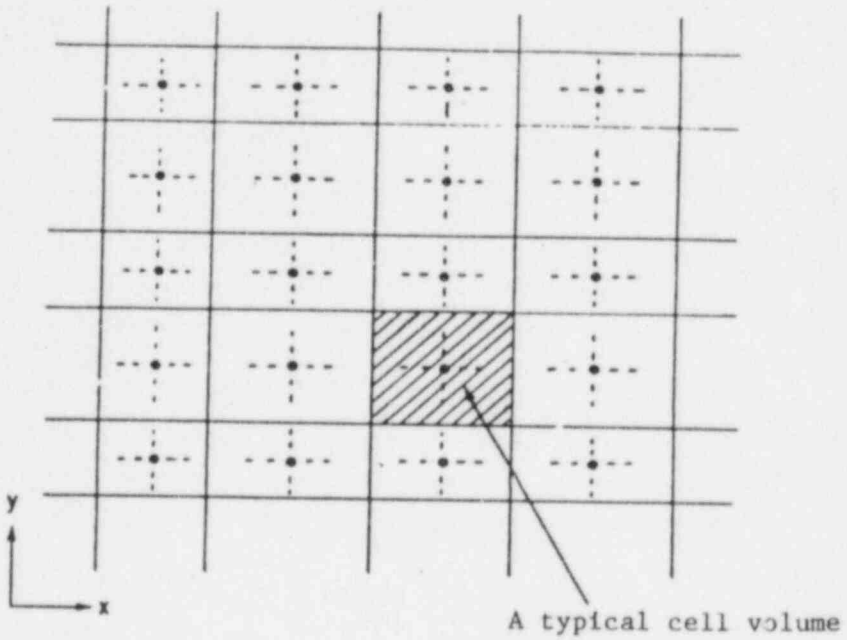

Fig. 3.1. Construction of Cell Volumes

Table 3.1. Convention used in COMMIX-1B to Define Neighboring-Cell Control Volumes

Subscript	Cell Centers	Cell-Face Centers
0	i, j, k	
1	i-1, j, k	i-1/2, j, k
2	i+1, j, k	i+1/2, j, k
3	i, j-1, k	i, j-1/2, k
4	i, j+1, k	i, j+1/2, k
5	i, j, k-1	i, j, k-1/2
6	i, j, k+1	i, j, k+1/2

3.2 CONTROL VOLUME FOR FIELD VARIABLES

In COMMIX, we use the staggered grid system, in which all dependent field variables are calculated at a cell center and flow variables are calculated at the surfaces of a cell.

For a field variable, we consider the control volume to be as shown in Fig. 3.2. It is constructed around a grid point 0, which has grid points 1 (i-1) and 2 (i+1) as its west and east neighbors; grid points 3 (j-1) and 4 (j+1) as its south and north neighbors; and grid points 5 (k-1) and 6 (k+1) as its bottom and top neighbors. We integrate each term of the conservation equation, step by step, over the control volume to derive the finite-difference equation.

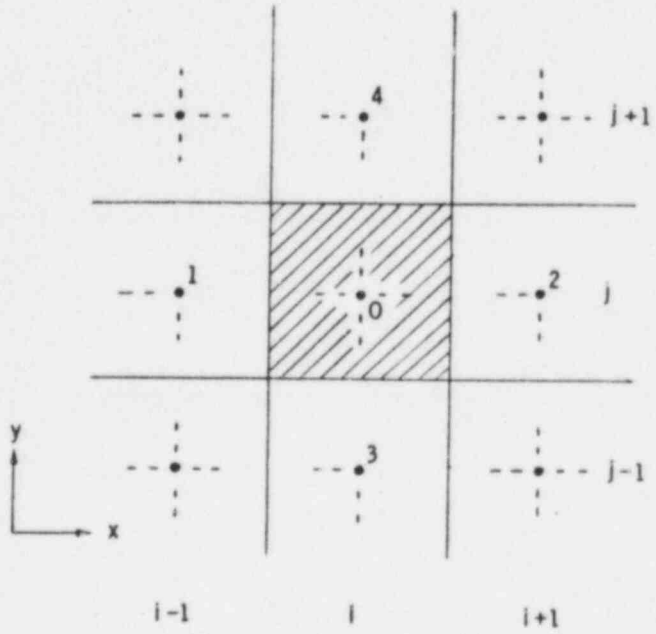

Fig. 3.2. Cell Volume around Point 0 in i,j,k Notation

3.3 CONTROL VOLUME FOR FLOW VARIABLES

Although all dependent variables are calculated for a grid point, the velocity components u, v, and w are an exception. They are calculated for displaced or "staggered" locations, and **not** at the grid point. The displaced locations of the velocity components are such that they are placed on the faces of a control volume. Thus, the i-direction velocity u is calculated at the faces that are normal to the i direction.

Figure 3.3 shows the locations of u and v by short arrows on a two-dimensional grid; the three-dimensional counterpart can be easily imagined. With respect to a grid point, the u location is displaced only in the i direction, the v location only in the j direction, and so on. The location for u thus lies in the i direction link joining two adjacent grid points. It is the pressure difference between these grid points that will be used to drive the velocity u located between them. This is the main consequence of the staggered grid.

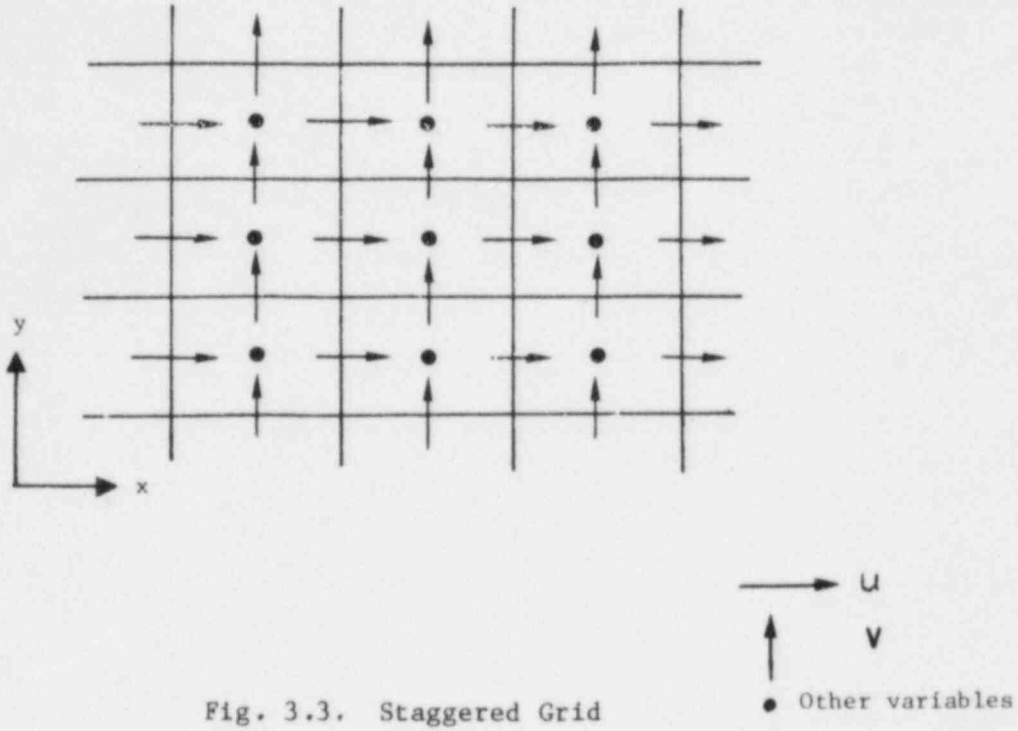

Fig. 3.3. Staggered Grid

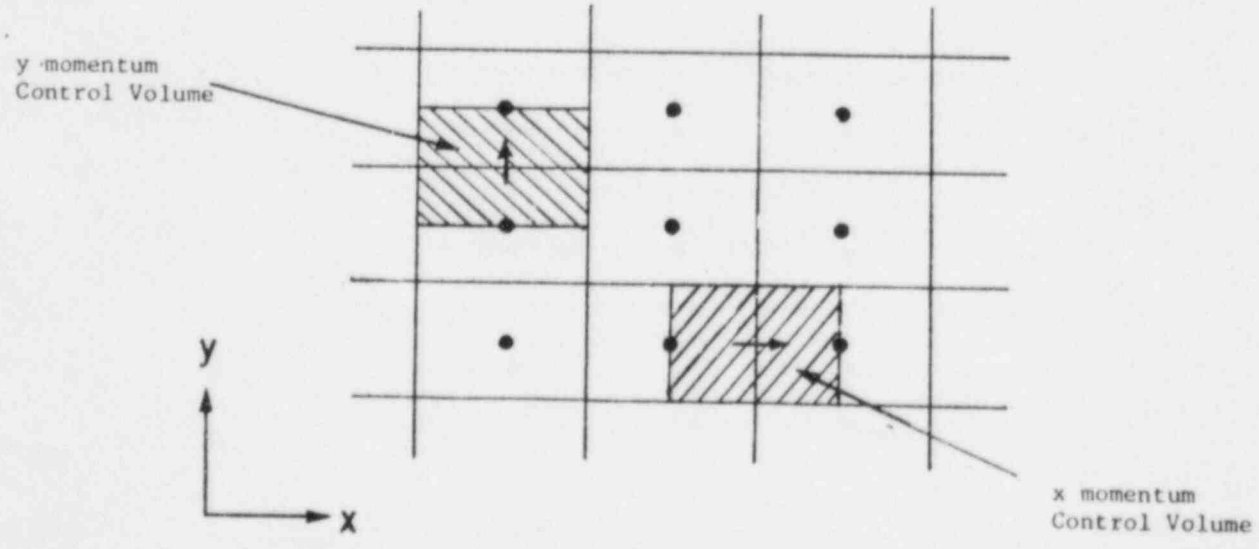

Fig. 3.4. Momentum Control Volumes

A direct consequence of the staggered grid is that the control volumes to be used for the conservation of momentum must also be staggered. The control volumes shown in Figs. 3.1 and 3.2 will now be referred to as the main control volumes. The control volumes for momentum will be staggered in the direction of the momentum such that the faces normal to that direction pass through the grid points (see Fig. 3.4). Thus, the pressures at these grid points can be directly used for calculating the pressure force on the momentum control volume. Table 3.2 shows the convention used for the subscripts, and Fig. 3.4 shows the momentum control volumes for the i and j directions.

Table 3.2. Convention Used in COMMIX-1B to Define Neighboring Control Volumes for i Direction Momentum Equations

Subscript	Momentum Control Volume Centers	Momentum Control Volume Face Centers
0	i+1/2, j, k	
1	i-1/2, j, k	i, j, k
2	i+3/2, j, k	i+1, j, k
3	i+1/2, j-1, k	i+1/2, j-1/2, k
4	i+1/2, j+1, k	i+1/2, j+1/2, k
5	i+1/2, j, k-1	i+1/2, j, k-1/2
6	i+1/2, j, k+1	i+1/2, j, k+1/2

4. FINITE-DIFFERENCE FORMULATION

Although the finite-difference formulation is applied to a grid in both the Cartesian and cylindrical coordinate systems, only a Cartesian coordinate grid system is used here to demonstrate the formulation of the finite-difference equations. Similarly, we have used only the x momentum equation to illustrate the formulation of the momentum equation.

The finite-difference equations are derived by integrating the governing equation (Eq. 2.1) over a control volume. We integrate each term separately.

4.1 UNSTEADY TERM

4.1.1 Main Control Volume

Representation of the term $\partial(\gamma_v \rho\phi)$ is obtained assuming that the values ρ_0 and ϕ_0 prevail over the control volume surrounding point 0 (see Fig. 4.1). Integration of the unsteady terms over the control volume then gives

$$\int \frac{\partial}{\partial t}(\gamma_v \rho\phi)\, dx\, dy\, dz = \frac{(\rho\phi)_0 - (\rho\phi)_0^n}{\Delta t} V_0 , \qquad (4.1)$$

where $V_0 = \gamma_v \Delta x \Delta y \Delta z$ is the volume of the fluid; the superscript n refers to known old time-step values, and the superscript n+1 for new time-step values is omitted for simplicity.

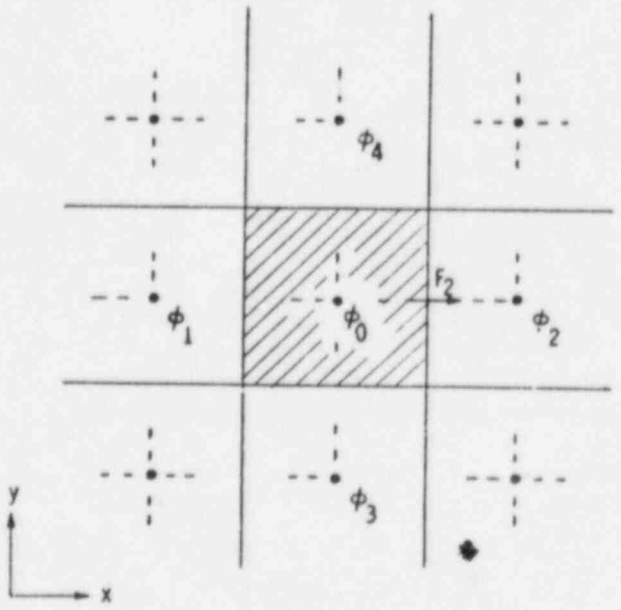

Fig. 4.1. Control Volume for Field Variables

4.1.2 Momentum Control Volume

Because the momentum control volumes are staggered, there are differences (mainly geometrical) in the resulting finite-difference equations. To illustrate these differences, we consider the x momentum control volume as shown in Fig. 4.2. If we integrate the unsteady term, we can obtain the same form as Eq. 4.1, but we express it a little differently.

$$\int \frac{\partial}{\partial t}\left(\gamma_v \rho\phi\right)\, dxdydz = \int \left(\rho \frac{\partial\phi}{\partial t} + \phi \frac{\partial\rho}{\partial t}\right)\gamma_v\, dxdydz$$

$$= \left[\left(\frac{\bar{\rho} + \bar{\rho}^n}{2}\right)\left(\frac{\phi - \phi^n}{\Delta t}\right) + \left(\frac{\phi + \phi^n}{2}\right)\left(\frac{\partial\bar{\rho}}{\partial t}\right)\right]\bar{V}_0 . \qquad (4.1a)$$

Here, the bar over a variable is to suggest that the variable now refers to the momentum control volume and not the main control volume. The geometrical differences between Eq. 4.1 and Eq. 4.1a are the following:

- Volume of fluid is for the x momentum control volume, i.e.,

$$\bar{V}_0 = \frac{1}{2}\left(\gamma_i + \gamma_{i+1}\right)\frac{1}{2}\left(\Delta x_i + \Delta x_{i+1}\right)\Delta y\, \Delta z\ , \qquad (4.2)$$

and

- The property values are evaluated at the center of the x-momentum control volume, e.g.,

$$\bar{\rho}_0 = \rho_{i+1/2} = \frac{\Delta x_i \rho_i + \Delta x_{i+1}\rho_{i+1}}{\Delta x_i + \Delta x_{i+1}}\ . \qquad (4.3)$$

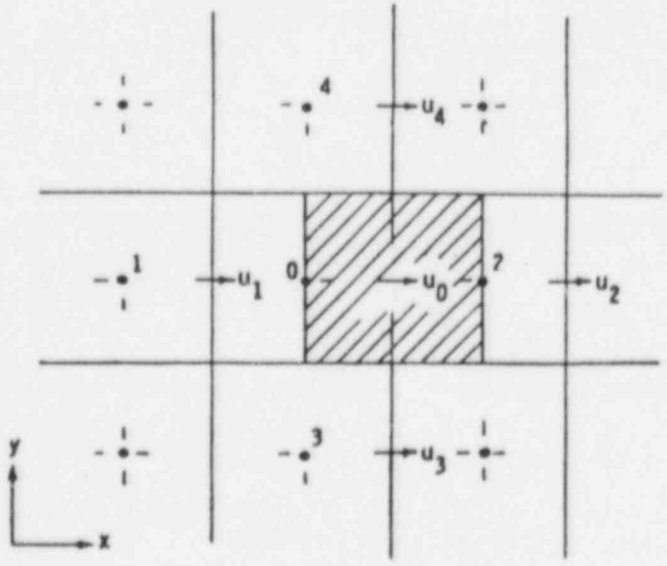

Fig. 4.2. Control Volume for x momentum

In Eq. 4.1a, we have used the symbol ϕ for the dependent variable (i.e., the x direction velocity) instead of u. This is only because our desire here is to illustrate the formulation of a general equation rather than to describe the derivation of a specific equation.

For the momentum equation, we express the right side of Eq. 4.1a little differently. We assume

$$\frac{\bar{\rho} + \bar{\rho}^{n}}{2} \sim \bar{\rho}, \text{ and } \left(\frac{\partial \bar{\rho}}{\partial t}\right) \sim \left(\frac{\partial \bar{\rho}}{\partial t}\right)^{n} ;$$

therefore, the transient term for the x-momentum control volume shown in Fig. 4.2 is

$$\int \frac{\partial}{\partial t}(\gamma_v \rho\phi)\, dx\, dy\, dz = \left[\bar{\rho}\left(\frac{\phi - \phi^{n}}{\Delta t}\right) + \left(\frac{\phi + \phi^{n}}{2}\right)\left(\frac{d\bar{\rho}}{dt}\right)^{n}\right]_{i+1/2} \bar{V}_0$$

$$= \left\{\left[\frac{\bar{\rho}}{\Delta t} + \frac{1}{2}\left(\frac{\partial \bar{\rho}}{\partial t}\right)^{n}\right]\phi - \left[\frac{\bar{\rho}}{\Delta t} - \frac{1}{2}\left(\frac{\partial \rho}{\partial t}\right)^{n}\right]\phi^{n}\right\}_{i+1/2} \bar{V}_0 \quad . \quad (4.4)$$

It will become clear later, when we assemble the full equation, why we have formulated the transient term for the flow variables differently from that of the field variables.

4.2 CONVECTION TERM

4.2.1 Main Control Volume

The integration of the convection terms over the control volume gives

$$\int \left[\frac{\Delta(\gamma_x \rho u\phi)}{\Delta x} + \frac{\Delta(\gamma_y \rho v\phi)}{\Delta y} + \frac{\Delta(\gamma_z \rho w\phi)}{\Delta z}\right] dx\, dy\, dz$$

$$= F_2\langle\phi\rangle_2^0 - F_1\langle\phi\rangle_0^1 + F_4\langle\phi\rangle_4^0 - F_3\langle\phi\rangle_0^3 + F_6\langle\phi\rangle_6^0 - F_5\langle\phi\rangle_0^5 \quad . \quad (4.5)$$

Here, F (= density x velocity x flow area) is the mass flux across the surface of the control volume and subscripts 2, 1, 4, 3, 6, and 5 stand for the east, west, north, south, top, and bottom surfaces, respectively (see Fig. 4.3a). For example,

$$F_2 = F_{i+1/2} = \langle\rho\rangle_2^0 \left(\gamma_x u \Delta y \Delta z\right)_2 = \langle\rho\rangle_2^0 \left(uA_x\right)_2 = \langle\rho\rangle_{i+1}^{i} \left(uA_x\right)_{i+1/2} \quad (4.6)$$

is the mass flux at the east surface, as shown in Fig. 4.1. We use the upwind-difference scheme to define a property value at the surface of a cell; i.e.,

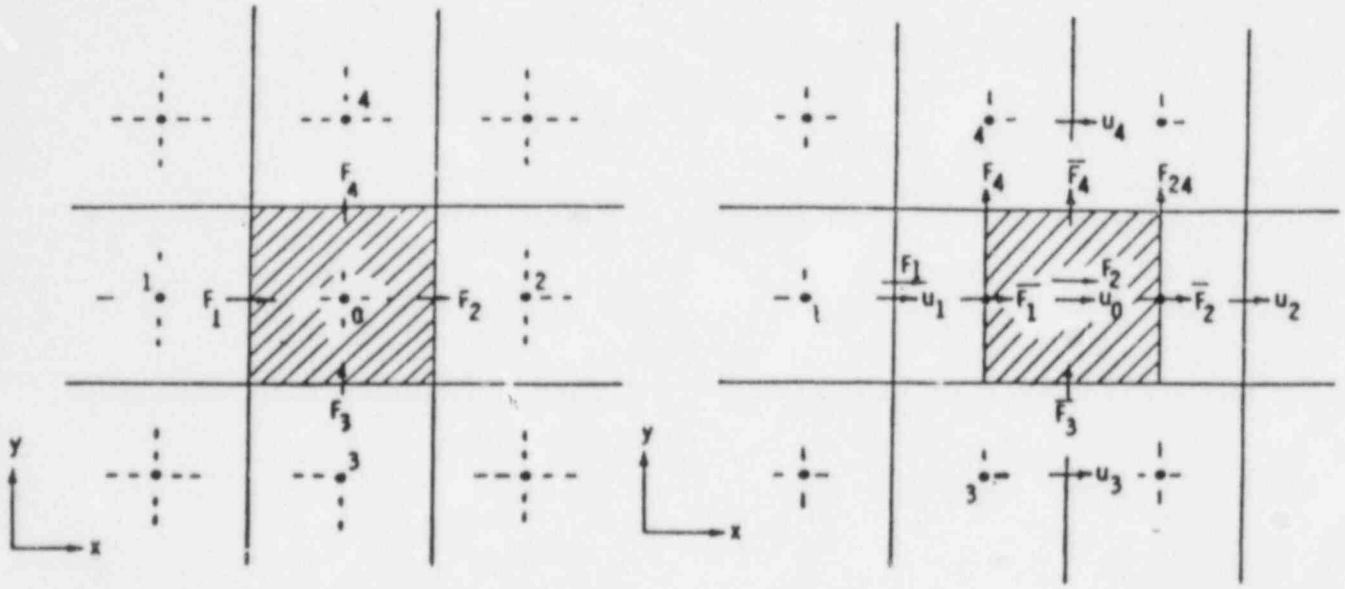

(a) Field Variable (b) x momentum

Fig. 4.3. Control Volume Showing Convective Fluxes

$$F_2\langle\phi\rangle_2^0 = F_{i+1/2}\langle\phi\rangle_{i+1}^i = F_2\,\phi_0 = F_{i+1/2}\phi_i \quad \text{(if } F_2 \text{ is +ve)}\,, \tag{4.7a}$$

$$= F_2\,\phi_2 = F_{i+1/2}\phi_{i+1} \quad \text{(if } F_2 \text{ is -ve)}\,. \tag{4.7b}$$

The superscript location value is to be used for positive velocity and subscript location value is to be used for negative velocity. Equation 4.7 can also be written as

$$F_2\langle\phi\rangle_2^0 = |0,F_2|\phi_0 - |0,-F_2|\phi_2\,. \tag{4.8}$$

The operator $|\ |$ is to be interpreted as equal to the greater of two arguments; i.e.,

$$|A,B| = A \quad \text{if} \quad A > B,$$

$$= B \quad \text{if} \quad B > A. \tag{4.9}$$

In accordance with the above convention and after some simplification, we rewrite Eq. 4.5 as

$$\int \left[\frac{\Delta(\gamma_x \rho u \phi)}{\Delta x} + \frac{\Delta(\gamma_y \rho v \phi)}{\Delta y} + \frac{\Delta(\gamma_z \rho w \phi)}{\Delta z} \right] dx\, dy\, dz$$

$$= \left[|0,F_2| + |0,F_4| + |0,F_6| + |0,-F_1| + |0,-F_3| + |0,-F_5| \right] \tilde{\phi}_0$$

$$- \left[|0,-F_2| \tilde{\phi}_2 + |0,-F_4| \tilde{\phi}_4 + |0,-F_6| \tilde{\phi}_6 \right.$$

$$\left. + |0,F_1| \tilde{\phi}_1 + |0,F_3| \tilde{\phi}_3 + |0,F_5| \tilde{\phi}_5 \right] . \qquad (4.10)$$

Please note that we have introduced a curly bar over the dependent variable ϕ in Eq. 4.10. We define

$$\tilde{\phi} = \alpha \phi^{n+1} + (1 - \alpha) \phi^{n} , \qquad (4.11)$$

where α is an implicitness parameter. The introduction of the implicitness parameter α makes the convective flux formulation, Eq. 4.10, very general, i.e. from the semi-implicit formulation where some variables are at old-time values ($\alpha = 0$) to a fully implicit formulation where all variables are at new-time values ($\alpha = 1$).

All six convective fluxes for the main control volume are listed in Table 4.1.

Table 4.1. Convective Fluxes for Main Control Volume

F_1	:	$(A_x u)_{i-1/2}$	$\langle \rho \rangle_0^1$
F_2	:	$(A_x u)_{i+1/2}$	$\langle \rho \rangle_2^0$
F_3	:	$(A_y v)_{j-1/2}$	$\langle \rho \rangle_0^3$
F_4	:	$(A_y v)_{j+1/2}$	$\langle \rho \rangle_4^0$
F_5	:	$(A_z w)_{k-1/2}$	$\langle \rho \rangle_0^5$
F_6	:	$(A_z w)_{k+1/2}$	$\langle \rho \rangle_6^0$

4.2.2 **Momentum Control Volume**

We consider the x momentum control volumes as shown in Fig. 4.3b. If we compare the main and x momentum control volumes (Figs. 4.3a and 4.3b), we can define the total j direction flowrate at the upper face of the momentum control volume as

$$\bar{F}_4 = \frac{1}{2}\left(F_4 + F_{24}\right)$$

$$= \frac{1}{2}\left[\left(A_y v\right)_{i,j+1/2} \langle\rho\rangle^{j}_{j+1} + \left(A_y v\right)_{i+1,j+1/2} \langle\rho\rangle^{i+1}_{i+1,j+1}\right] . \qquad (4.12)$$

Similarly, the i direction flowrate entering the momentum control volume can be defined as

$$\bar{F}_1 = \frac{1}{2}\rho_0\left[\left(A_x u\right)_{i-1/2} + \left(A_x u\right)_{i+1/2}\right] . \qquad (4.13)$$

The convective fluxes $\bar{F}_1 \ldots . \bar{F}_6$ for the x momentum control volume are listed in Table 4.2.

Table 4.2 Convective Fluxes for x Momentum Control Volume

$$\bar{F}_1 : \rho_0 \frac{1}{2}\left[\left(uA_x\right)_{i-1/2} + \left(uA_x\right)_{i+1/2}\right]$$

$$\bar{F}_2 : \rho_2 \frac{1}{2}\left[\left(uA_x\right)_{i+1/2} + \left(uA_x\right)_{i+3/2}\right]$$

$$\bar{F}_3 : \frac{1}{2}\left[\langle\rho\rangle^{3}_{0}\left(vA_y\right)_{i,j-1/2} + \langle\rho\rangle^{23}_{2}\left(vA_y\right)_{i+1,j-1/2}\right]$$

$$\bar{F}_4 : \frac{1}{2}\left[\langle\rho\rangle^{0}_{4}\left(vA_y\right)_{i,j+1/2} + \langle\rho\rangle^{2}_{24}\left(vA_y\right)_{i+1,j+1/2}\right]$$

$$\bar{F}_5 : \frac{1}{2}\left[\langle\rho\rangle^{5}_{0}\left(wA_z\right)_{i,k-1/2} + \langle\rho\rangle^{25}_{2}\left(wA_z\right)_{i+1,k-1/2}\right]$$

$$\bar{F}_6 : \frac{1}{2}\left[\langle\rho\rangle^{0}_{6}\left(wA_z\right)_{i,k+1/2} + \langle\rho\rangle^{2}_{26}\left(wA_z\right)_{i+1,k+1/2}\right]$$

Thus, when we integrate the convective terms over the momentum control volume, we have the same form of equation as Eq. 4.10, except that we use the momentum control volume fluxes $\bar{F}$ (Table 4.2) instead of the main control volume fluxes F (Table 4.1).

$$\int \left[\frac{\Delta(\rho u \gamma_x \phi)}{\Delta x} + \frac{\Delta(\rho v \gamma_y \phi)}{\Delta y} + \frac{\Delta(\rho w \gamma_z \phi)}{\Delta z}\right] dx\, dy\, dz$$

$$= \left[\,|0,\bar{F}_2| + |0,\bar{F}_4| + |0,\bar{F}_6| + |0,-\bar{F}_1| + |0,-\bar{F}_3| + |0,-\bar{F}_5|\right] \tilde{\phi}_0$$

$$- \left[\,|0,-\bar{F}_2|\,\tilde{\phi}_2 + |0,-\bar{F}_4|\,\tilde{\phi}_4 + |0,-\bar{F}_6|\,\tilde{\phi}_6\right.$$

$$\left. + |0,\bar{F}_1|\,\tilde{\phi}_1 + |0,\bar{F}_3|\,\tilde{\phi}_3 + |\,0,\bar{F}_5|\,\tilde{\phi}_5\right] . \qquad (4.14)$$

Please note, once again, that the dependent variable ϕ has a curly bar over it. Thus, it represents (as defined in Eq. 4.11) a combination of old and new time values.

4.3 DIFFUSION TERM

4.3.1 Main Control Volume

The integration of diffusion terms over a main control volume (Fig. 4.4a) gives

$$\int \left[\frac{\Delta\left(\gamma_x \Gamma_\phi \frac{\partial\phi}{\partial x}\right)}{\Delta x} + \frac{\Delta\left(\gamma_y \Gamma_\phi \frac{\partial\phi}{\partial y}\right)}{\Delta y} + \frac{\Delta\left(\gamma_z \Gamma_\phi \frac{\partial\phi}{\partial z}\right)}{\Delta z}\right] dx\, dy\, dz$$

$$= D_2(\tilde{\phi}_2 - \tilde{\phi}_0) - D_1(\tilde{\phi}_0 - \tilde{\phi}_1) + D_4(\tilde{\phi}_4 - \tilde{\phi}_0) - D_3(\tilde{\phi}_0 - \tilde{\phi}_3)$$

$$+ D_6(\tilde{\phi}_6 - \tilde{\phi}_0) - D_5(\tilde{\phi}_0 - \tilde{\phi}_5) ,$$

$$= D_1\tilde{\phi}_1 + D_2\tilde{\phi}_2 + D_3\tilde{\phi}_3 + D_4\tilde{\phi}_4 + D_5\tilde{\phi}_5 + D_6\tilde{\phi}_6$$

$$- \left(D_1 + D_2 + D_3 + D_4 + D_5 + D_6\right) \tilde{\phi}_0 . \qquad (4.15)$$

Here, D (= effective diffusivity x flow area/distance between the centers of two control volumes) is the diffusion strength across the surface of the control volume, ϕ (Eq. 4.11) represents the sum of the contributions of old and new time values, and Γ_ϕ is the effective diffusivity for the variable ϕ.

To determine the value of D at a surface, we assume a uniform value of diffusivity Γ prevails over each main control volume and use harmonic interpolation, e.g.,

$$D_2 = (A_x)_{i+1/2} \left[\left(\frac{\Delta x}{2\Gamma}\right)_0 + \left(\frac{\Delta x}{2\Gamma}\right)_2\right]^{-1} . \qquad (4.16)$$

The values of diffusion strength for main control volume are listed in Table 4.3.

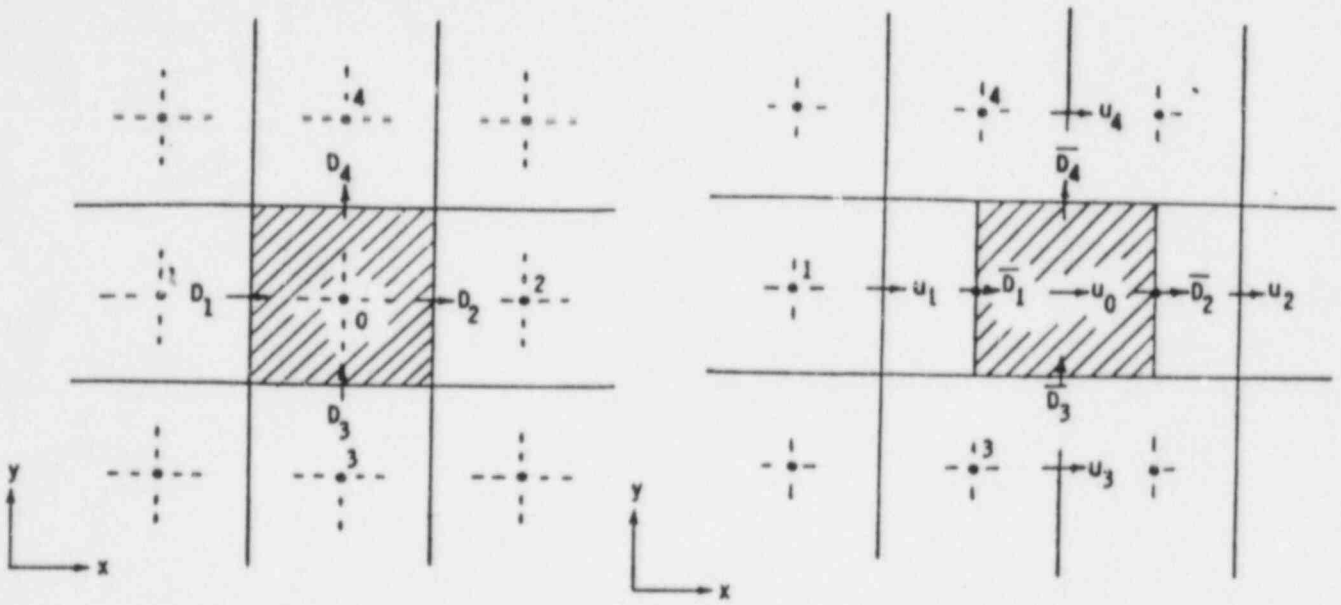

(a) Field Variable (b) x momentum

Fig. 4.4 Control Volume Showing Diffusive Fluxes

Table 4.3 Diffusion Strengths for Main Control Volume

$$D_1 : (A_x)_{i-1/2} \left[\left(\frac{\Delta x}{2\Gamma}\right)_0 + \left(\frac{\Delta x}{2\Gamma}\right)_1\right]^{-1}$$

$$D_2 : (A_x)_{i+1/2} \left[\left(\frac{\Delta x}{2\Gamma}\right)_0 + \left(\frac{\Delta x}{2\Gamma}\right)_2\right]^{-1}$$

$$D_3 : (A_y)_{j-1/2} \left[\left(\frac{\Delta y}{2\Gamma}\right)_0 + \left(\frac{\Delta y}{2\Gamma}\right)_3\right]^{-1}$$

$$D_4 : (A_y)_{j+1/2} \left[\left(\frac{\Delta y}{2\Gamma}\right)_0 + \left(\frac{\Delta y}{2\Gamma}\right)_4\right]^{-1}$$

$$D_5 : (A_z)_{k-1/2} \left[\left(\frac{\Delta z}{2\Gamma}\right)_0 + \left(\frac{\Delta z}{2\Gamma}\right)_5\right]^{-1}$$

$$D_6 : (A_z)_{k+1/2} \left[\left(\frac{\Delta z}{2\Gamma}\right)_0 + \left(\frac{\Delta z}{2\Gamma}\right)_6\right]^{-1}$$

4.3.2 Momentum Control Volume

The integration of i diffusion terms over x momentum control volume (Fig. 4.4b) also results in an expression similar to Eq. 4.15:

$$\int \left[\frac{\Delta \left(\gamma_x \Gamma_\phi \frac{\partial \phi}{\partial x} \right)}{\Delta x} + \frac{\Delta \left(\gamma_y \Gamma_\phi \frac{\partial \phi}{\partial y} \right)}{\Delta y} + \frac{\Delta \left(\gamma_z \Gamma_\phi \frac{\partial \phi}{\partial z} \right)}{\Delta z} \right] dx\, dy\, dz$$

$$= \bar{D}_1 \tilde{\phi}_1 + \bar{D}_2 \tilde{\phi}_2 + \bar{D}_3 \tilde{\phi}_3 + \bar{D}_4 \tilde{\phi}_4 + \bar{D}_5 \tilde{\phi}_5 + \bar{D}_6 \tilde{\phi}_6 +$$

$$- \left(\bar{D}_1 + \bar{D}_2 + \bar{D}_3 + \bar{D}_4 + \bar{D}_5 + \bar{D}_6 \right) \tilde{\phi}_0 \ . \qquad (4.17)$$

The only difference is that we now use the momentum control volume diffusion strength $\bar{D}$, instead of the main control volume diffusion strength D; e.g.,

$$\bar{D}_2 = \frac{1}{2} \left[(A_x)_{i+1/2} + (A_x)_{i+3/2} \right] \left(\frac{\Gamma_\phi}{\Delta x} \right)_2 \ . \qquad (4.18)$$

The values of diffusion strengths $\bar{D}$ for x momentum control volumes are listed in Table 4.4. In Eqs. 4.17 and 4.18, we have used the symbol Γ instead of μ for the diffusivity (viscosity) of the momentum equation. This is only for the purpose of retaining the generality of the formulation.

Table 4.4 Diffusion Strengths for x Momentum Control Volume

$$\bar{D}_1 : \frac{1}{2} \left[(A_x)_{i-1/2} + (A_x)_{i+1/2} \right] \left(\frac{\Gamma}{\Delta x} \right)_0$$

$$\bar{D}_2 : \frac{1}{2} \left[(A_x)_{i+1/2} + (A_x)_{i+3/2} \right] \left(\frac{\Gamma}{\Delta x} \right)_2$$

$$\bar{D}_3 : \frac{1}{2} \left[(A_y)_{i,j-1/2} + (A_y)_{i+1,j-1/2} \right] \left[\frac{\Delta y_{j-1}}{(\Gamma_3 + \Gamma_{23})} + \frac{\Delta y_j}{(\Gamma_0 + \Gamma_2)} \right]^{-1}$$

$$\bar{D}_4 : \frac{1}{2} \left[(A_y)_{i,j+1/2} + (A_y)_{i+1,j+1/2} \right] \left[\frac{\Delta y_{j+1}}{(\Gamma_4 + \Gamma_{24})} + \frac{\Delta y_j}{(\Gamma_0 + \Gamma_2)} \right]^{-1}$$

$$\bar{D}_5 : \frac{1}{2} \left[(A_z)_{i,k-1/2} + (A_z)_{i+1,k-1/2} \right] \left[\frac{\Delta z_{k-1}}{(\Gamma_5 + \Gamma_{25})} + \frac{\Delta z_k}{(\Gamma_0 + \Gamma_2)} \right]^{-1}$$

$$\bar{D}_6 : \frac{1}{2} \left[(A_z)_{i,k+1/2} + (A_z)_{i+1,k+1/2} \right] \left[\frac{\Delta z_{k+1}}{(\Gamma_6 + \Gamma_{26})} + \frac{\Delta z_k}{(\Gamma_0 + \Gamma_2)} \right]^{-1}$$

4.4 SOURCE TERM

The finite-difference representation of the source term S in Eq. 2.1 is expressed as

$$S_\phi = S_{c\phi} + S_{p\phi}\,\phi_0 \,, \tag{4.19}$$

where $S_{c\phi}$, $S_{p\phi}$, and ϕ_0 are assumed to prevail over the control volume surrounding point 0. This "linearization" of the source term is an effective device for stability and convergence. The exact expressions for the source term coefficients $S_{c\phi}$ and $S_{p\phi}$ depend on the actual form of the source S_ϕ. The coefficient $S_{p\phi}$ is always less than or equal to zero; otherwise instability, divergence or physically unrealistic solutions would result.

The integration of the source term over the control volume gives

$$\int S_\phi \, dx\, dy\, dz = S_{c\phi}\, V_0 + S_{p\phi}\, V_0\, \tilde{\phi}_0 \tag{4.20a}$$

for the main control volume, and

$$\int S_\phi \, dx\, dy\, dz = S_{c\phi}\, \bar{V}_0 + S_{p\phi}\, \bar{V}_0\, \tilde{\phi}_0 \tag{4.20b}$$

for the momentum control volume.

4.5 GENERAL FINITE-DIFFERENCE EQUATION

Having looked at each term of the general equation separately, we now assemble all terms of Eqs. 4.1, 4.10, 4.15, and 4.20 for the main control volume to obtain the general finite-difference equation.

$$\begin{aligned}
&\int [\,(\text{Unsteady}) + (\text{Convection}) - (\text{Diffusion}) - (\text{Source})\,]\, dx\, dy\, dz \\
&= \underbrace{\frac{(\rho\phi)_0 - (\rho\phi)_0^n}{\Delta t}\, V_0}_{(\text{Unsteady})} + \underbrace{\{\,|0,-F_1| + |0,F_2| + \cdots\,\}\,\tilde{\phi}_0}_{(\text{Convection})} \\
&\quad - \underbrace{\{\,|0,F_1|\,\tilde{\phi}_1 + |0,-F_2|\,\tilde{\phi}_2 + \cdots\,\}}_{(\text{Convection})} + \underbrace{(D_1 + D_2 + \cdots)\,\tilde{\phi}_0}_{(\text{Diffusion})} \\
&\quad - \underbrace{\{\,D_1\tilde{\phi}_1 + D_2\tilde{\phi}_2 + \cdots\,\}}_{(\text{Diffusion})} - \underbrace{S_{c\phi}\, V_0 - S_{p\phi}\,\tilde{\phi}_0\, V_0}_{(\text{Source})} = 0 \,.
\end{aligned} \tag{4.21}$$

We now rearrange Eq. 4.21 such that only the terms containing ϕ_0 are on the left-hand side of the equation, noting that

$$\tilde{\phi} = \alpha\phi + (1-\alpha)\,\phi^n \,. \tag{4.22}$$

After some algebra and rearrangement, we obtain

$$\phi_o \left\{ \frac{\rho_0 V_0}{\Delta t} + \alpha[(|0,-F_1| + \cdots + |0,F_6|) + (D_1 + \cdots + D_6) - S_{p\phi} V_0] \right\}$$

$$= [(|0,F_1| + D_1)\phi_1 + \cdots + (|0,-F_6| + D_6)\phi_6]\alpha$$

$$+ \left[(|0,F_1| + D_1)\phi_1^n + \cdots + (|0,-F_6| + D_6)\phi_6^n\right](1-\alpha)$$

$$- \phi_o^n (1-\alpha)[(|0,-F_1| + \cdots |0,F_6|) + (D_1 + \cdots D_6) - S_{p\phi} V_0]$$

$$+ \left(\frac{\rho_0^n \phi_0^n}{\Delta t} V_o + S_{C\phi} V_o\right), \tag{4.23}$$

or

$$\boxed{a_0^\phi \phi_0 = \left(a_1^\phi \phi_1 + a_2^\phi \phi_2 + a_3^\phi \phi_3 + a_4^\phi \phi_4 + a_5^\phi \phi_5 + a_6^\phi \phi_6\right)\alpha + b_0^\phi ,} \tag{4.24}$$

where

$$b_0^\phi = b1^\phi{}_0 + b2_0^\phi + b3_0^\phi . \tag{4.25}$$

For ease in reading, the coefficients of Eqs. 4.24 and 4.25 for the main control volumes are given in Table 4.5. As we have combined the extreme semi-implicit and fully implicit formulations in one general form, the coefficients of Table 4.5 may appear somewhat confusing. We have therefore also included Tables 4.6 and 4.7, which give the coefficients for extreme semi-implicit (α = 0) formulation and fully implicit (α = 1) formulation.

For the x momentum control volume, we follow the same procedure to assemble all the terms of Eqs. 4.4, 4.14, 4.17, and 4.21. The resulting equation has the same form as Eq. 4.24, except that the coefficients are slightly different. The coefficients for the x momentum control volume are presented in Tables 4.8, 4.9, and 4.10.

It may be noted from Table 4.5 that we have expressed the coefficient a_0^ϕ in two forms. The first form $a_0^\phi(1)$ is obtained by assembling all the terms of Eqs. 4.1, 4.10, 4.15, and 4.20. The second form $a_0(2)$ is obtained by subtracting the continuity equation from the first form $a_0(1)$; that is,

$$a_0(1) - \{\text{continuity equation}\} = a_0(2) . \tag{4.26}$$

We use only the first form $a_0(1)$ for the momentum equations because during the solution of the momentum equations, the continuity equation might not have been satisfied. The use of the second form $a_0(2)$ may introduce inconsistencies. However, when we solve the energy equation, the continuity

Table 4.5. General Finite-Difference Equation for the Main Control Volume (Eqs. 4.24 and 4.25) and Its Coefficient

$$a_0^{\phi}\phi_0 = \alpha\left(a_1^{\phi}\phi_1 + \cdots + a_6^{\phi}\phi_6\right) + \left(b1_0^{\phi} + b2_0^{\phi} + b3_0^{\phi}\right)$$

$a_1^{\phi} : \left(\lvert 0, F_1\rvert + D_1\right)$	$a_2^{\phi} : \left(\lvert 0, -F_2\rvert + D_2\right)$
$a_3^{\phi} : \left(\lvert 0, F_3\rvert + D_3\right)$	$a_4^{\phi} : \left(\lvert 0, -F_4\rvert + D_4\right)$
$a_5^{\phi} : \left(\lvert 0, F_5\rvert + D_5\right)$	$a_6^{\phi} : \left(\lvert 0, -F_6\rvert + D_6\right)$

$$b1_0^{\phi} : (1-\alpha)\left(a_1^{\phi}\phi_1^{n} + a_2^{\phi}\phi_2^{n} + a_3^{\phi}\phi_3^{n} + a_4^{\phi}\phi_4^{n} + a_5^{\phi}\phi_5^{n} + a_6^{\phi}\phi_6^{n}\right)$$

$$b2_0^{\phi} : -(1-\alpha)\left[\left(\lvert 0, -F_1\rvert + \cdots + \lvert 0, F_6\rvert\right) + \left(D_1 + \cdots + D_6\right) - S_{p\phi}V_0\right]\phi_0^{n}$$

$$b3_0^{\phi} : \left(\frac{\rho^{n}\phi^{n}}{\Delta t} + S_{c\phi}\right)_0 V_o$$

$$a_0^{\phi}(1) : \frac{\rho_0 V_0}{\Delta t} + \alpha\left[\left(\lvert 0, -F_1\rvert + \cdots + \lvert 0, F_6\rvert + \left(D_1 + D_2 \cdots + D_6\right) - S_{p\phi}\, V_0\right]\right.$$

(1st form)

$$a_0^{\phi}(2) : \alpha\left(a_1^{\phi} + a_2^{\phi} + \cdots a_6^{\phi}\right) + \left(\frac{\rho^{n}}{\Delta t} - S_{p\phi}\right)V_0$$

(2nd form)

$$+ (1-\alpha)\left(F_1 - F_2 + F_3 - F_4 + F_5 - F_6\right)$$

Table 4.6. Extreme Semi-Implicit ($\alpha = 0$) Finite-Difference Equation for the Main Control Volume (Eqs. 4.24 and 4.25) and Its Coefficients

$$a_0^{\phi}\phi_0 = \left(b1_0^{\phi} + b2_0^{\phi} + b3_0^{\phi}\right)$$

$$b1_0^{\phi} : \left(a_1^{\phi}\phi_1^n + a_2^{\phi}\phi_2^n + a_3^{\phi}\phi_3^n + a_4^{\phi}\phi_4^n + a_5^{\phi}\phi_5^n + a_6^{\phi}\phi_6^n\right)$$

$$b2_0^{\phi} : -\left[\left(\left|0,-F_1\right| + \cdots + \left|0,F_6\right|\right) + \left(D_1 + \cdots + D_6\right) - S_{p\phi}V_0\right]$$

$$b3_0^{\phi} : \left(\frac{\rho_0^n \phi^n}{\Delta t} + S_{c\phi}\right)_0 V_0$$

$$a_0^{\phi}(1) : \frac{\rho_0 V_0}{\Delta t}$$

(1st form)

$$a_0^{\phi}(2) : \left(\frac{\rho^n}{\Delta t} - S_{p\phi}\right) V_0 + \left(F_1 - F_2 + F_3 - F_4 + F_5 - F_6\right)$$

(2nd form)

Table 4.7. Fully Implicit ($\alpha = 1$) Finite-Difference Equation for the Main Control Volume (Eqs. 4.24 and 4.25) and Its Coefficients

$$a_0^{\phi}\phi_0 = \left(a_1^{\phi}\phi_1 + \cdots + a_6^{\phi}\phi_6 + b3_0^{\phi}\right)$$

$a_1^{\phi} : \left(\left\|0,F_1\right\| + D_1\right)$	$a_2^{\phi} : \left(\left\|0,-F_2\right\| + D_2\right)$
$a_3^{\phi} : \left(\left\|0,F_3\right\| + D_3\right)$	$a_4^{\phi} : \left(\left\|0,-F_4\right\| + D_4\right)$
$a_5^{\phi} : \left(\left\|0,F_5\right\| + D_5\right)$	$a_6^{\phi} : \left(\left\|0,-F_6\right\| + D_6\right)$

$$b3_0^{\phi} : \left(\frac{\rho_0^n \phi^n}{\Delta t} + S_{c\phi}\right)_0 V_0$$

$$a_0^{\phi}(1) : \frac{\rho_0 V_0}{\Delta t} + \left[\left(\left|0,-F_1\right| + \cdots + \left|0,F_6\right|\right) + \left(D_1 + D_2 \cdots + D_6\right) - S_{po\phi}V_0\right]$$

(1st form)

$$a_0^{\phi}(2) : \left(a_1^{\phi} + a_2^{\phi} + \cdots a_6^{\phi}\right) + \left(\frac{\rho^n}{\Delta t} - S_{p\phi}\right) V_0$$

(2nd form)

Table 4.8. Coefficients of General Finite-Difference Equation for x Momentum Control Volume

$$a_0^{\phi}\phi_0 = \alpha\left(a_1^{\phi}\phi_1 + \cdots\cdots + a_6^{\phi}\phi_6\right) + \left(b1_0^{\phi} + b2_0^{\phi} + b3_0^{\phi}\right)$$

$a_1^{\phi} : \left(\lvert 0, \bar{F}_1\rvert + \bar{D}_1\right)$	$a_2^{\phi} : \left(\lvert 0, -\bar{F}_2\rvert + \bar{D}_2\right)$
$a_3^{\phi} : \left(\lvert 0, \bar{F}_3\rvert + \bar{D}_3\right)$	$a_4^{\phi} : \left(\lvert 0, -\bar{F}_4\rvert + \bar{D}_4\right)$
$a_5^{\phi} : \left(\lvert 0, \bar{F}_5\rvert + \bar{D}_5\right)$	$a_6^{\phi} : \left(\lvert 0, -\bar{F}_6\rvert + \bar{D}_6\right)$

$$b1_0^{\phi} : (1-\alpha)\left(a_1^{\phi}\phi_1^n + a_2^{\phi}\phi_2^n + \cdots\cdots + a_6^{\phi}\phi_6^n\right)$$

$$b2_0^{\phi} : -(1-\alpha)\left[\left(\lvert 0, -\bar{F}_1\rvert + \cdots\cdots + \lvert 0, \bar{F}_6\rvert\right) + \left(D_1 + \cdots\cdots + D_6\right) - S_{p\phi} V_0\, \phi_0^n\right]$$

$$b3_0^{\phi} : \left\{\phi^n\left[\frac{\bar{\rho}_0}{\Delta t} - \frac{1}{2}\left(\frac{\partial \bar{\rho}}{\partial t}\right)_0^n\right] + S_{c\phi}\right\} \bar{V}_0$$

$$a_0(1) : \left[\frac{\bar{\rho}_0}{\Delta t} + \frac{1}{2}\left(\frac{\partial \bar{\rho}}{\partial t}\right)_0^n\right] \bar{V}_0 + \alpha\left(\lvert 0, -\bar{F}_1\rvert + \cdots\cdots + \lvert 0, \bar{F}_6\rvert\right) + \left(\bar{D}_1 + \cdots\cdots + \bar{D}_6\right) - S_{p\phi}\, \bar{V}_0$$

Table 4.9. Coefficients of Extreme Semi-Implicit ($\alpha = 0$) Finite-Difference Equation for x Momentum Control Volume

$$a_0^\phi \phi_0 = b1_0^\phi + b2_0^\phi + b3_0^\phi$$

$b1_0^\phi$	$a_1^\phi \phi_1^n + a_2^\phi \phi_2^n + \cdots\cdots + a_6^\phi \phi_6^n$
$b2_0^\phi$	$-\left[\left(\left\|0,-F_1\right\| + \cdots\cdots + \left\|0,F_6\right\|\right) + \left(D_1 + \cdots\cdots + D_6\right) - S_{p\phi} V_0\right] \phi_0^n$
$b3_0^\phi$	$\left\{\phi^n \left[\frac{\bar{\rho}_0}{\Delta t} - \frac{1}{2}\left(\frac{\partial \bar{\rho}}{\partial t}\right)_0^n\right] + S_{c\phi}\right\} \bar{V}_0$
$a_0^\phi(1)$	$\left[\frac{\bar{\rho}_0}{\Delta t} + \frac{1}{2}\left(\frac{\partial \bar{\rho}}{\partial t}\right)_0^n\right] \bar{V}_0$

Table 4.10. Coefficients of Fully Implicit ($\alpha = 1$) Finite-Difference Equation for x Momentum Control Volume

$$a_0^\phi \phi_0 = \left(a_1^\phi \phi_1 + \cdots\cdots + a_6^\phi \phi_6 + b3_0^\phi\right)$$

a_1^ϕ	$\left(\left\|0,\bar{F}_1\right\| + \bar{D}_1\right)$	a_2^ϕ	$\left(\left\|0,-\bar{F}_2\right\| + \bar{D}_2\right)$
a_3^ϕ	$\left(\left\|0,\bar{F}_3\right\| + \bar{D}_3\right)$	a_4^ϕ	$\left(\left\|0,-\bar{F}_4\right\| + \bar{D}_4\right)$
a_5^ϕ	$\left(\left\|0,\bar{F}_5\right\| + \bar{D}_5\right)$	a_6^ϕ	$\left(\left\|0,-\bar{F}_6\right\| + \bar{D}_6\right)$

$b3_0^\phi$	$\left\{\phi^n \left[\frac{\bar{\rho}_0}{\Delta t} - \frac{1}{2}\left(\frac{\partial \bar{\rho}}{\partial t}\right)_0^n\right] + S_{c\phi}\right\} \bar{V}_0$
a_0^ϕ	$\left[\frac{\bar{\rho}_0}{\Delta t} + \frac{1}{2}\left(\frac{\partial \bar{\rho}}{\partial t}\right)_0^n\right] \bar{V}_0 + \left[\left(\left\|0,-\bar{F}_1\right\| + \cdots\cdots + \left\|0,\bar{F}_6\right\|\right) + \left(\bar{D}_1 + \cdots\cdots + \bar{D}_6\right) - S_{p\phi}\, \bar{V}_0\right]$

equation is satisfied. The use of the second form $a_0(2)$ is therefore acceptable during the solution of the energy equation.

In deriving the second form of the coefficient a_0 for the main control volume, we have made use of the continuity equation in the following way. (If a reader is not interested in details, the rest of this section can be skipped.)

If we substitute $\phi = 1$, $S_\phi = 0$, and $\Gamma_\phi = 0$ in the general equation (Eq. 2.1), we have the continuity equation. Therefore, all formulations derived so far also are applicable to the continuity equation.

To derive the continuity equation, we substitute $\phi = 1$ in Eq. 4.23, remembering that $D = 0$ and $S = 0$ for the continuity equation. After simplification, we have the following:

Continuity Equation in the Discretized Form:

$$\frac{\rho_0 V_0}{\Delta t} + \alpha \left[|0,-F_1| + \cdots + |0,F_6| \right]$$

$$- \alpha \left[|0,F_1| + \cdots + |0,-F_6| \right]$$

$$- (1-\alpha) \left[|0,F_1| + \cdots + |0,-F_6| \right]$$

$$+ (1-\alpha) \left[|0,-F_1| + \cdots + |0,F_6| \right] - \frac{\rho^n V_0}{\Delta t} = 0 \ . \qquad (4.27)$$

Please note that the first density term in the continuity equation (Eq. 4.27) is at the new time, while the second density term is at the old time. The subtraction of Eq. 4.27 from $a_0(1)$, after some algebra, results in the second form $a_0(2)$:

$$a_0^\phi(2) = a_0^\phi(1) - \text{Continuity Equation 4.27}$$

$$= \alpha \left[(D_1 + \cdots + D_6) - S_{p\phi} V_0 \right]$$

$$+ \alpha \left[|0,F_1| + \cdots + |0,-F_6| \right]$$

$$+ (1-\alpha) \left[|0,F_1| + \cdots + |0,-F_6| \right]$$

$$- (1-\alpha) \left[|0,-F_1| + \cdots + |0,F_6| \right] + \frac{\rho^n V_0}{\Delta t}$$

$$= \alpha \left[(|0,F_1| + D_1) + \cdots + (|0,-F_6| + D_6) \right]$$

$$+\left(\frac{\rho^n}{\Delta t} - \alpha\ S_{p\phi}\right) V_0$$

$$+ (1 - \alpha)\left[\left(|0,F_1| - |0,-F_1|\right) + \cdots\cdot + \left(|0,-F_6| - |0,F_6|\right)\right]$$

$$= \alpha\left(a_1^\phi + a_2^\phi + a_3^\phi + a_4^\phi + a_5^\phi + a_6^\phi\right) + \left(\frac{\rho^n}{\Delta t} - \alpha\ S_{p\phi}\right) V_0$$

$$+ (1 - \alpha)\left(F_1 - F_2 + F_3 - F_4 + F_5 - F_6\right), \qquad (4.28)$$

because

$$|0,F_1| - |0,-F_1| = F_1$$

and

$$|0,-F_2| - |0,F_2| = -F_2.$$

4.6 FINITE DIFFERENCE OF MOMENTUM EQUATIONS

We have derived the finite-difference equation for x momentum following the same procedure as for the general equation. We see that the pressure term gradient appears in the momentum equation, but the pressure field is neither known beforehand nor directly obtainable from some sort of "conservation equation for pressure." Therefore, we consider pressure as unknown and determine it indirectly from the constraint that the velocity field satisfies the continuity equation. For this reason, we display the pressure-containing term in the finite-difference form of the momentum equation separately and do not include it in the source term.

From these considerations, the x momentum finite-difference equation for the control volume shown in Fig. 4.3 is written as

$$a_0^u u_0 = a_1^u u_1 + a_2^u u_2 + a_3^u u_3 + a_4^u u_4 + a_5^u u_5 + a_6^u u_6$$

$$+ b_0^u - d_u\left(P_2 - P_0\right). \qquad (4.29)$$

Here,

$$d_u = \frac{1}{2}\left(\gamma_0 + \gamma_2\right)\Delta y\,\Delta z. \qquad (4.30)$$

The other coefficients, $a_0^u \cdots\cdot a_6^u$, and $b_0^u = b1_0^u + b2_0^u + b3_0^u$, are given in Tables 4.8, 4.9, and 4.10.

The contributions of the source term that enter a_0^u and b_0^u do not contain the pressure gradient; the effect of the pressure gradient is expressed by the last term in Eq. 4.29. The momentum equation for the j and k directions are obtained in a similar manner.

5. PRESSURE EQUATION

The pressure appearing in the momentum equation (4.20) is unknown and must be determined from the conservation-of-mass equation. In this section, we present the derivation of the pressure equation and the solution procedures employed in COMMIX-1B.

The conservation-of-mass equation for the cell around point 0 (Fig. 4.1) can be derived from Eq. 4.23 by substituting $\phi = 1$, diffusion strength $D = 0$, and $S = 0$:

$$V_0\left(\frac{\partial \rho}{\partial t}\right) - (A_x u)_{i-1/2} \langle\rho\rangle_0^1 + (A_x u)_{i+1/2} \langle\rho\rangle_2^0 - (A_y v)_{j-1/2} \langle\rho\rangle_0^3 + (A_y v)_{j+1/2} \langle\rho\rangle_4^0 - (A_z w)_{k-1/2} \langle\rho\rangle_0^5 + (A_z w)_{k+1/2} \langle\rho\rangle_6^0 = \delta_0 . \qquad (5.1)$$

Here, $V_0 = \gamma_v \Delta x \Delta y \Delta z$ is the control volume, δ_0 is the mass residual of the continuity equation, $\langle\rho\rangle$ is the upwind density, u, v, and w are the normal velocities at the surface of the control volume, and A is the flow area. We define the flow area as the product of surface area and surface permeability.

When mass is precisely conserved, the right side of Eq. 5.1 vanishes, i.e., $\delta = 0$. However, because Eq. 5.1 is solved by an iterative-solution procedure, the mass residual δ, in general, may not be zero.

To convert the indirect specification of pressure in the continuity equation to an explicit form, we write the momentum Eq. 4.20 as

$$\phi = \hat{\phi} - d^{\phi} \Delta P \qquad (\phi = u, v, w) , \qquad (5.2)$$

where

$$\hat{\phi} = \frac{\alpha \sum_{\ell=1}^{6} a_\ell^{\phi} \phi_\ell + b1_0^{\phi} + b2_0^{\phi} + b3_0^{\phi}}{a_0^{\phi}} \quad \text{(for the general case)} \qquad (5.2a)$$

$$\hat{\phi} = \frac{b1_0^{\phi} + b2_0^{\phi} + b3_0^{\phi}}{a_0^{\phi}} \quad \text{(for the extreme semi-implicit case, } \alpha = 0), \qquad (5.2b)$$

and

$$\hat{\phi} = \frac{\sum_{\ell=1}^{6} a_\ell^{\phi} \phi_\ell + b3_0^{\phi}}{a_0^{\phi}} \quad \text{(for the fully implicit case, } \alpha = 1). \qquad (5.2c)$$

For example, the x direction velocity u at east surface of the main control volume is expressed as

$$u_2 = \hat{u}_2 - d_2^u \left(P_2 - P_0 \right) , \tag{5.3a}$$

where

$$d_2^u = \frac{1}{2} \frac{\left(\gamma_{v0} + \gamma_{v2} \right) \quad \Delta y \, \Delta z}{a_0^u} . \tag{5.3b}$$

With similar definitions for $\hat{v}$, $\hat{w}$, and d, the other velocities appearing in Eq. 5.1 can be expressed as

$$u_1 = \hat{u}_1 - d_1^u \left(P_0 - P_1 \right) ,$$

$$v_4 = \hat{v}_4 - d_4^v \left(P_4 - P_0 \right) ,$$

$$v_3 = \hat{v}_3 - d_3^v \left(P_0 - P_3 \right) ,$$

$$w_6 = \hat{w}_6 - d_6^w \left(P_6 - P_0 \right) ,$$

and

$$w_5 = \hat{w}_5 - d_5^w \left(P_0 - P_5 \right) . \tag{5.4}$$

Here, the subscripts 1 .... 6 for velocities refer to the surfaces of the main control volume. Substitution of Eqs. 5.3 and 5.4 into Eq. 5.1 yields

$$a_0^P P_0 - \sum_{\ell=1}^{6} a_\ell^P P_\ell - b_0^P = \delta_0 . \tag{5.5}$$

The coefficients of Eq. 5.5 are listed in Table 5.1.

Equation 5.5 is the required pressure equation. In the above equations, the superscripts for coefficients a and b indicate the equations they belong to; e.g., a^u and b^u are coefficients of the u momentum equation.

Table 5.1. Coefficients of Pressure Equation (Eq. 5.5)

$$a_1^P : \left(\frac{A_x}{a_0^u}\right)_{i-1/2} \langle\rho\rangle_0^1 \frac{1}{2}(\gamma_{v0} + \gamma_{v1})\,\Delta y\,\Delta z$$

$$a_2^P : \left(\frac{A_x}{a_0^u}\right)_{i+1/2} \langle\rho\rangle_2^0 \frac{1}{2}(\gamma_{v0} + \gamma_{v2})\,\Delta y\,\Delta z$$

$$a_3^P : \left(\frac{A_y}{a_0^v}\right)_{j-1/2} \langle\rho\rangle_0^3 \frac{1}{2}(\gamma_{v0} + \gamma_{v3})\,\Delta x\,\Delta z$$

$$a_4^P : \left(\frac{A_y}{a_0^v}\right)_{j+1/2} \langle\rho\rangle_4^0 \frac{1}{2}(\gamma_{v0} + \gamma_{v4})\,\Delta x\,\Delta z$$

$$a_5^P : \left(\frac{A_z}{a_0^w}\right)_{k-1/2} \langle\rho\rangle_0^5 \frac{1}{2}(\gamma_{v0} + \gamma_{v5})\,\Delta x\,\Delta y$$

$$a_6^P : \left(\frac{A_z}{a_0^w}\right)_{k+1/2} \langle\rho\rangle_6^0 \frac{1}{2}(\gamma_{v0} + \gamma_{v6})\,\Delta x\,\Delta y$$

$$a_0^P : a_1^P + a_2^P + a_3^P + a_4^P + a_5^P + a_6^P$$

$$b_0^P : -V_0 \left(\frac{\partial \rho}{\partial t}\right)_0 + (A_x\hat{u})_{i-1/2} \langle\rho\rangle_0^1 - (A_x\hat{u})_{i+1/2} \langle\rho\rangle_2^0$$

$$+ (A_y\hat{v})_{j-1/2} \langle\rho\rangle_0^3 - (A_y\hat{v})_{j+1/2} \langle\rho\rangle_4^0$$

$$+ (A_z\hat{w})_{k-1/2} \langle\rho\rangle_0^5 - (A_z\hat{w})_{k+1/2} \langle\rho\rangle_6^0$$

6. TURBULENCE MODELING

6.1 INTRODUCTION

For turbulent flow, the diffusivity in the governing conservation equation (2.1) is considered as a time-averaged value. Therefore, the viscosity μ and thermal conductivity λ in the momentum and energy equations are the effective transport coefficients of momentum and energy, respectively. Thus,

$$\mu = \mu_{eff} = \mu_{lam} + \mu_{tur} \tag{6.1}$$

and

$$\lambda = \lambda_{eff} = \lambda_{lam} + \lambda_{tur} = \frac{\mu_{lam} + \mu_{tur}}{Pr} \ . \tag{6.2}$$

Here, the subscripts lam and tur stand for laminar (molecular) and turbulent properties, and Pr is the effective Prandtl number. There are four models in COMMIX-1B for calculation of turbulent diffusivities:

- Constant turbulent diffusivity model,
- Zero-equation mixing-length model,
- One-equation (k) turbulence model, and
- Two-equation (k-ϵ) turbulence model.

After a brief background on turbulence modeling, we present here the details of these models.

6.2 BACKGROUND ON TURBULENCE MODELING

The subject of turbulence has attracted countless researchers over a period of more than 80 years. In 1895, Reynolds proposed that a fluid particle in turbulent flow is in randomly unsteady motion. He averaged the Navier Stokes equation over a time scale that is long compared with the turbulent time scale, and derived the equations that describe the mean turbulent motion. In spite of the long time span and large research effort since Reynolds averaged the Navier-Stokes equation, the problem of turbulence has not been resolved completely for the following reasons.

The appearance of the time-averaged correlations, such as $\rho\overline{u'v'}$ in the governing equations, gives rise to the so-called "closure" problem (more unknowns than equations available for the solution of unknowns). Here ρ denotes fluid density, u' and v' are the fluctuating velocity components in the coordinate directions x and y, and the overbar denotes the time averaging. The correlations u'v' are known as Reynolds stresses.

Another difficulty is that the constituents of the turbulence phenomenon normally take place in scales of motion that are very small orders of magnitude in size, while the whole flow domain may extend over meters or even

kilometers. Important details of turbulence are small-scale in character (although it is not the details but the time-averaged consequences that are of interest in practical application). As a result, the computational nodes required to resolve small-scale motions of turbulence will far exceed the storage capacity of current computers. The corresponding computer running time also will be unfeasibly long.

An alternative approach to resolve these difficulties is to employ some form of turbulence modeling in which we solve only the time-averaged equations of motion along with a set of transport equations of turbulence quantities, e.g., k the turbulence kinetic energy, ϵ the rate of dissipation of k, etc. Even this approach requires a significant amount of numerical computation. It is only in the last 20 years, with the recent advances in computer power, that this alternative turbulence modeling approach has been made feasible.

Many turbulence models have been proposed to resolve the above-mentioned difficulties by providing solvable equations for computation of turbulent flows. The central idea in most of the turbulence models, except the Reynolds-stress model or algebraic stress modeling, is the employment of an artificial turbulent viscosity μ_{tur} to account for the additional diffusional flux due to the turbulent motion. To do that, the Reynolds stress term is expressed as

$$-\rho\,\overline{u'v'} = \mu_{tur}\left(\frac{\partial u}{\partial x} + \frac{\partial v}{\partial y}\right) - \frac{1}{3}\rho\left(\overline{u'^2} + \overline{v'^2} + \overline{w'^2}\right) . \qquad (6.3)$$

We must note here that the turbulent viscosity μ_{tur} is a property of the local state of turbulence and not a physical property of the fluid. The turbulence model in this category is therefore generally referred to as a viscosity model.

The most popular model among these viscosity models, yet the simplest, is Prandtl's mixing-length hypothesis[53]. We refer to the mixing-length hypothesis as a zero-equation model because it does not require solution of any transport equation of turbulence parameters.

In 1945, Prandtl[54] suggested a more general approach than the mixing-length hypothesis. His new approach is generally referred to as a one-equation turbulence model. In this model, the turbulent viscosity is assumed to be a function of the square root of the turbulence kinetic energy k. To determine the value of k, we need to solve its transport equation. Since then, many one-equation turbulence models have been proposed. The transport equation for the shear stress developed by Bradshaw et al.[55] and the transport equation for the turbulent viscosity developed by Nee and Kovasznay[56] are typical turbulent viscosity models.

Undoubtedly, one-equation models generally produce more reliable results than the mixing-length hypothesis produces for most computations. However, a need to obtain a more accurate estimate of the length scale distribution, especially in a separated flow region, leads to the suggestion of two-equation turbulence models.

There are several two-equation turbulence models (k-ϵ model, k-ℓ model, k-W model, etc.). Here, the symbol k is the kinetic energy of turbulence, ϵ is the dissipation rate of turbulence energy, ℓ is a macroscopic length scale of turbulence, and W is interpreted as the time-averaged square of the velocity fluctuations. Among the two-equation models, the k-ϵ model, as proposed by Harlow and Nakayama[57] and Jones and Launder[58], is the most widely used.

The next level in turbulence modeling is represented by the complex Reynolds stress models[59-62]. These models are still in the development stages. We have therefore programmed in COMMIX only the 0, 1, and 2 equation turbulence models for the analysis of turbulent flows. These models are described in this section.

As we increase the level of turbulence modeling from 0 to 1 equation, from 1 to 2 equations, and so forth, we are increasing complexity in the turbulence modeling and, therefore, computer cost as well. So during selection of a turbulence model, we must balance the increase in accuracy with the cost of computing.

6.3 CONSTANT TURBULENT DIFFUSIVITY MODEL

This is a very simplified turbulence model in which the turbulent viscosity and the turbulent conductivity are assumed to be constant. The value of turbulent viscosity is a user-prescribed single input constant.

It is preferable to prescribe values of turbulent viscosity and turbulent conductivity obtained from experimental data. If the experimental information is not available, then turbulent viscosity can be estimated using the following equation suggested by Sha and Launder[62]:

$$\mu_{tur} = 0.007 c_\mu \rho U_{max} \ell \ , \tag{6.4}$$

where

$$c_\mu = 0.1 \qquad \text{for } Re_{max} > 2000 \ ,$$

$$c_\mu = 0.1\left(0.001 Re_{max} - 1\right) \qquad \text{for } 1000 \leq Re_{max} \leq 2000 \ ,$$

and

$$c_\mu = 0 \qquad \text{for } Re_{max} < 1000 \ . \tag{6.5}$$

Here,

$$U_{max} = \text{Max}(u, v, w) \quad \text{and} \tag{6.6}$$

$$Re_{max} = \text{Max}(Re_x, Re_y, Re_z) \ , \tag{6.7}$$

the mixing length scale

$$\ell = C_\ell D_h \ , \tag{6.8}$$

the coefficient

$$C_{\ell} = 0.4 \ , \tag{6.9}$$

and D_h is the hydraulic diameter.

If the information about turbulent conductivity λ_{tur} is not available and not prescribed, then we can approximate it using the following relation:

$$\lambda_{tur} = \frac{c_p \mu_{tur}}{Pr_{tur}}$$

$$= \frac{C_p \mu_{tur}}{0.8\left[1 - \exp\left(-6 \times 10^{-5} \ Re \ Pr^{1/3}\right)\right]^{-1}} \ , \tag{6.10}$$

where Re is the user-specified characteristic Reynolds number and $Pr = C_p\mu/\lambda$ is the molecular Prandtl number, calculated based on the simplified property option and user-specified characteristic temperature. Equation 6.10 is based on the proposal of Nijsing and Eiffel[63].

6.4 ZERO-EQUATION MIXING-LENGTH MODEL

In the 0-equation mixing-length model, the turbulent viscosity is computed from the relation

$$\mu_{tur} = \rho \ell^2 \left[\frac{\partial u_m}{\partial x_n}\left(\frac{\partial u_m}{\partial x_n} + \frac{\partial u_n}{\partial x_m}\right)\right]^{1/2} \ . \tag{6.11}$$

Here, u's are the time-averaged velocities and x's are the Cartesian or cylindrical coordinates. We have adopted the usual summation convention where the use of repeated subscripts implies summation over the three coordinate components. The mixing length ℓ is related to the distance y from the nearest wall as

$$\ell = \kappa y \quad (\text{for } y < y_{max}),$$

$$= \kappa y_{max} \ (\text{for } y > y_{max}). \tag{6.12}$$

Here, κ is the von Karman constant with recommended value $\kappa = 0.42$, y_{max} ($= 0.175 * D_H$) is the cutoff value, and D_H is the hydraulic diameter.

6.5 ONE-EQUATION MODEL

In the 1-equation (k) model, we solve the transport equation (Secs. 6.7 and 6.8) for turbulence kinetic energy k and compute turbulent viscosity using the relation

$$\mu_{tur} = \frac{C_D \rho k^2}{\epsilon} \ , \tag{6.13}$$

where ϵ, the dissipation rate of turbulent kinetic energy is given by

$$\varepsilon = \frac{C_D^{3/4}\, k^{3/2}}{\ell} , \tag{6.14}$$

C_D is a constant having the recommended value 0.09, and ℓ is the length scale related to the distance y from the nearest wall as described in Eq. 6.12.

In the case of multidimensional flow with more than one wall co-existing, the value of y, used to compute ℓ, is the nearest distance from a wall. The cutoff value y_{max} is either 0.175 D_H or a preassigned length, where D_H is the hydraulic diameter.

After computation of turbulent viscosity, we compute the thermal conductivity using the relation

$$\lambda_{tur} = \frac{C_p \mu_{tur}}{Pr_{tur}} , \tag{6.15}$$

where Pr_{tur} is the user-specified turbulent Prandtl number.

6.6 TWO-EQUATION MODEL

In the 2-equation (k-ε) turbulence model, we first solve the transport equations (Secs. 6.7 and 6.8) for turbulence kinetic energy k and the dissipation rate of turbulence kinetic energy ε. After obtaining the values of k and ε, we compute the turbulent viscosity μ_{tur} using the relation

$$\mu_{tur} = \left(\frac{C_D \rho k^2}{\varepsilon} \right) . \tag{6.16}$$

Here, C_D is a constant having the recommended value 0.09,

$$k = \frac{1}{2} \left(\overline{u'^2 + v'^2 + w'^2} \right) \tag{6.17}$$

is the turbulence kinetic energy,

$$\varepsilon = \nu \overline{\frac{\partial u_i'}{\partial x_j} \frac{\partial u_i'}{\partial x_j}} \tag{6.18}$$

is the dissipation rate of turbulent kinetic energy and ν is the kinematic viscosity. After computing turbulent viscosity, we compute the thermal conductivity using the relation

$$\lambda_{tur} = \frac{C_p \mu_{tur}}{Pr_{tur}} , \tag{6.19}$$

where Pr_{tur} is the user-specified turbulent Prandtl number.

6.7 TRANSPORT EQUATIONS OF k AND ε

6.7.1 Transport Equation for k

If we multiply the fluctuating velocity equations by fluctuating velocity components, add them, perform time-averaging, and use the definition $k = \frac{1}{2}\overline{u_i'u_i'}$, we obtain

$$\rho\frac{\partial k}{\partial t} + \rho\, u_j\frac{\partial k}{\partial x_j} = -\rho\overline{u_i'u_j'}\frac{\partial u_i}{\partial x_j} + \overline{\rho' u_i'}\, g_i - \mu\,\overline{\frac{\partial u_i'}{\partial x_j}\left(\frac{\partial u_i'}{\partial x_j} + \frac{\partial u_j'}{\partial x_i'}\right)}$$

A B C

$$+ \frac{\partial}{\partial x_j}\left[\mu\left(\frac{\partial k}{\partial x_j} + \frac{\partial\overline{u_i'u_j'}}{\partial x_i}\right) - \rho\,\frac{\overline{u_i'u_i'u_j'}}{2} - \overline{pu_i'}\,\delta_{ij}\right] . \quad (6.20)$$

D

Equation 6.20 is the exact form of the transport equation for k. Here, the terms are

A : source due to mean shear,

B : buoyancy interactions,

C : loss of k through viscous dissipation, and

D : diffusive transport of k and randomizing action of the pressure-strain correlation.

We can see that Eq. 6.20 has the closure problem. Adoption of the gradient-transport notion of Sha and Launder[62] eliminates the closure problem and simplifies Eq. 6.20 to

$$\rho\frac{\partial k}{\partial t} + \rho\, u_j\frac{\partial k}{\partial x_j} = P_k + G_k - \rho\varepsilon + \frac{\partial}{\partial x_j}\left[\left(\frac{\mu_{tur} + \mu_{lam}}{\sigma_k}\right)\frac{\partial k}{\partial x_j}\right] . \quad (6.21)$$

Here,

$$P_k = \mu_{tur}\left[\frac{\partial u_i}{\partial x_j}\left(\frac{\partial u_i}{\partial x_j} + \frac{\partial u_j}{\partial x_i}\right)\right] \quad (6.22)$$

is the source due to mean shear, and

$$G_k = -\frac{\mu_{tur}}{\rho\sigma_h}\frac{\partial\rho}{\partial T}\left(\frac{\partial T}{\partial x_j}\, g_j\right) \quad (6.23)$$

is the source due to thermal buoyancy. The term containing σ_k in Eq. 6.21 represents the diffusion of k. σ_k is called the turbulent Prandtl number for k. Launder et al[61] have recommended the value 1.0 for σ_k.

6.7.2 Transport Equation for ε

The exact form of the transport equation for ε is obtained by taking the derivative of Eq. 6.3, with respect to x_j, and multiplying it by

$$2\nu \left(\frac{\partial u_i'}{\partial x_j} + \frac{\partial u_j'}{\partial x_i} \right) . \tag{6.24}$$

The resulting equation is discussed in detail by Daly and Harlow[64], Hanjalic and Launder[60], and Lumley and Khajeh-Nouri[65]. The only feasible approach toward devising an ε equation is to apply both intuition and intelligent dimensional analysis. The ε equation contains several empirical coefficients that require adjusting to account for different behaviors of different shear flows. The equation proposed by Jones and Launder[58] and Daly and Harlow[64] is

$$\rho \frac{\partial \varepsilon}{\partial t} + \rho u_j \frac{\partial \varepsilon}{\partial x_j} = C_1 \frac{\varepsilon}{k} (P_k + G_k) - C_2 \frac{\rho \varepsilon^2}{k} + \frac{\partial}{\partial x_j} \left[\left(\frac{\mu_{tur} + \mu_{lam}}{\sigma_\varepsilon} \right) \frac{\partial \varepsilon}{\partial x_j} \right] . \tag{6.25}$$

Here, the source term P_k has the same form as Eq. 6.23, the second term on the right is the dissipation term, and the last term represents diffusion. The variable σ_ε is the turbulent Prandtl number for ε; the recommended value[62] is 1.3. The coefficient of the production term C_1 is normally chosen by reference to near-wall turbulence, whereas the coefficient C_2 is determined from the decay of grid turbulence. The values of C_1 and C_2 recommended by Launder et al.[66] are 1.44 and 1.92, respectively.

6.8 BOUNDARY CONDITIONS FOR TRANSPORT EQUATIONS

There are three types of boundaries:

A line or surface (plane) of symmetry,

Inlet and outlet boundaries, and

A solid wall.

The first two boundaries are discussed here and a solid wall boundary is discussed in Sec. 6.10.

6.8.1 Symmetry Boundary

The simplest boundary is the line or plane of symmetry; at a symmetry line, the normal velocity is zero. The gradients of scalar quantities k and ε normal to the symmetry line are also zero.

6.8.2 Inlet and Outlet Boundaries

At the outlet plane (free boundary), the gradient of turbulence quantities are assumed to be zero. The inlet plane requires special treatment. The inlet turbulence kinetic energy k_{in} can be obtained from measurement if available. For the uniform inlet velocity u_{in} the inlet turbulence kinetic energy k_{in} can be estimated as follows:

$$k_{in} = C_{k,in} u_{in}^2 , \tag{6.26}$$

where $C_{k,in}$ is the user-specified coefficient. The recommended value of $C_{k,in}$ is 0.001. The inlet dissipation rate of turbulence kinetic energy ϵ_{in} can be estimated using the relation

$$\epsilon_{in} = C_{\epsilon,in} k_{in}^{3/2} , \tag{6.27}$$

where $C_{\epsilon,in}$ is a coefficient that can be determined empirically or by using the following equation

$$C_{\epsilon,in} = \frac{C_\mu^{3/4}}{\ell_{in}} . \tag{6.28}$$

Here ℓ_{in} ($= \kappa y_{in} \leq \kappa\ 0.175\ D_H$) is the length scale at the inlet.

If the profile of the mean velocity at the inlet plane is known or can be guessed, then k_{in} can be estimated from

$$k_{in} = \ell_{in}^2 \left[\left(\frac{\partial u_{in}}{\partial y} \right)^2 + \left(\frac{\partial u_{in}}{\partial z} \right)^2 \right] , \tag{6.29}$$

where u_{in} is the mean velocity component in the main flow direction. The inlet dissipation rate ϵ_{in} can be computed pointwise using the same relation (Eq. 6.27) as for the uniform velocity case.

6.9 WALL FUNCTION TREATMENT

In the immediate vicinity of a solid wall, there is large variation in the values of turbulence properties. Therefore, to predict the correct values of momentum flux, energy flux, and the gradients of k and ϵ, we apply a special treatment called the wall-function treatment. In this procedure, we implicitly account for steep variation near a wall and avoid the need for a fine mesh. This procedure is described briefly here; more detailed information can be found in Sha and Launder[14].

6.9.1 Wall Shear Stress in the Momentum Equation

The illustration of the model used for a near-wall region is shown in Fig. 6.1. P is the node adjacent to the wall and outside the viscosity-affected zone (viscous sublayer), NP is the node next to P, and the distance

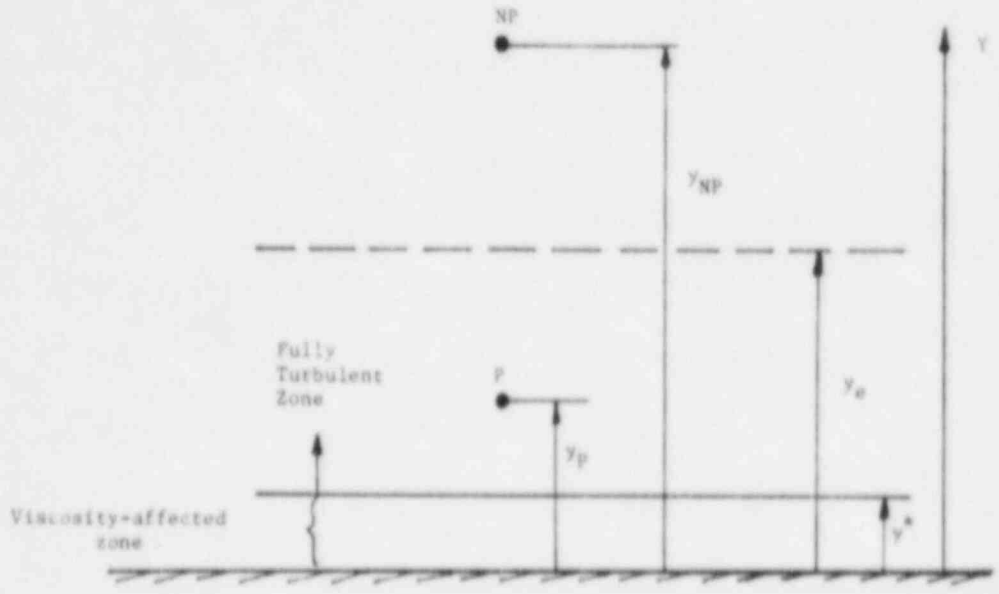

Fig. 6.1. Model of a Near-Wall Region

y_p is the distance from P to the wall. The sublayer thickness y^* is determined such that the Reynolds number R_t^* at the edge of the region is ~20.

$$R_t^* \equiv \frac{y^* k^{*1/2}}{\nu} = 20 \ . \tag{6.30}$$

The level of turbulent kinetic energy k^* at y^* is obtained by linearly extrapolating the values of k_p and k_{NP} to $y = y^*$:

$$k^* = k_p + \frac{y_p - y^*}{y_{NP} - y_p} \left(k_p - k_{NP} \right) \ . \tag{6.31}$$

Based on the assumption of logarithmic velocity profile from turbulent Couette flow, the wall shear stress between the node P and the wall is modified to account for the frictional force at the wall. The modified wall shear stress, in lieu of the normally calculated value, is

$$\tau_w = \frac{\rho k_p^{1/2} \ u_p \ \kappa \ C_\mu^{1/4}}{\ell n \left(\frac{E y_p \ C_\mu^{1/4} \ k_p^{1/2}}{\nu} \right)} \ , \tag{6.32}$$

which is deduced from the velocity profile

$$\frac{u_p}{\tau_w/\rho} \ k_p^{1/2} = C_\mu^{-1/4} \ \frac{1}{\kappa} \ \ell n \left(\frac{E y_p \ C_\mu^{1/4} \ k_p^{1/2}}{\nu} \right) \ . \tag{6.33}$$

The constant E has the value of 9.0 and u_p is the velocity parallel to the wall at node P. The shear stress calculated from Eq. 6.32 is assumed invariant from node P to the wall.

6.9.2 Wall Heat Flux in the Energy Equation

In the energy equation, the heat flux near the wall is modified using a logarithmic temperature profile. The modification for the wall heat flux is similar to that made for the wall shear stress in the momentum equation except that an additional term is introduced to include the resistance of the laminar sublayer. For the case of a laminar Prandtl number $\sigma_{h,\ell am}$ of the order of 1 or greater, the wall heat flux is

$$q_w = \frac{\rho k_p^{1/2} C_\mu^{1/4} (h_w - h_p)}{\frac{1}{\kappa} \ell n \left(\frac{E y_p C_\mu^{1/4} k_p^{1/2}}{\nu} \right) + P_f} , \tag{6.34}$$

where

$$P_f = 9.24 \left(\frac{\sigma_{h,\ell am}}{\sigma_{h,tur}} - 1 \right) \left(\frac{\sigma_{h,tur}}{\sigma_{h,\ell am}} \right)^{1/4} . \tag{6.35}$$

In Eq. 6.34, h is the enthalpy and subscripts w and P represent the values at the wall and node P, respectively. P_f is generally referred to as the P-function and $\sigma_{h,tur}$ is the turbulent Prandtl number for thermal energy transfer, as defined previously.

For the case of a low Prandtl number, such as liquid metal flow where $\sigma_{h,\ell am}$ is on the order of 10^{-2}, the turbulence contribution to the wall heat flux is small. The temperature profile between the wall and node P can be assumed linear.

6.9.3 Turbulence Quantities k and ε Near a Solid Wall

For treatment of the transport equations of k, the diffusive flux from node P to the wall is first set to zero. The production term P_k in the k equation is modified as

$$P_k = \tau_w u_p / y_p ; \tag{6.36}$$

instead of using mean shear, τ_w is the modified wall shear stress computed from Eq. 6.32.

In the transport equation of ε, the dissipation rate at node P is computed as

$$\varepsilon_p = \frac{C_\mu^{3/4} k_p^{3/4}}{\ell} \tag{6.37}$$

instead of solving the transport equation for ϵ. In addition, the average value of ϵ is computed by integrating the nonlinear variation of ϵ for the near-wall cell. Thus,

$$\bar{\epsilon} = \frac{1}{y_e} \int_0^{t_e} \epsilon \, dy$$

$$= \frac{C_\mu^{3/4} \, k_P^{3/2}}{\kappa y_e} \ln \left(\frac{E y_e \, C_\mu^{1/4} \, k_P^{1/2}}{\nu} \right), \qquad (6.38)$$

where y_e is the value at the edge of the control volume of node P as shown in Fig. 6.1. The value of $\bar{\epsilon}$ is used to evaluate the dissipation term in the equation for k for the near-wall cell.

7. VOLUME-WEIGHTED SKEW-UPWIND DIFFERENCE SCHEME

7.1 INTRODUCTION

In fluid-dynamic calculations, the pure-upwind difference scheme is generally preferred over the central-difference scheme to discretize convective terms. The reason is that for high-Peclet number flows, the pure-upwind scheme prevents instability and provides a more accurate solution than that obtained with the central-difference scheme. However, it has been observed that for flows inclined to grid lines, the pure-upwind scheme causes an increased amount of numerical diffusion. To reduce numerical diffusion, we have developed and implemented a volume-weighted skew-upwind difference scheme, which is described in this section.

7.2 PURE-UPWIND DIFFERENCE SCHEME

7.2.1 One-Dimensional

Because of its stabilizing effect, the pure-upwind difference scheme is used extensively in one-dimensional hydrodynamic computer programs[79]. The basic concept is briefly discussed here in reference to Fig. 7.1.

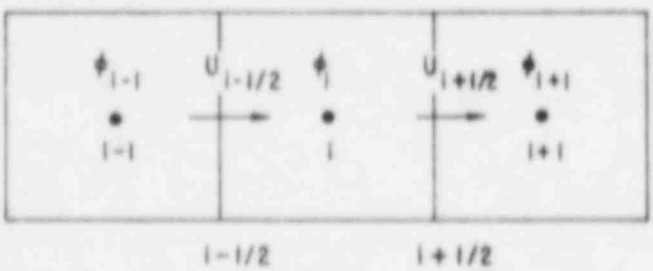

Fig. 7.1 One-Dimensional Upwind or Donor Cell

It is easy to difference the model equation

$$\frac{\partial}{\partial x}(u\phi) = 0 \tag{7.1}$$

at node i, where ϕ is some scalar and u is the velocity. Equation 7.1 can be differenced at center node i as

$$\frac{(u\phi)_{i+1/2} - (u\phi)_{i-1/2}}{\Delta x} = 0 , \tag{7.2}$$

where the subscript i+1/2 refers to the values of $(u\phi)$ at the cell edges. In a staggered mesh system, ϕ and u are not known at the same points. If it is assumed that ϕ is continuous, Eq. 7.2 can be approximated as

$$\frac{(u\phi)_{i+1/2} - (u\phi)_{i-1/2}}{\Delta x} \approx \frac{u_{i+1/2}\,\phi_i - u_{i-1/2}\,\phi_{i-1}}{\Delta x} \tag{7.3a}$$

for the case $u_{i+1/2} > 0$, and

$$= \frac{u_{i+1/2}\phi_{i+1} - u_{i-1/2}\phi_i}{\Delta x} \tag{7.3b}$$

for $u_{i+1/2} < 0$. That is, the values of ϕ are considered "donated" (or upwinded) to the cell edge, depending on the signs of $u_{i+1/2}$.

7.2.2 **Two-Dimensional**

Now consider the two-dimensional situation as shown in Fig. 7.2. The application of the one-dimensional pure-upwind difference scheme to the two-dimensional model equation

$$\frac{\partial}{\partial x}(u\phi) + \frac{\partial}{\partial y}(v\phi) = 0 \tag{7.4}$$

produces

$$\frac{\partial(u\phi)}{\partial x} = \frac{(u\phi)_{i+1/2,j} - (u\phi)_{i-1/2,j}}{\Delta x}$$

$$\approx \frac{(u_{i+1/2,j}\,\phi_{i,j}) - (u_{i-1/2,j}\,\phi_{i-1,j})}{\Delta x} \tag{7.5}$$

and

$$\frac{\partial(v\phi)}{\partial y} = \frac{(v\phi)_{i,j+1/2} - (v\phi)_{i,j-1/2}}{\Delta y}$$

$$\approx \frac{(v_{i,j+1/2}\,\phi_{i,j}) - (v_{i,j-1/2}\,\phi_{i,j-1})}{\Delta y}\,, \tag{7.6}$$

assuming u and v are both positive. This extension assumes that the velocities are locally one-dimensional, i.e., each cell face is associated with only one velocity component, as shown in Fig. 7.2.

7.2.3 **Numerical Diffusion**

This apparently straightforward application of the one-dimensional pure-upwind concept to two and three dimensions has been identified as one of the main sources of numerical diffusion[68-70]. It has been shown that for a steady-state two-dimensional flow with constant velocity components u and v and equal grid sizes $\Delta x = \Delta y = \Delta$, the numerical diffusion coefficient Γ_f resulting from using Eqs. 7.5 and 7.6 in Eq. 7.4 is given approximately by

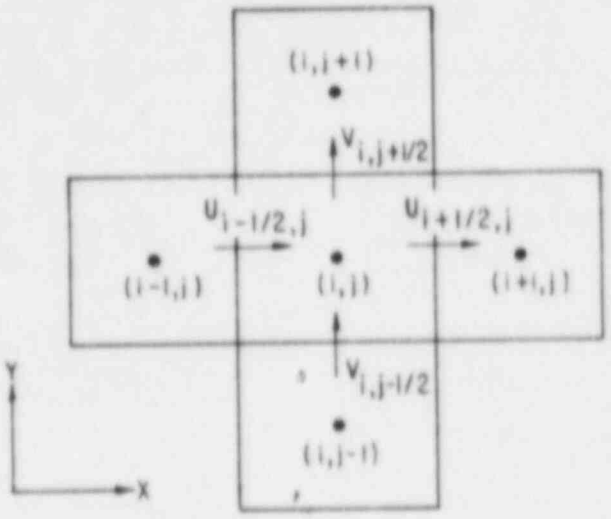

Fig. 7.2. Two-Dimensional Upwind or Donor Cell

$$\Gamma_f = \frac{\sqrt{2}}{4} \sin\left(\frac{\pi}{4} + \theta\right) |\vec{V}| \Delta \sin(2\theta) , \tag{7.7}$$

where

$$\theta = \tan^{-1}\left(\frac{u}{v}\right) . \tag{7.7a}$$

The maximum value of the numerical diffusion coefficient occurs for $\theta = \pi/4$, i.e., $u = v$.

7.3 WHAT IS NUMERICAL DIFFUSION

The term "numerical diffusion" is highly misunderstood among the practitioners of numerical analysis. Accordingly, we get different interpretations from different practitioners.

The concept of numerical diffusion can be described as follows. If we subtract the finite-difference approximation from its partial differential equation in a Taylor series expanded form, the resulting equation is generally termed a "truncation error". Here, we are assuming that a Taylor series expanded form is an accurate representation of the partial differential equation under consideration.

The truncation error usually contains many odd and even derivative terms. The effect of even derivative terms is generally to reduce all gradients in the solution, whether physically correct or artificially induced. This effect, called dissipation, is often looked on as if we have introduced an artificial viscosity. This is why dissipation is often referred to as false, artificial, or numerical diffusion. The odd derivative terms, on the other hand, have a tendency to produce an oscillatory solution. This effect is termed dispersion.

The lowest-order term of the truncation error defines the order of the numerical scheme. In general, if the lowest-order term in the truncation error is an even derivative, than the dissipative error will predominate; if it is an odd derivative, then the dispersive error will predominate.

When we use an upwind-differencing scheme, the lowest-order term in the truncation error is a first-order even derivative of the order $O(\Delta x)$. The effect of upwind differencing is therefore to distort sharp gradients by dissipation, as shown in Fig. 7.3b. In the case of central differencing, the even-derivative term gets cancelled, so the lowest-order term is a second-order odd derivative of the order $O(\Delta x^2)$. The effect of central differencing is therefore dispersive, as shown in Fig. 7.3c.

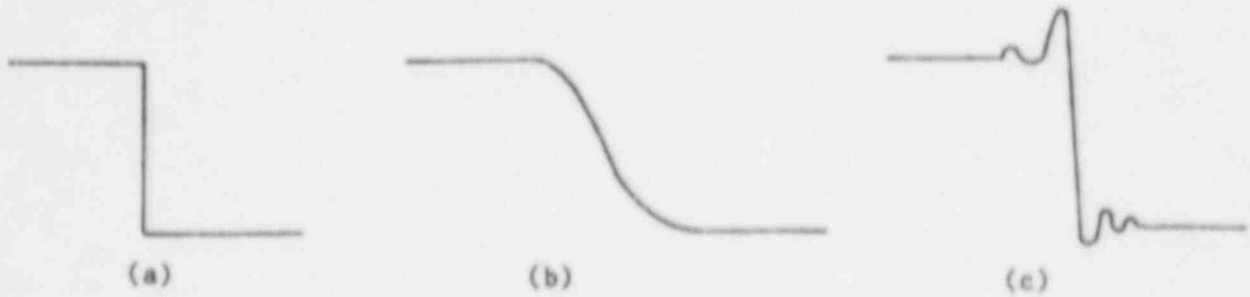

Fig. 7.3. Effects of Dissipation and Dispersion: (a) Exact Solution; (b) Numerical Solution Distorted Primarily by Dissipation Errors (Typical of First-Order Methods); (c) Numerical Solution Distorted Primarily by Dispersion Errors (Typical of Second-Order Methods)

Since a pure-upwind scheme introduces dissipation, we need not consider it as inaccurate or a misrepresentation of reality. On the contrary, for convection diffusion flows parallel to grid lines and at high Peclet number the pure-upwind scheme actually gives a better and more stable solution than that we would obtain from a central-differencing scheme. However, for flows inclined to grid lines, we need modification to reduce numerical diffusion.

7.4 HOW TO REDUCE NUMERICAL DIFFUSION

The apparent ways to reduce numerical diffusion are

- to use very fine mesh and
- to use higher-order finite-difference approximations.

But these procedures are not possible in practice when one is trying to analyze a large, complex, real engineering situation. In addition, it may be very uneconomical to do so.

What is needed is a scheme that is simple to implement, permits the use of coarser mesh for given accuracy, and has acceptable numerical diffusion.

7.5 REVIEW OF AVAILABLE SCHEMES

Numerous methods for reducing numerical diffusion have been proposed in the open literature. We are presenting here our brief review of several of these procedures that we had looked into for implementation in the COMMIX code.

The method of Truncation Error Cancellation (TEC), used by LASL[71], involves adding diffusive terms to make sure that the coefficients of all second-order terms are positive. In the upwind scheme, the coefficients are already positive. Therefore, the procedure requires the use of negative diffusion coefficients. We tried this procedure and found that it decreases the stability of a solution.

The Flux-Corrected Transport (FCT) theory was developed by Boris and Book[72] and extended by Zalesak[73]. As described by Zalesak, the method requires the governing equations to be in conservation law form and computes the net transportive flux as a weighted average of a flux computed by a low-order scheme (e.g., upwind) and a flux computed by a higher-order scheme (e.g., a leapfrog trapezoidal algorithm with fourth-order spatial differences). Filtering is required to suppress overshoots and undershoots ("wiggles"). The procedure is a very high-order scheme and its implementation in COMMIX would require major code modifications. Furthermore, the procedure would become computationally more expensive.

The use of the Asymmetric Weighted Residual method, as propounded by Romstedt and Werner[74], was not considered because it would require substantial modification of COMMIX, it is an untried technique for multidimensional fluid-flow problems, and is inappropriate for a COMMIX-type code.

R. G. Steinke[75] describes the use of a step function rather than a flat shape in the pure-upwind scheme. This approach does not address numerical diffusion due to cross-flow; instead, it is concerned only with numerical diffusion due to pure-upwind differencing.

A nonlinear fitting technique (FRAM) presented by Chapman[76] is for multidimensional homogeneous equations in conservative form. The basic idea is to use a higher-order scheme and then locally introduce artificial diffusion when spurious oscillations appear. The technique seems to offer several advantages over FCT. In particular, the high-order scheme can be like Crowley's[77,78], which is akin to central differences. Thus, the basic scheme would be a nine-point scheme in two dimensions and a 27-point scheme in three dimensions. Also, artifical diffusion is introduced locally rather than globally, as in FCT. The modification can be moderate in scope. We wanted to see if we could find a simpler alternative.

A skew-upwind difference (SUD) scheme is described by Raithby[68] and Lillington[79]. In this approach, one applies upwind difference in the stream direction and uses a linear variation differencing in the cross-stream direction. This technique addresses the problem of numerical diffusion due to cross-flow gradients in the pure-upwind scheme. In two dimensions, this scheme leads to, at most, a nine-point formula.

7.6 SELECTION OF A SCHEME

After reviewing the alternatives described, we decided to do the following:

1. Extend Raithby's two-dimensional SUD scheme to three dimensions,

2. Develop the VWSUD scheme, and

3. Implement both these schemes (SUD and VWSUD) into the energy equation in COMMIX-1B.

The following were our important considerations for the development of the VWSUD scheme.

- As mentioned earlier, our objective was to develop a scheme that is simple to implement, computationally efficient, and displays acceptable numerical diffusion for flows oblique to the computational grids.

- The pure-upwind scheme is simple. It is based on the assumption that for a steady-state convection-dominated flow, the variation of property value in the streamwise direction is very small. This is a valid assumption. A major deficiency of the pure-upwind scheme is that it produces numerical diffusion when a flow is inclined to the computational grid lines.

- The skew-upwind scheme, an extension of the pure-upwind scheme, reduces the deficiency of the pure-upwind scheme. But SUD has two other problems: it predicts results that may overshoot or undershoot, and it requires an arbitrary cutoff value during linear interpolation.

We therefore developed a scheme called the volume-weighted skew-upwind difference (VWSUD) scheme, which is a modification of the SUD scheme. It eliminates the two problems of the SUD scheme. It approximates the property value at the surface of a computational cell using the volumes of two upstream cells as weighting factors.

We have implemented the VWSUD scheme in COMMIX-1B only in the energy equation and not in the momentum equation for the following reasons:

- All our analyses have shown that the numerical diffusion due to pure-upwind approximation is mainly through the energy equation and not through the momentum equation.

- The analysis of Hassan et al[78] has shown that increasing the order of approximation (from pure-upwind to central difference) in the momentum equation, in general, does not make any appreciable difference in the velocity field.

So that a reader can clearly understand the VWSUD scheme, we have included Raithby's skew-upwind difference (SUD) scheme as background information before describing the alternative volume-weighted skew-upwind difference (VWSUD) scheme.

7.7 RAITHBY'S TWO-DIMENSIONAL SKEW-UPWIND DIFFERENCE (SUD) SCHEME

Raithby[68] developed what is called the skew-upwind difference (SUD) scheme applicable to a two-dimensional flow field. It is based on the assumption that in a small domain surrounding the center of a cell surface, a scalar property function ϕ (e.g., density, temperature, etc.) is continuous, linearly varying and constant along a streamline.

Mathematically,

$$\frac{d\phi}{d\psi} = 0 \ . \tag{7.8}$$

Here, $d/d\psi$ is the directive derivative along the stream direction ψ. Let us consider the west face of node (i,j), as shown in Fig. 7.4.

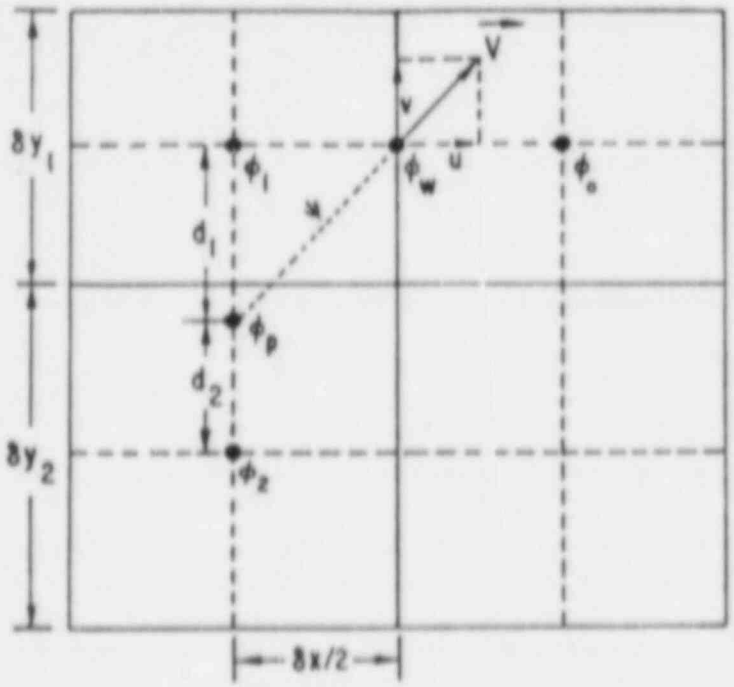

Fig. 7.4. Two-Dimensional Skew-Upwind Differencing Scheme

We denote, for clarity,

$$\phi_o = \phi_{i,j},$$

$$\phi_w = \phi_{i-1/2,j},$$

$$\phi_1 = \phi_{i-1,j}, \text{ and}$$

$$\phi_2 = \phi_{i-1,j-1} \ . \tag{7.9}$$

Equation 7.8 implies that

$$\phi_w = \phi_p \ , \tag{7.10}$$

where ϕ_p is the value of ϕ at the point of intersection between the projection of the velocity vector $\vec{V}$ and the vertical line connecting ϕ_1 and ϕ_2. The property value ϕ_p in turn can be evaluated from the values ϕ_1 and ϕ_2, using simple linear interpolation, as

$$\phi_w = \phi_p = \left(\frac{\delta y - d_1}{\delta y}\right)\phi_1 + \left(\frac{\delta y - d_2}{\delta y}\right)\phi_2 \ , \tag{7.11}$$

where

$$\delta y = (\delta y_1 + \delta y_2)/2 \tag{7.11a}$$

and δy_1 and δy_2 are the cell heights. The lengths d_1 and d_2 are determined from

$$d_1 = \left|\frac{v}{u}\right| (\delta x/2) \tag{7.12}$$

and

$$d_2 = \delta y - d_1 \ . \tag{7.12a}$$

Here u and v are the components of the velocity vector $\vec{V}$, considered centered at the middle of the west face, and δx is the grid width for the cell containing ϕ_1 (or ϕ_2). When d_1 is greater than δ_y, then d_1 is set equal to δ_y and d_2 is set equal to zero, and vice versa for the case of d_2 greater than δ_y. These are Raithby's artificial cutoffs to prevent the possibility of negative coefficients in the interpolation formula given by Eq. 7.11. Equation 7.11 can be rewritten as

$$\phi_w = \phi_p = \left(1 - \frac{1}{2}\frac{\delta x}{\delta y}\left|\frac{v}{u}\right|\right)\phi_1 + \left(\frac{1}{2}\frac{\delta x}{\delta y}\left|\frac{v}{u}\right|\right)\phi_2 \ . \tag{7.13}$$

This is the same as Raithby's results for both u and v positive. Thus, Raithby's SUD scheme is a method to replace ϕ_w by a linear interpolation between ϕ_1 and ϕ_2 using velocity components u and v. The flux on the west face is then computed in the usual manner as

$$F_w = \phi_w \delta y_1 \, u \ . \tag{7.14}$$

One benefit of the method is reduction in the numerical diffusion in the direction normal to the stream direction introduced by the indiscriminate extension of the one-dimensional pure-upwind difference scheme to two and three dimensions. The method does not address the problem of numerical diffusion that persists in that direction; neither does it address numerical diffusion resulting from time-dependent terms.

The interpretation of the method as an interpolation procedure for ϕ_w allows easy implementation in our existing COMMIX computer code without major reprogramming.

In the following section, we explain the extension of the method to the three-dimensional situation.

7.8 EXTENSION OF RAITHBY'S 2D-SUD SCHEME

The approach employed in Sec. 7.7 to derive the skew-upwind difference (SUD) scheme in a two-dimensional flow field is simple and straightforward. All the terms involved in Eq. 7.11 can be interpreted with physical and geometrical meanings. The same approach is used to derive the three-dimensional skew-upwind difference scheme shown in Fig. 7.5. To illustrate the configuration easily and without losing generality, we will assume that the velocity components u, v, and w of $\vec{V}$, passing through the center of the north face (+y) of the cell containing ϕ_0 (Fig. 7.5), are all positive.

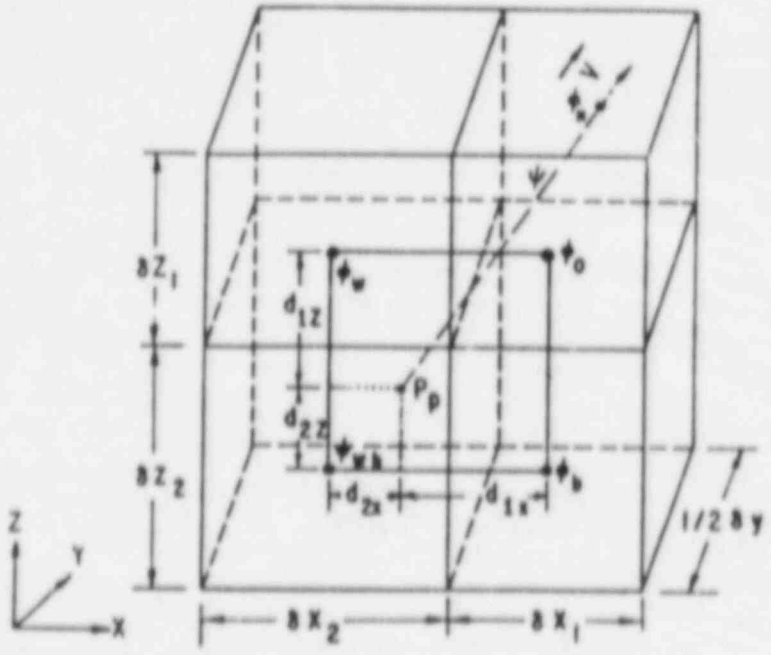

Fig. 7.5. Three-Dimensional Skew-Upwind Differencing Scheme

The three-dimensional model equation under consideration is given by

$$\frac{\partial}{\partial x}(u\phi) + \frac{\partial}{\partial y}(v\phi) + \frac{\partial}{\partial z}(w\phi) = 0 \ . \qquad (7.15)$$

Equation 7.15 can also be written as Eq. 7.8 and the same considerations described in Sec. 7.7 are then directly extended to three dimensions.

The location of point P_p is the intersection of the projection of velocity $\vec{V}$ with the plane containing the scalar values ϕ_0, ϕ_w, ϕ_{wb}, and ϕ_b. The length of d_{lz} and d_{lx} can be derived easily from Fig. 7.5 as

$$d_{lz} = \frac{w}{v}(\delta y/2) \tag{7.16}$$

and

$$d_{lx} = \frac{u}{v}(\delta y/2) \ . \tag{7.17}$$

If the center of the north face (+y) of the cell containing ϕ_0 is considered to be the origin of the local coordinate system, then the coordinates of point P_p can be written as

$$(P_p)_{local} = P_p(-d_{lx},\ -\delta y/2,\ -d_{lz}) \ . \tag{7.18}$$

We define the interpolation coefficients as

$$\alpha_z = \left(\frac{\delta z - |d_{lz}|}{\delta z}\right) \qquad \text{if } \delta z > |d_{lz}| \ , \tag{7.19}$$

$$\alpha_z = 0 \qquad \text{otherwise} \ ,$$

and

$$\alpha_x = \left(\frac{\delta x - |d_{lx}|}{\delta x}\right) \qquad \text{if } \delta x > |d_{lx}| \ , \tag{7.20}$$

$$\alpha_x = 0 \qquad \text{otherwise} \ ,$$

where

$$\delta z = \frac{1}{2}(\delta z_1 + \delta z_2) \tag{7.20a}$$

and

$$\delta x = \frac{1}{2}(\delta x_1 + \delta x_2) \ . \tag{7.20b}$$

Therefore, the intensive property ϕ_N defined on the north face of the cell containing ϕ_0 can be simply written, analogous to the two-dimensional case given by Eq. 7.11, as

$$\phi_N = \phi_p = (\alpha_z\,\alpha_x)\,\phi_0 + [(1-\alpha_z)\alpha_x]\,\phi_w + [\alpha_z\,(1-\alpha_x)]\,\phi_b$$

$$+ [(1-\alpha_z)\,(1-\alpha_x)]\,\phi_{wb} \ . \tag{7.21}$$

7.9 VOLUME-WEIGHTED SKEW-UPWIND DIFFERENCING (VWSUD) SCHEME

In this section, we describe the volume-weighted skew-upwind difference (VWSUD) scheme, which overcomes some of the deficiencies of the skew-upwind difference (SUD) scheme.

7.9.1 Two-Dimensional Volume-Weighted Skew-Upwind Difference (VWSUD) Scheme

As discussed in the preceding sections, the only assumption made to derive the SUD scheme is

$$\frac{d\phi}{d\psi} = 0 \tag{7.22}$$

and the only conclusive implication from this assumption in two or three dimensions (shown in Figs. 7.4 and 7.5) is that

$$\phi_w = \phi_p \ . \tag{7.23}$$

Nevertheless, the expression of ϕ_p in terms of ϕ_1 and ϕ_2 in Eq. 7.2, or ϕ_o, ϕ_w, ϕ_b, ϕ_{wb} in Eq. 7.21, is straightforward but not necessarily unique.

In some cases, the interpolation may result in significant undershoots or overshoots. For the case of highly angled flow, shown in Fig. 7.6, the projected point P_p falls outside of the line connecting ϕ_1 and ϕ_2.

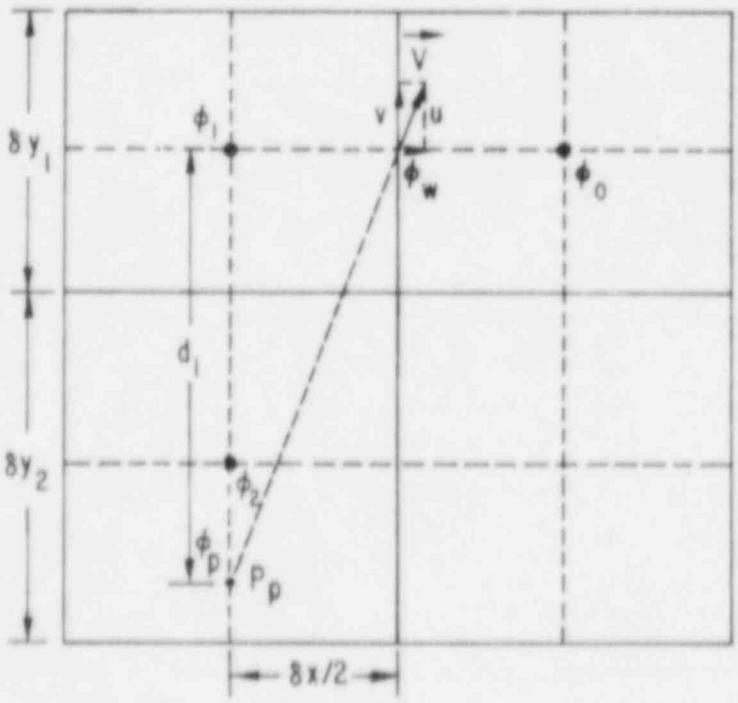

Fig. 7.6. Deficiency of Skew-Upwind Differencing Scheme

To avoid the extrapolation, which may result in gross errors[68], we can simplify Eq. 7.11 using the cutoff

$$\phi_w = \phi_p = \phi_2 \ . \tag{7.24}$$

However, based on physical intuition, the intensive property of the flow passing the west face of the cell containing ϕ_o should involve both ϕ_2 and ϕ_1.

To correct this situation, we consider the volume of flow passing through the west face of the cell containing ϕ_0, as shown in Fig. 7.7. The volume of flow passing through the west face originating from the portion of the control volume containing ϕ_1 is $A_1 h$, where h is the unit depth of the flow. The remainder of the flow that passes through the west face originating from the control volume containing ϕ_2 is given by $A_2 h$. Therefore, the average of the intensive property associated with the volume of the flow passing through the west face can be expressed as

$$\phi_w = \phi_p = \frac{A_1}{A_1 + A_2} \phi_1 + \frac{A_2}{A_1 + A_2} \phi_2 \ . \tag{7.25}$$

Since the coefficients in Eq. 7.25 are always between 0 and 1, there is no need for any artificial cutoffs in the VWSUD scheme.

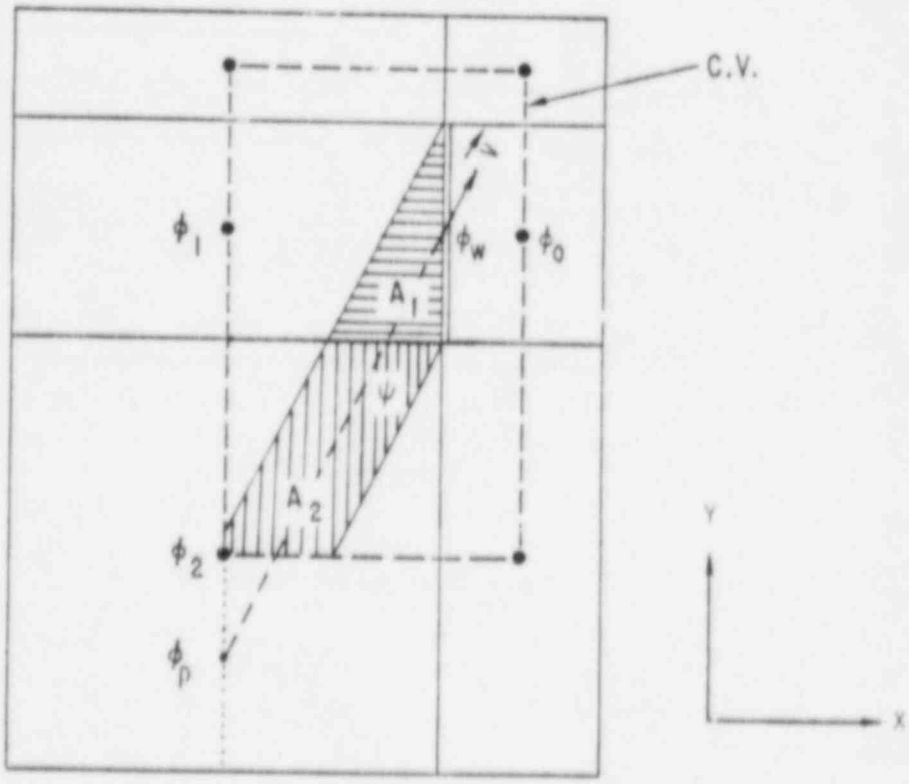

Fig. 7.7. Concept of Volume-Weighted Skew-Upwind Scheme

7.10 EXTENSION OF 2D-VWSUD TO THREE-DIMENSION

The extension of the two-dimensional VWSUD scheme to three dimensions is quite straightforward but difficult to visualize. As shown in Fig. 7.8, the projection line τ of the vector $\vec{V}$ that passes through the north face (+y) of the cell containing ϕ_0 may result in the formation of subvolumes inside the surrounding cells. To simplify the representation, we number the cells 1 through 4 counterclockwise, starting with the cell containing ϕ_0, as shown in Fig. 7.8. Detailed configurations of the constituent subvolumes resulting from the projection line τ are shown in Figs. 7.9 through 7.12.

The extension of Eq. 7.25 to three-dimensional flow field can be written as

$$\phi_N = \phi_p = \left(\frac{V_1}{V_{tot}}\right)\phi_1 + \left(\frac{V_2}{V_{tot}}\right)\phi_2 + \left(\frac{V_3}{V_{tot}}\right)\phi_3 + \left(\frac{V_4}{V_{tot}}\right)\phi_4 , \qquad (7.26)$$

where

$$V_{tot} = V_1 + V_2 + V_3 + V_4 \qquad (7.26a)$$

and V_1, V_2, V_3, and V_4 are the volumes as shown in Fig. 7.8.

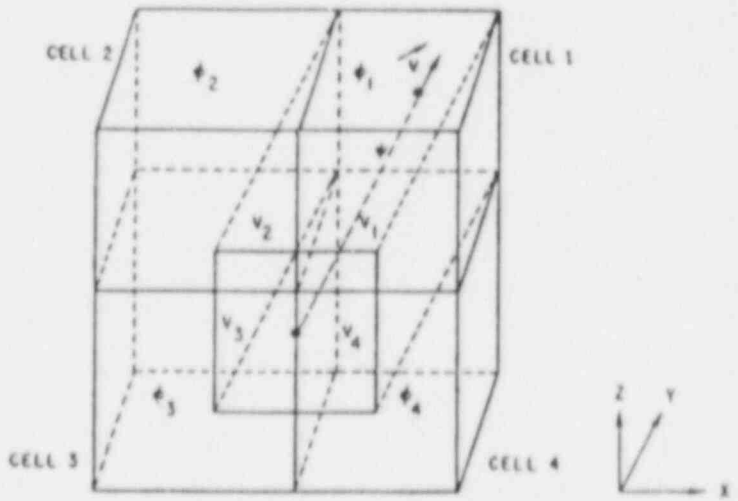

Fig. 7.8. Three-dimensional Volume-Weighted Differencing Scheme

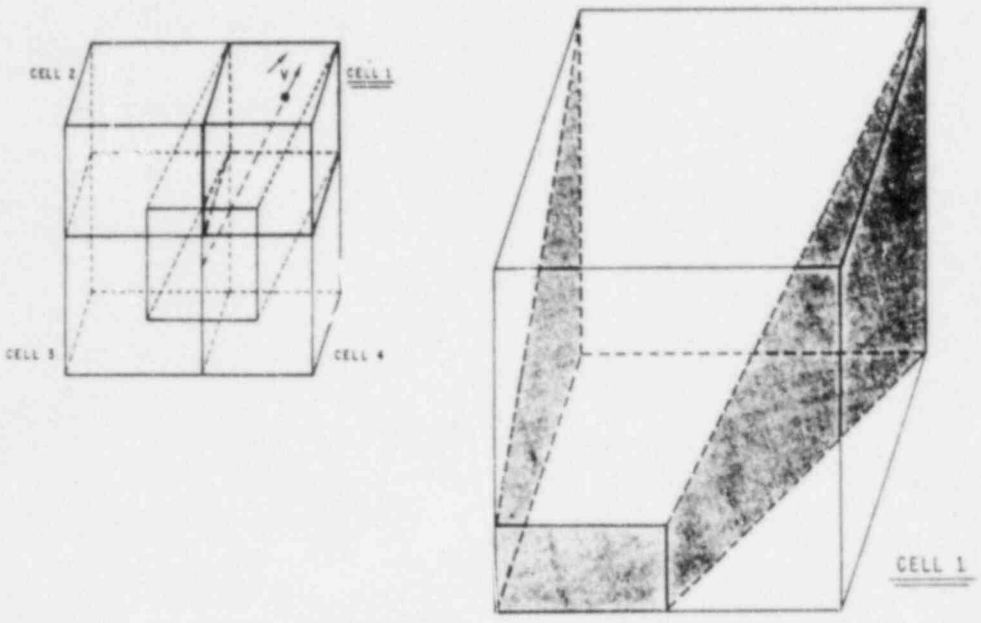

Fig. 7.9. Projected Element in Cell 1

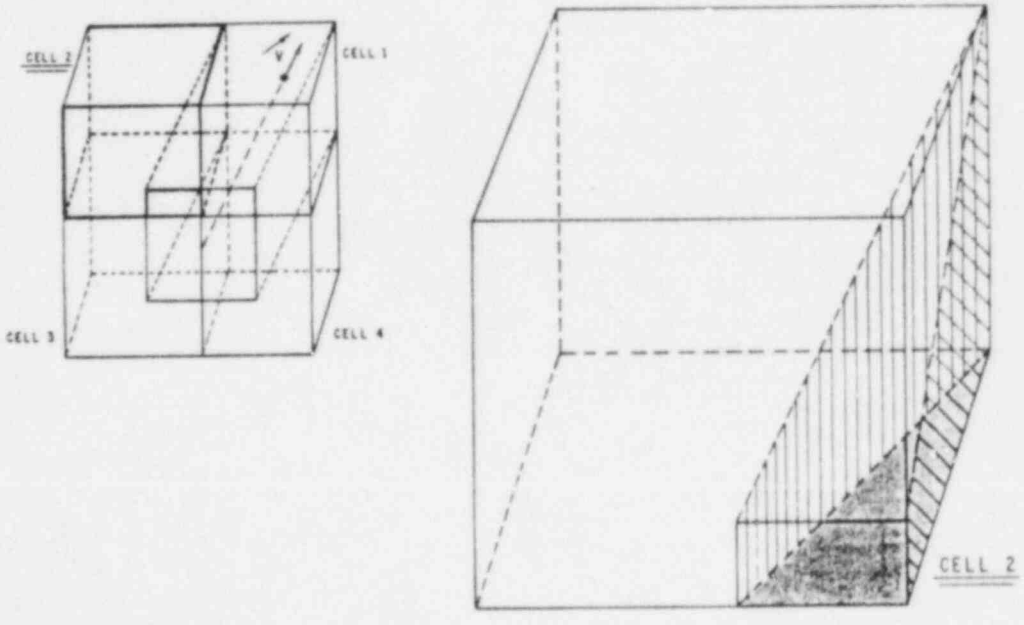

Fig. 7.10. Projected Element in Cell 2

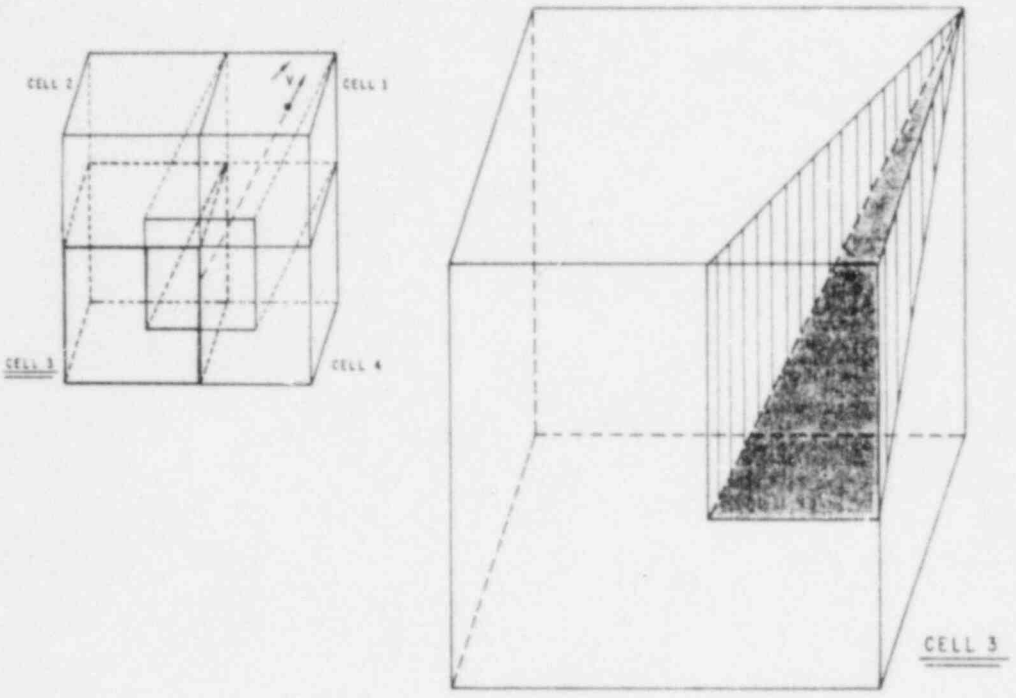

Fig. 7.11. Projected Element in Cell 3

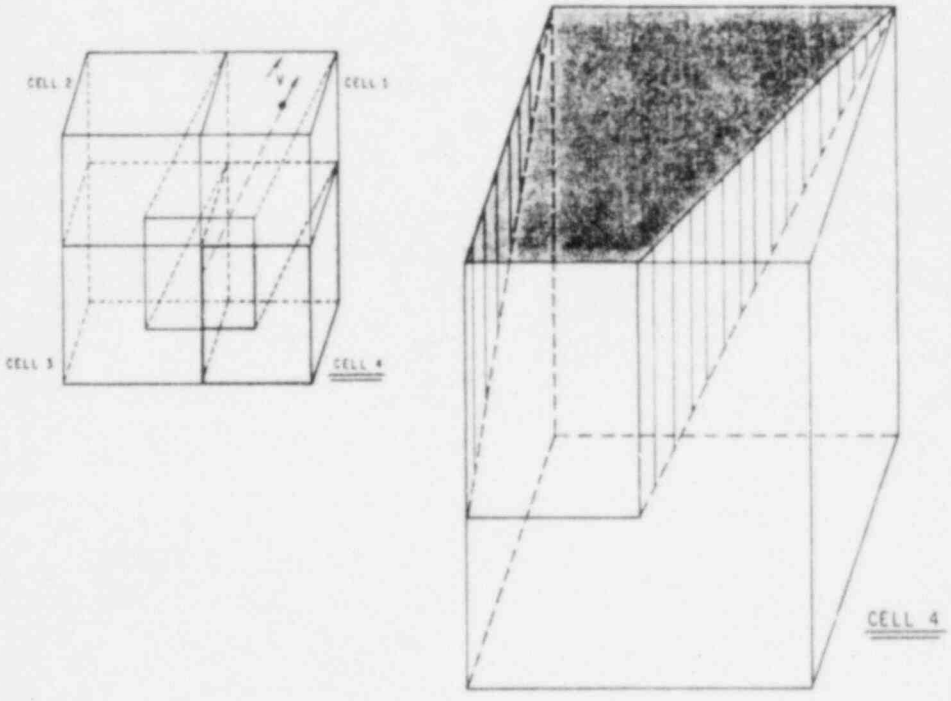

Fig. 7.12. Projected Element in Cell 4

7.11 REMARKS ON THE SUD AND VWSUD SCHEMES

The SUD and VWSUD schemes have been implemented in the energy equation of COMMIX-1B. These schemes have been tested by performing several multidimensional steady-state and transient simulations of thermal-mixing benchmark problems and two thermal mixing experiments. We have observed the following:

- The SUD scheme can significantly reduce numerical diffusion for steady-state thermal mixing problems with flow oblique to grid lines. However, significant undershoots and overshoots occur and appear greater in three dimensions than in two dimensions.

- The SUD scheme appears less stable than the VWSUD scheme and may require high underrelaxation.

- For the same mesh size, the computer running time for the SUD and VWSUD schemes are larger than that for the pure-upwind scheme, but numerical diffusion is less. So there is a price to be paid for reducing numerical diffusion. The additional running time is highly problem-dependent.

Overall, the VWSUD scheme

- is numerically stable (the stability analysis is presented in Appendix A),

- has the same order of accuracy as the SUD scheme, but eliminates all of the undershoots and overshoots (computational values below and above the limits of physically allowable values) observed in the SUD scheme in this study,

- retains the simplicity of the SUD scheme without resorting to artificial cutoffs needed in the SUD scheme; this advantage is crucial in many thermal-hydraulic applications,

- significantly reduces the numerical diffusion for steady-state and transient thermal mixing with flow oblique to computational grids--hence, the VWSUD scheme permits more realistic analysis of thermal mixing to help resolve many critical engineering problems such as the pressurized thermal shock issue, and

- permits use of a coarser mesh than with pure-upwind and still provides results that are of the same order of accuracy, saving significant computer running time by a factor of 4 to 8.

8. HEXAGONAL FUEL ASSEMBLY

In the initial COMMIX development period, major emphasis was on the analysis of hexagonal fuel assemblies. Consequently, several features and models have been implemented in COMMIX that are specifically for hexagonal fuel assemblies. These are described briefly in this section.

8.1 HEX-GEOMETRY OPTION

The hex-geometry option is available in COMMIX-1B for the calculation of all required geometrical parameters for hexagonal fuel assemblies. The subroutines for this option have been developed so that a minimum amount of information is required as input, relieving the user from the tedious work of preparing geometrical data. The user has to provide only the following input data:

Pins	Number of pins, pin diameter, distance between pin centers, and clearance between pin and wall.
Wire wrap	Diameter of wires next to wall, diameter of wires away from wall, and type of wire wrap option desired (see Sec. 8.3).
Partitioning	Number of axial partitions, size of each axial partition, and type of cross-sectional partitioning (see Figs. 8.1 and 8.2).

With this minimum information, the code calculates all required geometrical parameters--grid sizes in x and y directions, directional surface porosities, volume porosities, wetted perimeters, hydraulic diameters, surface areas, etc.

During calculation of all of the parameters, we have assumed that

- Axial length is along the z direction,
- One flat surface of the hex assembly lies on the x axis, and
- Eight surfaces of the hex assembly have the following locations:

Surface No.	Location
1	Lower left diagonal in x-y plane
2	Upper left diagonal in x-y plane
3	Lower right diagonal in x-y plane
4	Upper right diagonal in x-y plane
5	Lower flat along x axis
6	Upper flat parallel to x axis
7	Entrance; z = 0 plane
8	Exit plane normal to z axis

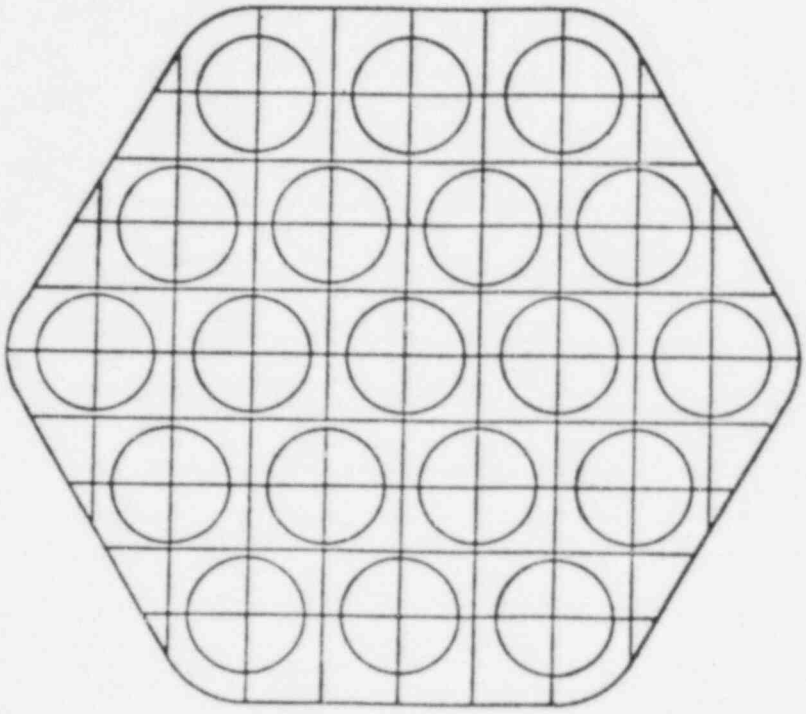

Fig. 8.1. Quarter-Pin Partitioning of 19-Pin Fuel Assembly in Hexagonal Duct

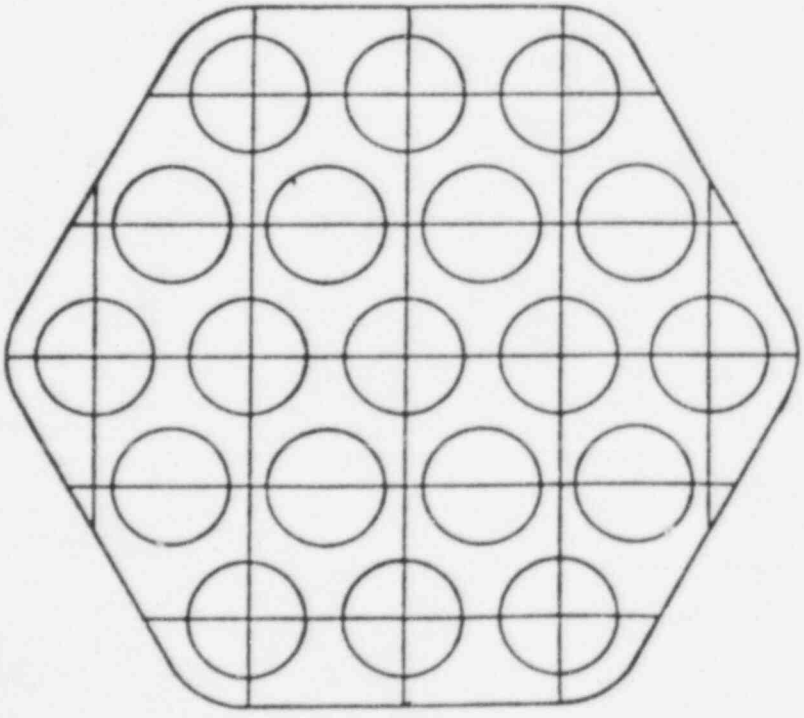

Fig. 8.2. Single-Pin Partitioning of 19-Pin Fuel Assembly in Hexagonal Duct

We have designed this option with two types of cross-sectional partitioning:

- Quarter-pin and
- Full-pin.

To illustrate the differences, a quarter-pin partitioning and a full-pin partitioning of a 19-pin hexagonal fuel assembly are shown in Figs. 8.1 and 8.2.

The hex-geometry option can also be used even if the hexagonal fuel assembly under analysis has some deviations from a regular hex-geometry, and contains some internal structures, e.g., blockage, that affect the values of volume porosity and directional surface porosities. The only difference is that the user now has to input the values of volume porosity and directional surface porosities that are different from a regular geometry. The user-prescribed values in the internal-cell-initialization cards override the code-calculated values.

If the hex-geometry is very irregular, e.g., different fuel-pin diameters, nonuniform spacing with different pitches, etc., then the user may bypass the hex-geometry option and use the normal box-geometry option. Of course, with the box-geometry option the user has to provide all the required geometrical details.

8.2 WIRE WRAP MODEL

8.2.1 Introduction

The presence of helical wire wrapping around a fuel pin has two effects on fluid flow.

- The geometrical effect, where the presence of wire wrap influences the fluid flow by reducing the available flow space (this effect is accounted for by modifying the volume porosities and directional surface porosities), and
- The physical effect, where the presence of wire produces additional drag on the fluid flow (this effect is accounted for by including additional resistance terms in the momentum equation).

In this model, we have provided two options. They are described here.

8.2.2 Smeared Wire Option

In this option, the volume porosities and directional surface porosities are modified uniformly across the section. This is done by distributing total wire volume equally over all cells and total wire-wrap cross-sectional area equally over all cells in each axial plane. Physical effects are neglected.

8.2.3 Cell Integrated Option

8.2.3.1 Geometrical Effects

The geometrical effects due to the presence of wire wrap are accounted for by modifying volume porosities and directional surface porosities. This is done using the relations

$$\gamma_v^w = \gamma_v - \frac{1}{(\Delta x \Delta y \Delta z)} \int_{z_1}^{z_2} A_z^w \, \delta z \ , \tag{8.1}$$

$$\gamma_{x,i+1/2}^w = \gamma_{x,i+1/2} - \frac{1}{(\Delta y \Delta z)} \int_{z_1}^{z_2} \delta A_{x,i+1/2}^w \ , \tag{8.2}$$

$$\gamma_{y,j+1/2}^w = \gamma_{y,j+1/2} - \frac{1}{(\Delta x \Delta z)} \int_{z_1}^{z_2} \delta A_{y,j+1/2}^w \ , \tag{8.3}$$

and

$$\gamma_{z,k+1/2}^w = \gamma_{z,k+1/2} - \frac{A_{z,k+1/2}^w}{(\Delta x \Delta y)} \ , \tag{8.4}$$

where the superscript w refers to the wire wrap and A is the cross-sectional area of the wire wrap. The right sides of Eqs. 8.1-8.3 are integrated numerically. At each axial position, A^w is computed by determining its proper location in a cell. The step size for numerical integration is taken to be equal to three degrees of angular rotation, i.e.,

$$\delta z = \frac{\text{wire pitch}}{120} \ . \tag{8.5}$$

8.2.3.2 Wire Drag Effect

The resistance force due to the wire wrap is modeled as

$$\vec{F}_w = \frac{C \rho |w| w \vec{A}}{(\Delta x \Delta y \Delta z)} \ , \tag{8.6}$$

where

$$\vec{F}_w = f_x \vec{i} + f_y \vec{j} + f_z \vec{k} \tag{8.7}$$

is the resistance force per unit volume, C is the drag coefficient, and

$$\vec{A} = A_x\vec{i} + A_y\vec{j} + A_z\vec{k} \tag{8.8}$$

is the projected area of the wire wrap. The calculation of $\vec{A}$ is briefly described here.

Figure 8.3 shows a typical wire wrap arrangement. Consider the wire wrap as a spiral ring of width d_w attached to the fuel pin and located at position S(x,y,z) as shown in Fig. 8.4. The projected area is

$$\begin{aligned} d\vec{A} &= d\vec{S} \times d_w\vec{n} \\ &= (dx\vec{i} + dy\vec{j} + dz\vec{k}) \times d_w(\vec{i}\cos\alpha + \vec{j}\sin\alpha) , \end{aligned} \tag{8.9}$$

where

$$\vec{n} = \vec{i}\cos\alpha + \vec{j}\sin\alpha \tag{8.10}$$

is the unit normal vector,

$$\begin{aligned} \vec{S} &= (x\vec{i} + y\vec{j} + z\vec{k}) \\ &= \vec{i}r_p\cos\alpha + \vec{j}r_p\sin\alpha + \vec{k}\left(z_0 + \frac{\alpha}{2\pi}P_w\right) \end{aligned} \tag{8.11}$$

is the wire wrap position vector,

$$d\vec{s} = \left[\vec{i}\left(-r_p\sin\alpha\right) + \vec{j}\,r_p\cos\alpha + \vec{k}\,\frac{P_w}{2\pi}\right]d\alpha \tag{8.12}$$

is the change in the wire wrap position vector, r_p is the radius of fuel pin, and P_w is the wire pitch. Substituting Eq. 8.12 into Eq. 8.9, we obtain, after simplification,

$$d\vec{A} = \frac{P_w d_w}{2\pi}\left[\vec{i}(-\sin\alpha) + \vec{j}\cos\alpha - \vec{k}\tan\theta\right]d\alpha , \tag{8.13}$$

where

$$\theta = \tan^{-1}\left(\frac{2\pi r_p}{P_w}\right) \tag{8.14}$$

is the angle between the wire wrap centerline and the fuel pin centerline. Integrating Eq. 8.13 between two z planes [k-1/2 and k+1/2] for a given cell, we obtain

$$\vec{A} = \frac{P_w d_w}{2\pi}\left[\vec{i}(\cos\alpha_2 - \cos\alpha_1) + \vec{j}(\sin\alpha_2 - \sin\alpha_1) - \vec{k}(\alpha_2 - \alpha_1)\tan\theta\right] , \tag{8.15}$$

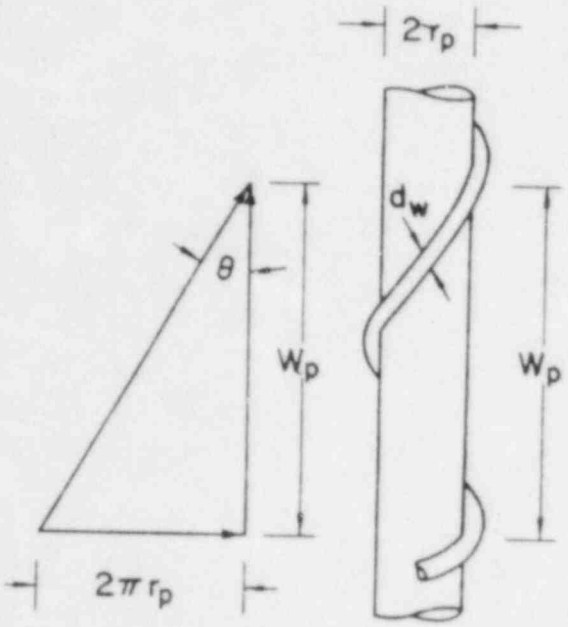

Fig. 8.3. Typical Wire Wrap Arrangement

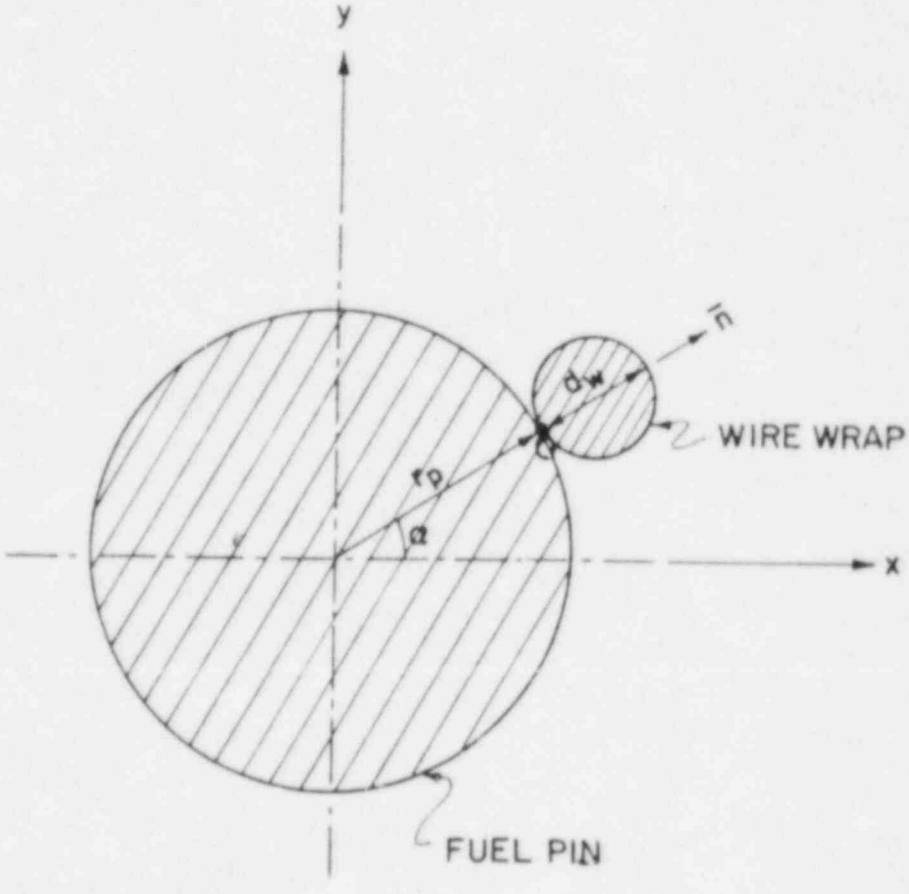

Fig. 8.4 Cross-Section of a Helical Wire Wrap around a Fuel Pin

where

$$\alpha = \frac{2\pi\left(z - z_o\right)}{P_w} , \tag{8.16}$$

$$\alpha_2 - \alpha_1 = \frac{2\pi}{P_w}\left[z_{k+1/2} - z_{k-1/2}\right] , \tag{8.17}$$

and z_0 is the axial location when the wire wrap position is on the x axis passing through the centerline of a fuel pin.

8.3 FUEL PIN RESISTANCE

We model the distributed resistance forces R_x, R_y, and R_z (defined in Table 2.1) due to fuel pins in the following way:

$$R_x = \frac{1}{\gamma_v}\frac{1}{2} f_x \rho u^2 , \tag{8.18}$$

where R is the distributed resistance force per unit volume, f is the friction factor per unit length, and the subscript x refers to the x direction.

When a rod bundle is aligned along the z axis, the cross-flow friction factor f_x is given by[62]

$$f_x = 2\frac{u}{|u|}\bar{f}_x \frac{\gamma_v^2 W_p}{1 - \left(\frac{d}{P_y}\right)^2} , \tag{8.19}$$

where

W_p = the wetted perimeter per unit cross-sectional area ,

d = the rod diameter ,

P_y = the pitch in the y direction ,

and

$\bar{f}_x$ = the largest of the following three expressions:

$$\bar{f}_x = 3Re_x^{-1}\left(\frac{P_y - d}{P_y - 0.93d}\right)^2 , \tag{8.20}$$

$$\bar{f}_x = 0.6\frac{P_y}{d}\left[0.25 + \frac{0.118}{\left(P_y/d - 1\right)^{1.08}}\right]Re_x^{*-0.15} , \tag{8.21}$$

and

$$\bar{f}_x = 3\left(\frac{P_y - d}{P_y - 0.93d}\right)^2 \left[\frac{\mu}{\mu_{eff}} Re_x \left(1 + \frac{2.16d}{P_y - d}\right)\right]^{-1} . \qquad (8.22)$$

In these expressions,

$$Re_x = \frac{\rho |u| P_y \gamma_v}{\mu} \qquad (8.23)$$

and

$$Re_x^* = \frac{\rho |u| d\gamma_v}{\mu(1 - d/P_y)} . \qquad (8.24)$$

Analogous expressions are used for f_y, replacing u with v, P_y with P_x, and Re_x with Re_y in the above definitions.

The axial friction factor f_z is given by

$$f_z = 2 \frac{w}{|w|} W_p\left(aRe_z^b + c\right) , \qquad (8.25)$$

where

$$Re_z = \frac{\rho |w| D_h}{\mu} , \qquad (8.26)$$

D_h = the equivalent hydraulic diameter ,

and the constants a, b, and c are:

a	b	c	Re_z
8	-1	0	< 940
0.07	-0.32	0.0007	> 940

8.4 OTHER FEATURES

8.4.1 Heat Source

To provide an easy input of heat source from the fuel pins, three variables have been introduced in COMMIX: QIN, QK, and QFLUX. The variables QIN and QK are the normalized power distribution functions in a transverse plane and in an axial direction, respectively. QFLUX is an average heat source per unit area of fuel pin. With these three variables prescribed, the code calculates the heat source in a cell using the relation

$$Q(i,j,k) = QIN(i,j) * QK(k) * (\pi d \Delta Z)\ PINF * QFLUX * f_{nf}(t) , \qquad (8.27)$$

where PINF is the fraction of a pin in the cell under consideration, ($\pi d\Delta Z$) is the pin surface area, f is the transient function to account for the variation of heat source with time, and the subscript nf is the transient function number.

Equation 8.27 assumes that all axial planes have the same normalized power distribution QIN, and all vertical axes (cells with same (i,j) locations) have the same normalized power distribution QK.

Note that the power Q, calculated in Eq. 8.27, is added to the heat source term in the fluid-energy equation. Thermal inertia of fuel pins is not accounted for in this calculation. The use of the easy heat source input described here is therefore recommended only for

- Steady-state analysis and
- Slow transients.

For fast transients, it is recommended that fuel pins be considered as thermal structures (described in Sec. 9).

When we have nonuniform heat source distributions in all three directions, there are two other alternatives:

- Prescribe a volumetric heat source for each cell through a variable QSOUR, or
- Treat fuel pins as thermal structures and prescribe a heat source through thermal structure input.

8.4.2 Pressure-Boundary Conditions

Most simulations need a velocity boundary at the inlet and a pressure boundary at the exit. However, we may have situations needing pressure boundaries at both ends, inlet and exit. This additional capability of simulating with pressure-boundary conditions at both ends has been implemented and tested for hexagonal fuel assembly cases.

9. SUPPLEMENTARY PHYSICAL MODELS

To broaden the scope of COMMIX-1B applications and to more accurately account for phenomena that affect thermal-hydraulic simulation, a number of supplementary physical models have been incorporated into COMMIX-1B.

9.1 SIMPLIFIED FLUID PROPERTY OPTION

There are two fluid property packages in COMMIX, one for liquid sodium and one for water. Nominally, COMMIX makes use of the sodium property package. Use of the water property package requires the creation of a separate load module. Both property packages are developed and formulated in a modular fashion to accomodate replacement by any other fluid property package. The details of the two property packages and procedures for creation of the load module are given in Volume II.

Besides the two fluid property packages, another option is available to the COMMIX user. This option is known as a simplified property option. This option, when in force, automatically disconnects the sodium property package and calculates properties as specified by the user. Enthalpy, density, thermal conductivity, and viscosity are all assumed to be functions of only temperature, and are all assumed to have the functional forms

$$h = C_{0h} + C_{1h}T \ ,$$

$$\rho = C_{0\rho} + C_{1\rho}T \ ,$$

$$k = C_{0k} + C_{1k}T \ ,$$

and

$$\mu = C_{0\mu} + C_{1\mu}T \ . \qquad (9.1)$$

Here, C_0 and C_1 are constant coefficients and are required as input.

9.2 OTHER MATERIAL PROPERTIES

In many real applications, solid boundaries and immersed solid objects affect the thermal behavior of the fluid. When these effects are to be accounted for, the thermal properties of the solid materials must be prescribed. Volume II describes how the material types are prescribed and their properties evaluated.

In COMMIX, we can prescribe properties of as many materials as desired (steel, cladding, etc.). For each material, the density, thermal conductivity, and specific heat are assumed to be functions of temperature having the following functional forms:

$$\rho = C_{0\rho} + C_{1\rho}T + C_{2\rho}T^2 \ ,$$

$$k = C_{0k} + C_{1k}T + C_{2k}T^2 ,$$

and

$$c_p = C_{0cp} + C_{1cp}T + C_{2cp}T^2 . \qquad (9.2)$$

Here, C_0, C_1, and C_2 are the input coefficients.

9.3 HEAT-TRANSFER CORRELATIONS

To calculate the heat transfer between fluid and solid surfaces (either the solid boundaries of a flow domain or the surfaces of internal structures), a heat-transfer coefficient model is required in the code. In the model implemented in COMMIX, all heat transfer coefficient correlations are assumed to have the following form:

$$Nu = C_1 + C_2 \, Re^{C_3} . \qquad (9.3)$$

Here Nu is the Nusselt number, Re is the Reynolds number, and C_1, C_2, and C_3 are the constant coefficients for a given correlation number NH. The user can prescribe several correlations by inputting different values of coefficients C_1, C_2, and C_3. The Nusselt number and Reynolds number are based on the characteristic lengths of the structures. These characteristic lengths are input and must be prescribed by the user.

9.4 INTERACTIONS WITH STRUCTURES

As described before, the solid structures in a flow domain interact with fluid and influence the momentum and energy distributions. In the new porous-media formulation employed in COMMIX, these interactions are modeled using distributed resistances and distributed heat sources.

9.4.1 Structure-Fluid Momentum Interaction

9.4.1.1 Modeling in COMMIX-1B

As mentioned earlier, solid structures near fluid have the physical effect of influencing fluid flow by increasing flow resistance. In the quasi-continuum formulation, this effect is accounted for by providing an additional distributed resistance term in the momentum equation. This section describes how the calculation of distributed resistance, also known as force structure, is carried out, and how a wide range of generality and flexibility is provided in COMMIX.

The pressure drop due to stationary solid structures is expressed, in the literature, in many different forms, e.g.,

$$\Delta p = 4 \frac{L}{D} \frac{1}{2} \rho \, v^2 \, f , \qquad (9.4a)$$

$$\Delta p = \frac{L}{D} \frac{1}{2} \rho \, v^2 \, C_D , \text{ and} \qquad (9.4b)$$

$$\Delta p = \frac{1}{2} \rho \, v^2 \, K \, . \tag{9.4c}$$

The coefficients f, C_D, K, etc. have different names--Fanning friction factor, Darcy friction factor, drag coefficient, loss coefficient, etc.--depending on the form of the equation. To accommodate all friction loss equations, COMMIX employs the following general form:

$$\Delta p = c_1 \frac{L}{D} \rho \, v^2 \, f \, . \tag{9.5a}$$

In terms of distributed resistance R, the equation has the form

$$R = c_1 \rho \frac{v|v|}{D} f \, . \tag{9.5b}$$

Here, L(Δx, Δy, or Δz) is the length of the cell, D is the hydraulic diameter, and c_1 is the coefficient, depending on the form of the equation desired. The values of c_1 and D depend on the geometry and type of the structure and are required to be provided by the user.

There may be more than one structure in a flow domain of interest. Submerged structures usually have different geometries and so require different values for the parameters c_1 and D. In COMMIX we have provided this flexibility; details are given in Volume II.

The friction factor f in Eq. 9.5 is a function of the Reynolds number and is assumed to be of the form

$$f = a_{\ell am} \, Re^{b_{\ell am}} + c_{\ell am} \tag{9.6a}$$

for $Re \leq Re_{tr}$ and

$$f = a_{tur} \, Re^{b_{tur}} + c_{tur} \tag{9.6b}$$

for $Re > Re_{tr}$. Here, Re is the Reynolds number, and a, b, and c are constants. The subscripts ℓam, tur, and tr stand for laminar, turbulent, and transition. COMMIX has the flexibility of permitting as many correlations as the user desires. Each correlation requires seven input numbers--$a_{\ell am}$, $b_{\ell am}$, $c_{\ell am}$, a_{tur}, b_{tur}, c_{tur}, and Re_{tr}.

To simplify the specification of which fluid cells interact with which structure, a specific input arrangement has been implemented in COMMIX; details are presented in Volume II of this report.

A report[80] has been prepared that provides a convenient collection of resistance correlations that are most commonly needed by COMMIX users. This collection of resistance correlations are also included as an Appendix in Volume II.

9.4.1.2 Friction-Factor Library

Occasionally, the COMMIX-1B user may be faced with the situation that the desired correlation is not of a form directly suitable for input as described in Sec. 9.4.1. The user is then faced with two choices:

- Approximate the correlation to fit the input form, or
- Use the friction-factor library.

The friction-factor library has been created to accomodate up to 50 different additional correlations. Currently, only six correlations, as described in Table. 9.1, have been added to the library.

An ambitious user who wishes to define his or her own correlation may first examine the code to see what correlation numbers are free and available. Then, with other library correlations as a guide, the new correlation can be inserted appropriately in the code and recompiled. Every effort has been made to modularize this part of the subroutine so that a user has minimum difficulty in inserting new correlations in the code.

9.4.2 Structure-Fluid Thermal Interaction

9.4.2.1 Introduction

To determine the heat-transfer interaction between a structure and surrounding fluid, COMMIX contains a so-called thermal-structure module.

The heat transfer to fluid from a structure is calculated by solving the one-dimensional heat conduction equation for the structure. This assumes that heat conduction in the other two directions is negligible. The COMMIX numerical model has the following features:

- The model considers all internal structures. The input determines the total number of structures.
- A structure can be planar, cylindrical, or spherical with either one surface (e.g., solid cylinder or sphere) or two surfaces (plane or annular cylinder) having thermal interactions with surrounding fluid. The axis of alignment of the structure can be aligned with any of the three coordinate axes.
- Each structure can consist of more than one type of material, each separated by a gap.
- Radial variation and temperature dependence of thermal conductivity and specific heat of structures are incorporated.
- The effects of gaps in a structure element are accounted for in the model. The gap width and heat-transfer coefficient across a gap are input parameters.
- The heat source in a structure element is considered in the heat conduction equation. The heat source can be transient.

Table 9.1 Friction Factor Library

Correlation Number	Description	Correlation	CLENTH (hydraulic diameter, m)	REYLEN (length used to compute Reynolds number)
90	CRBR fuel	$f = \frac{81.7}{Re}\sqrt{1-\chi} + \frac{0.48}{Re^{0.25}}\sqrt{\chi}$ $\chi = 0;\ Re \leq 400,$ $\chi = (Re - 400)/4600;\ 400 < Re < 5000$ $\chi = 1;\ Re \geq 5000,$	3.25×10^{-3}	3.25×10^{-3}
91	CRBR blanket assembly	$f = \frac{99}{Re}\sqrt{1-\chi} + \frac{0.48}{Re^{0.25}}\sqrt{\chi}$ $\chi = 0;\ Re \leq 400,$ $\chi = (Re - 400)/4600;\ 400 < Re < 5000$ $\chi = 1;\ Re \geq 5000,$	3.39×10^{-4}	3.39×10^{-4}
92	Direct reactor heat exchanger	$f = \frac{A}{Re^{0.22}}$ $A = 0.171 + 0.012\ (P/D) - 0.07e^{-50(P/D-1)}$ $P/D = 1.84$	0.1055	0.1055

Table 9.1 (Contd.)

Correlation Number	Description	Correlation	CLENTH (hydraulic diameter, m)	REYLEN (length used to compute Reynolds number)
93	CRBR chimneys	$f = \frac{64}{Re}\sqrt{1-\chi} + \frac{0.3164}{Re^{0.25}}\sqrt{\chi}$	0.127	0.127
		$\chi = 0;\ Re \leq 1200$		
		$\chi = \frac{Re - 1200}{2800};\ 1200 < Re < 4000$		
		$\chi = 1;\ Re \geq 4000$		
94	FFTF pin bundle	$f = \frac{84}{Re};\ Re \leq 1000$	3.95×10^{-3}	3.95×10^{-3}
		$f = 1.075\, f_c \left[1 + 0.1746 \left(\frac{1000}{Re}\right)^2 + 0.0745 \left(\frac{1000}{Re}\right)^4\right]$		
		$\frac{1}{\sqrt{f_c}} = -0.8686 \log_e \left(\frac{2.51}{Re\sqrt{f_c}}\right)$		
95	CRBR control assembly	$f = \frac{60.68}{Re}\sqrt{1-\chi} + \frac{0.48}{Re^{0.25}}\sqrt{\chi}$	3.48×10^{-3}	3.48×10^{-3}
		$\chi = 0,\ Re \leq 400$		
		$\chi = (Re - 400)/4600;\ 400 < Re < 5000$		
		$\chi = 0;\ Re \geq 5000$		

- Each structure is divided into a desired number of axial elements. A set of discretization equations is obtained for each element using the proper boundary conditions. The equations are solved using the Tri-Diagonal Matrix Algorithm. The temperature variations in the element and heat transfer from the element to fluid are calculated.

9.4.2.2 **Geometrical Description**

To explain the geometrical features of the model, we consider a cylindrical structure with its axis aligned in the z direction, and its length extending over a number of Δz partitions (K levels), as shown in Fig. 9.1. Although the description and the subsequent formulation are geared toward cylindrical-type structure, the model in COMMIX-1B also is applicable to spherical and slab-type geometries.

Each Δz partition of the structure is referred to as a thermal-structure element. Each element has its own internal temperature distribution as it interacts with surrounding fluid cells. Each element has two surfaces, outer and inner. The outer surface interacts with surrounding fluid. The inner surface can either be adiabatic or interact with fluid, as shown in Fig. 9.2. Each element can interact with no more than one fluid cell per element surface, while each fluid cell can interact with more than one structure element; this can be seen in Figs. 9.3 and 9.4.

Figure 9.5 shows the cross-section of a typical structure element. The outside surface is considered as surface 1 and the inside as surface 2. Each element can be made up of more than one material. In Fig. 9.5, there are three materials. Each material region can be subdivided into a number of partitions, as shown in Fig. 9.5.

9.4.2.3 **Governing Equation**

The transient one-dimensional heat conduction equation is

$$\rho c_p \frac{\partial T}{\partial t} = \frac{1}{A} \frac{\partial}{\partial r} (-Aq) + \dot{q}''' \quad . \tag{9.7}$$

Here, ρ and c_p are the density and specific heat of the material, $\dot{q}'''$ is the heat source per unit volume, q is the surface heat flux per unit area, and A is the cross-sectional area.

9.4.2.4 **Finite-Difference Formulation**

Figure 9.6 shows the cross-section of a typical structure element under consideration. Each element is divided into a number of material regions and each material region is subdivided into a number of partitions. Let Δr be the partition size and let L be the total number of partition cells.

Consider the energy balance of cell ℓ, as shown in Fig. 9.7. The integrated energy equation for the control volume of cell ℓ gives

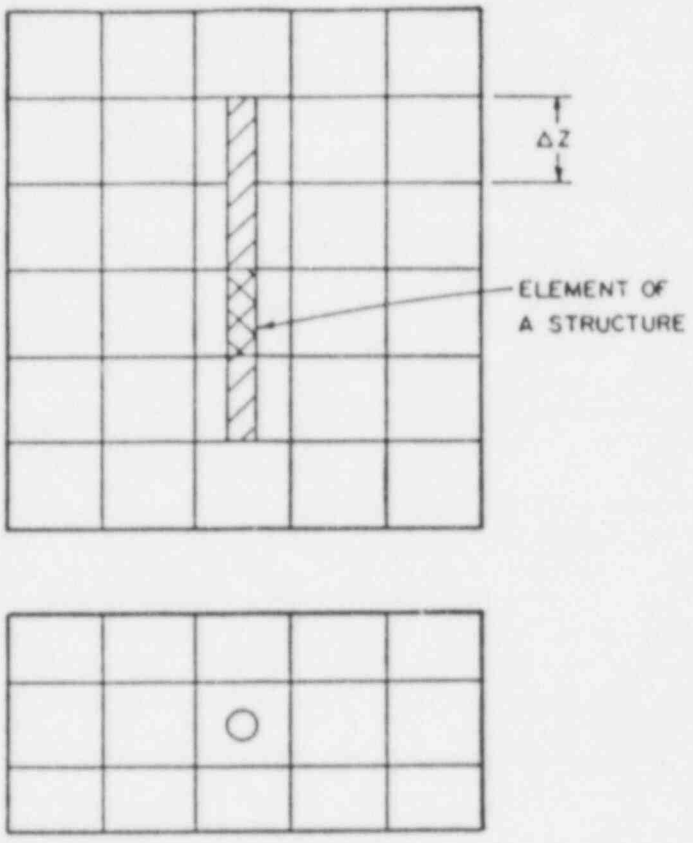

Fig. 9.1. Flow Domain Showing a Cylindrical Structure

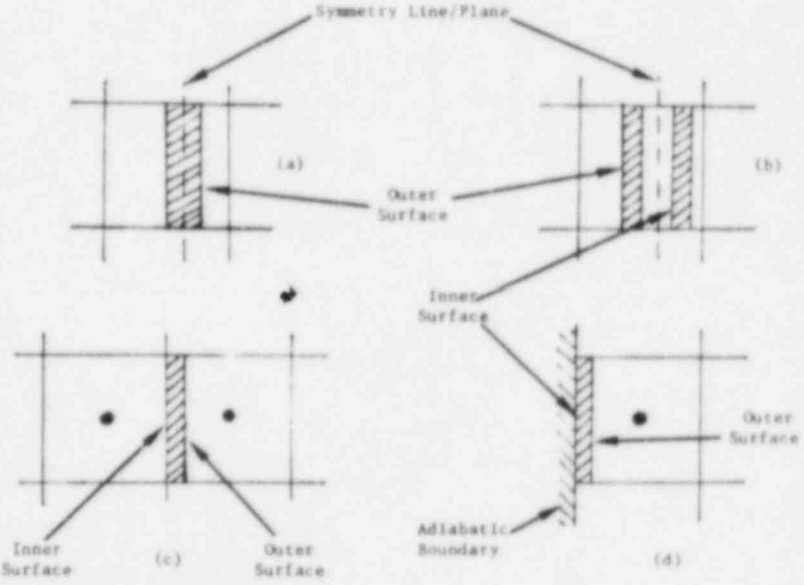

Fig. 9.2. Element of a Thermal Structure Showing Outer and Inner Surfaces

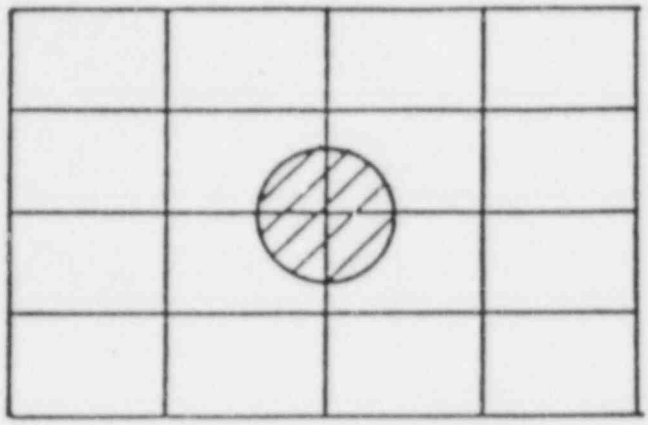

Fig. 9.3 Four Quarter Cylindrical Structures each Interacting with One Fluid Cell

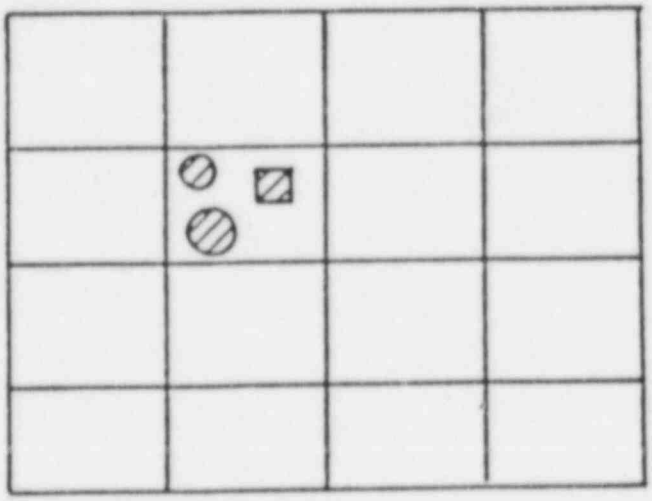

Fig. 9.4 More than one Structure Interacting with a Single Fluid Cell

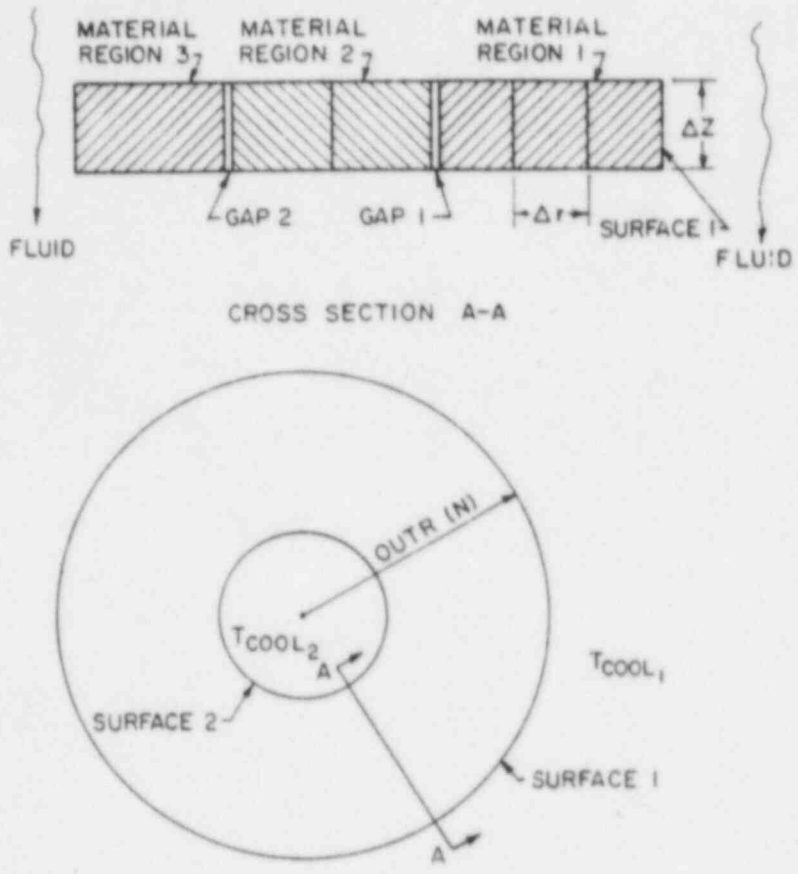

Fig. 9.5 Typical Structure Element showing Material Regions and Gaps

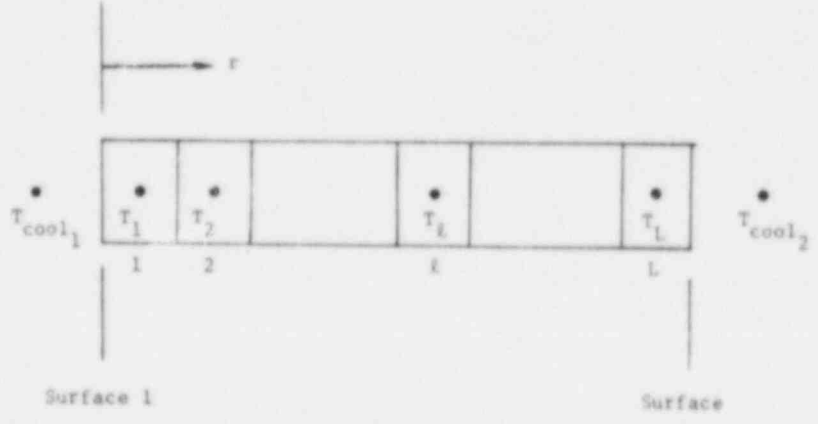

Fig. 9.6 Cross-Section of a Thermal Structure Element

$$\frac{\rho c_p V_\ell}{\delta t}\left(T_\ell - T_\ell^n\right) = -\left(A_{\ell+1}q_{\ell+1} - A_\ell q_\ell\right) + \dot{q}''' V_\ell \ . \tag{9.8}$$

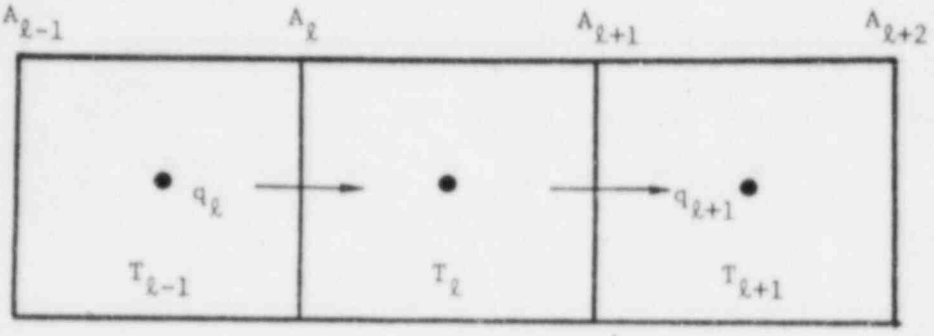

Fig. 9.7. Energy Balance of a Partition Cell ℓ

Here, V_ℓ is the cell volume. The heat flux q_ℓ can be expressed in terms of temperature difference:

$$q_\ell = U_\ell\left(T_{\ell-1} - T_\ell\right) = \left(T_{\ell-1} - T_\ell\right)/R_\ell \ . \tag{9.9}$$

Here, U_ℓ is the overall heat transfer coefficient (conductance) and R_ℓ is the overall thermal resistance between T_ℓ and $T_{\ell-1}$:

$$U_\ell = \frac{1}{R_\ell} = \frac{1}{\left(\frac{\Delta r}{2\lambda}\right)_{\ell-1} + \left(\frac{\Delta r}{2\lambda}\right)_\ell} \qquad \text{for conduction ,} \tag{9.10}$$

and

$$U_\ell = \frac{1}{R_\ell} = \frac{1}{\frac{1}{h} + \left(\frac{\Delta r}{2\lambda}\right)_\ell} \qquad \text{for conduction and convection (gap or surface),} \tag{9.11}$$

where λ is the thermal conductivity and h is the convective heat transfer coefficient. After substituting Eq. 9.9 in Eq. 9.8 and rearranging, we obtain

$$\left(a_\ell + b_\ell + b_{\ell+1}\right)T_\ell = b_\ell T_{\ell-1} + b_{\ell+1}T_{\ell+1} + d_\ell \ , \tag{9.12}$$

where

$$a = \rho c_p V/\delta t \ , \tag{9.13}$$

$$b = A\,U = A/R \ , \tag{9.14}$$

and

$$d = \dot{q}''' \, V + a \, T^n \ . \tag{9.15}$$

Here, T^n and T are the temperatures at time t and $(t + \delta t)$, respectively.

Cell Adjacent to Coolant

For the case of Cell 1 (Fig. 9.8), adjacent to the fluid, the integrated energy equation gives

$$(a_1 + b_1 + b_2)T_1 = b_1 T_{cool_1} + b_2 T_2 + d_1 \ . \tag{9.16}$$

Here, a, b, and d have the same meaning, except that b_1 now includes the convective contribution. Therefore,

$$b_1 = \frac{A_1}{R_1} = \frac{A_1}{\frac{1}{h_{cool_1}} + \left(\frac{\Delta r}{2\lambda}\right)_1} \ . \tag{9.17}$$

Similarly, if the other end of the thermal structure, say Cell L, is in contact with fluid, we get

$$(a_L + b_L + b_{L+1})T_L = b_L T_{L-1} + b_{L+1} T_{cool_2} + d_L \ , \tag{9.18a}$$

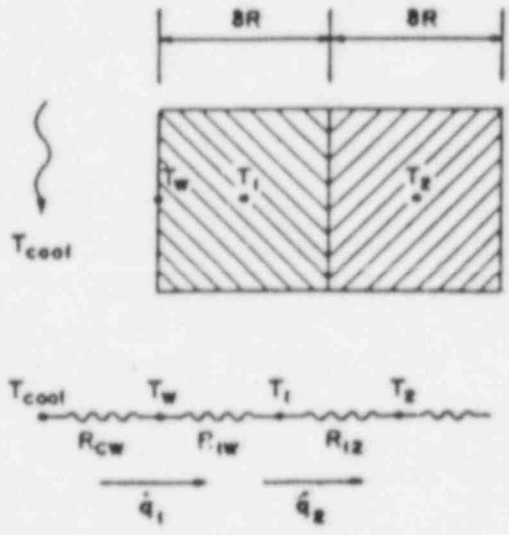

Fig. 9.8 Energy Balance of Cell 1 Adjacent to Coolant

where

$$b_{L+1} = \frac{A_{L+1}}{R_{L+1}} = \frac{A_{L+1}}{\frac{1}{h_{cool_2}} + \left(\frac{\Delta r}{2\lambda}\right)_L} \quad . \tag{9.18b}$$

Cell Adjacent to a Different Material

For a cell adjacent to a different material cell, as shown in Fig. 9.9,

$$(a_\ell + b_\ell + b_{\ell+1})T_\ell = b_\ell T_{\ell-1} + b_{\ell+1} T_{\ell+1} + d_\ell \quad . \tag{9.19}$$

Equation 9.19 is similar to Eq. 9.12, except that the term $b_{\ell+1}$ includes the gap resistance. Thus,

$$b_{\ell+1} = \frac{A_{\ell+1}}{R_{\ell+1}} = \frac{A_{\ell+1}}{\left(\frac{\Delta r}{2\lambda}\right)_\ell + \frac{1}{h_{gap}} + \left(\frac{\Delta r}{2\lambda}\right)_{\ell+1}} \quad . \tag{9.20}$$

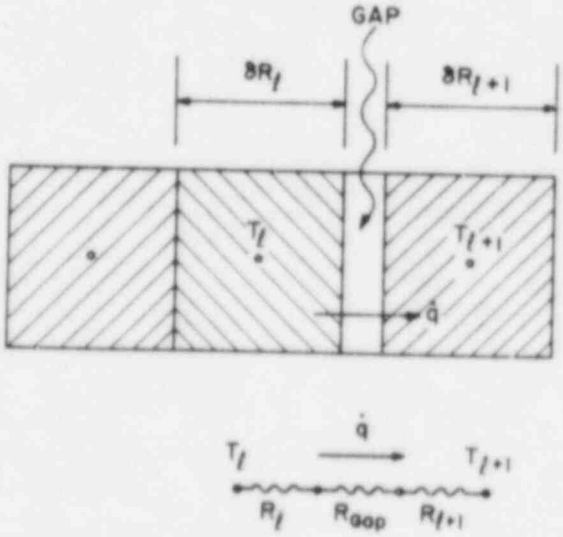

Fig. 9.9. Cell Surrounded by Different Materials with Air Gap between Them

End Cell with Adiabatic Boundary Condition

In solid cylindrical or spherical structures, the other end (symmetry line) has the adiabatic boundary condition. The end cell for this boundary condition is shown in Fig. 9.10. We have no heat transfer, so thermal resistance is infinite and the term b_{L+1} goes to zero.

The final equation, therefore, is

$$(a_L + b_L)T_L = b_L T_{L-1} + d_L \quad . \tag{9.21}$$

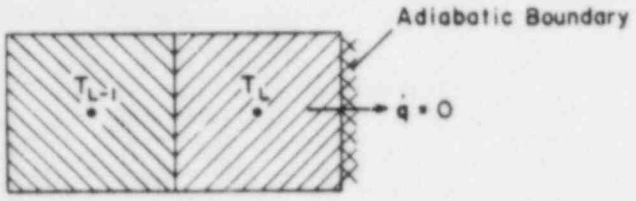

Fig. 9.10
Cell with Adiabatic Boundary

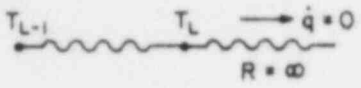

9.4.2.5 **Solution of the Discretization Equations**

We can see from the formulation of the preceding section that there are L number of equations for L number of unknown temperatures.

- Outside Surface Cell ($\ell = 1$)

$$(a_1 + b_1 + b_2)T_1 = b_2T_2 + \left(d_1 + b_1T_{cool_1}\right) \tag{9.22a}$$

- Intermediate Cells ($\ell = 2, \cdots\cdots L-1$)

$$(a_\ell + b_\ell + b_{\ell+1})T_\ell = b_\ell T_{\ell-1} + b_{\ell+1}T_{\ell+1} + d_\ell \quad .$$

$$(\ell = 2, \cdots\cdots L-1) \tag{9.22b}$$

- Inside Surface Cell ($\ell = L$)

$$(a_L + b_L + b_{L+1})T_L = b_LT_{L+1} + \left(b_{L+1}T_{cool_2}\right) + d_L \tag{9.22c}$$

if the inside surface is non-adiabatic, and

$$(a_L + b_L)T_L = b_LT_{L-1} + \left(d_L\right) \tag{9.22d}$$

if the inside surface is adiabatic.

Equation 9.22 can be transformed to

$$C_1'T_1 = b_2T_2 + A_1' \qquad (\ell = 1) \tag{9.23a}$$

$$C_\ell'T_\ell = b_{\ell+1}T_{\ell+1} + A_\ell' \quad , \qquad (\ell = 2, \cdots\cdots L-1) \tag{9.23b}$$

$$C'_L T_L = b_{L+1} T_{cool_2} + A'_L \qquad (\ell = L;\ \text{nonadiabatic}) \qquad (9.23c)$$

or

$$C'_L T_L = A'_L \qquad (\ell = L;\ \text{adiabatic}) \ . \qquad (9.23d)$$

Here,

$$A'_\ell = d_\ell + \left(b_\ell A'_{\ell-1}/C'_{\ell-1}\right) \ , \qquad (\ell = 2 \cdots\cdots L) \qquad (9.24a)$$

and

$$C'_\ell = a_\ell + b_\ell + b_{\ell+1} - \left(b_\ell^2/C'_{\ell-1}\right) \ . \ (\ell = 2, \cdots\cdots L) \ . \qquad (9.24b)$$

The first set of coefficients is

$$A'_1 = d_1 + b_1 T_{cool_1} \qquad (9.24c)$$

and

$$C'_1 = a_1 + b_1 + b_2 \ . \qquad (9.24d)$$

The inside-surface cell temperature is first calculated from Eqs. 9.23c or 9.23d. Then the rest of the temperatures are computed using Eqs. 9.23a and 9.23b.

9.4.2.6 **Heat Transfer to the Adjacent Fluid**

Once the temperature distribution in a structure element is computed, the heat transfer rate to the adjacent fluid is computed from

$$\dot{q} = \frac{A_1}{R_1}\left(T_1 - T_f\right)$$

$$= U_1 A_1 \left(T_1 - T_f\right) \quad \text{for outside surface } \left(T_f = T_{cool_1}\right) \text{ and} \qquad (9.25)$$

$$\dot{q} = \frac{A_{L+1}}{R_{L+1}}\left(T_L - T_f\right)$$

$$= U_{L+1}\, A_{L+1}\left(T_L - T_f\right) \quad \text{for inside surface } \left(T_f = T_{cool_2}\right) \ . \qquad (9.26)$$

Here, $\dot{q}$ is the heat transfer rate in watt, U is the overall heat transfer coefficient given by

$$U = \frac{1}{R} = \frac{1}{\dfrac{1}{h_{cool}} + \left(\dfrac{\Delta r}{2\lambda}\right)} \ , \qquad (9.27)$$

A is the surface area, T_l and T_L are the temperatures of the edge partition cells, and T_f is the respective fluid temperature. The heat transfer rate is then translated into an effective volumetric heat source for the fluid cell.

$$\dot{Q}_{rb} = \frac{\dot{q}}{\gamma_v V_0} , \tag{9.28}$$

where V_0 is the computation cell volume (e.g., $\Delta x \Delta y \Delta z$) of the adjacent fluid cell and $\dot{Q}_{rb}$ is the heat source from solids per unit fluid volume. The computation of the heat transfer coefficient is carried out as described in Sec. 9.3.

10. INITIAL AND BOUNDARY CONDITIONS

10.1 INITIAL CONDITIONS

Generally, before the solution sequence can begin, all values of variables must be assigned. In COMMIX, we can accomplish this either

- By continuing a previous run via the restart capability (recommended for all but the first run), or
- By specifying the initial distribution throughout the interior points and boundary of the space under consideration.

When the initialization is not a restart, we have to specify initial pressure, temperature, velocity and turbulence parameters distributions. The determination of these distributions and their subsequent input into the code are generally tedious. In COMMIX, we have provided several simplified input procedures, which make the initialization of velocity, pressure, and temperature less tedious. These procedures are described in Volume II. The procedures of initialization relating to turbulence parameters are described in Sec. 6 of Volume I and Sec. 8 of Volume II.

10.2 BOUNDARY CONDITIONS

This section describes the boundary conditions for mass, momentum, and energy equations. The boundary conditions for turbulence transport equations are described in Sec. 6 of Volume I and Sec. 8 of Volume II.

10.2.1 Velocity Boundary Conditions

The most common physical boundaries in an engineering system are solid impervious wall, inlet, symmetry, and outlet. To accommodate all possible velocity conditions at these four boundaries, we have provided seven boundary condition options. Here, we describe the meaning of these options in mathematical terms. In Table 10.1, we have summarized all seven velocity boundary options for the four most commonly occurring physical conditions. Volume II tells how to implement them in the input data.

- Constant Velocity

This boundary condition implies that normal velocity v_n = constant. In COMMIX, this is achieved by simply not altering the value of the normal velocity v_n specified during initialization. This option is applicable to a solid surface with zero normal velocity and to an inlet surface with constant inlet velocity.

- Transient Velocity

This option is applicable when an inlet velocity varies with time, e.g.,

$$v_n = v_0 f(t) \ . \qquad (10.1)$$

Table 10.1 Velocity-Boundary Options

Boundary	Suitable Option	Option No.	Remarks
Solid Impervious Surface	(i) Constant velocity	1	Specify normal velocity $v_n = 0$ during initialization
Inlet	(i) Constant velocity	1	Specify inlet velocity during initialization
	(ii) Transient velocity	2	Specify inlet velocity and appropriate transient function
Symmetry	(i) Free Slip	3	Axis through origin in cylindrical coordinate is a symmetry surface
Outlet	(i) Continuative mass flow	4	General outlet condition
	(ii) Continuative momentum	5	Suitable when areas are equal
	(iii) Continuative velocity	6	Suitable when areas and densities are equal
	(iv) Uniform velocity	7	Suitable when outlet is finely divided (Fig. 10.2)

Here,

v_n = surface-normal velocity at time t ,

v_0 = surface-normal velocity at time t = 0 ,

and

f(t) = transient function.

- Free Slip

The free-slip option means the shear stress at the surface is zero. Also,

$$v_n = 0.0 \ . \tag{10.2}$$

This option is applicable to a symmetry boundary. For a cylindrical coordinate system in COMMIX, the z axis passing through the origin is considered as a symmetry boundary with zero surface area.

- Continuative Mass Flow Outlet

This option is for an outlet surface as illustrated in Fig. 10.1. Here, ℓ and m are the outlet boundary cells and $\ell+1$ and $m-1$ are the neighboring cells. The continuative mass flow outlet implies that normal surface velocity at the outlet must be such as to balance the mass flow, i.e.,

$$(v_n)_{\ell-1/2} = \frac{(\rho A)_{\ell+1/2}}{(\rho A)_{\ell-1/2}} u_{\ell+1/2} \tag{10.3a}$$

and

$$(V_n)_{m+1/2} = - \frac{(\rho A)_{m-1/2}}{(\rho A)_{m+1/2}} u_{m-1/2} \, . \tag{10.3b}$$

The sign difference between Eqs. 10.3a and 10.3b is due to the COMMIX-1B convention that surface-normal velocity is directed into the flow domain.

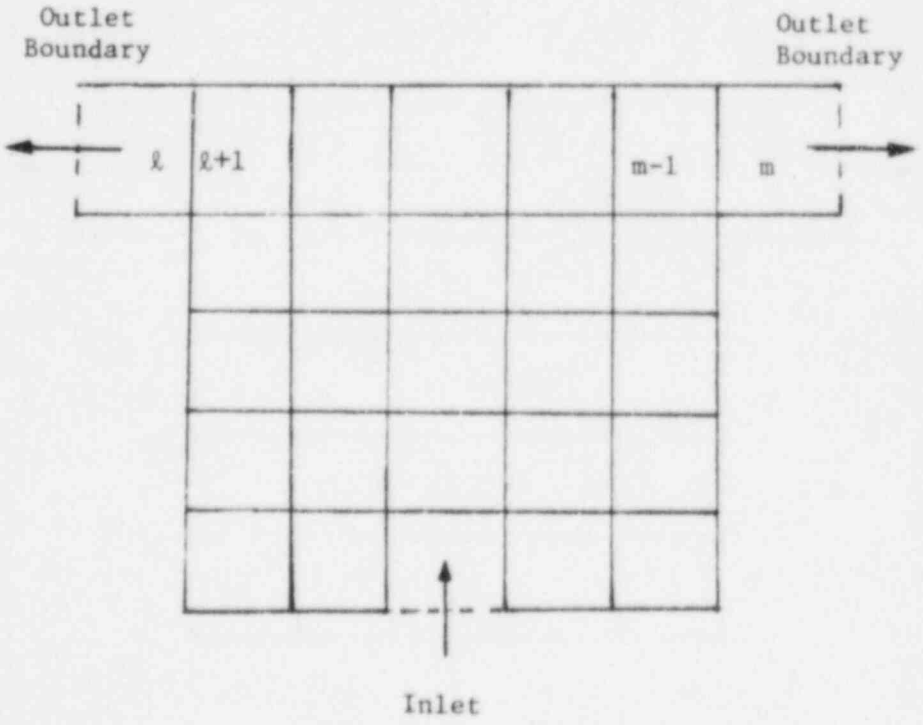

Fig. 10.1 Near Boundary Cells

- Continuative Momentum Outlet

When an outlet area is the same as the neighboring surface area, then Eq. 10.3a simplifies to

$$(v_n)_{\ell-1/2} = \frac{|\rho u|_{\ell+1/2}}{\rho_{\ell-1/2}} \quad . \tag{10.4}$$

We call this option continuative momentum because it appears that we are equating neighboring and outlet momentum fluxes.

- Continuative Velocity Outlet

If we have a constant area and equal densities, then Eq. 10.3a simplifies to

$$(v_n)_{\ell-1/2} = (u)_{\ell+1/2} \quad . \tag{10.5}$$

We call this option continuative velocity because it appears that we are equating neighboring and outlet velocities.

- Uniform Velocity Outlet

The uniform velocity outlet boundary condition option sets the normal velocity for all surface elements of a surface to the same value. This value is computed such that the total mass flow through a surface is the same as what would have been obtained from the continuative mass flow outlet boundary condition. Mathematically,

$$v_n = \frac{\sum (\rho Au)_{\ell+1/2}}{\sum (\rho A)_{\ell-1/2}} \quad . \tag{10.6}$$

Here the summation is taken over all surface elements of a surface. This option is suitable when an outlet is very finely divided, as shown in Fig. 10.2.

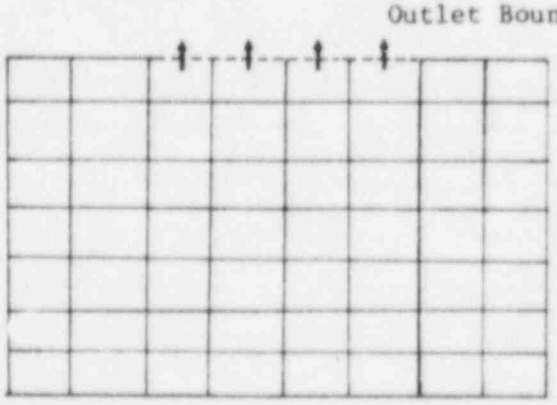

Fig. 10.2 Model Suitable for Uniform Velocity Outlet Option

10.2.2 **Temperature Boundary Conditions**

The six temperature boundary-condition options available in COMMIX-1B are briefly described here and summarized in Table 10.2.

Table 10.2 Suitable Temperature Boundary Options

Boundary/Option	Option No.	Remark
Solid surface		
Constant temperature	1	T_w = constant
Transient temperature	2	T_w = f(t)
Constant heat flux	3	q_w = constant
Transient heat flux	4	q_w = f(t)
Adiabatic	5	q_w = 0
Duct Wall	6	Considers thermal inertia of wall
Inlet		
Constant temperature	1	T_w = constant
Transient temperature	2	T_w = f(t)
Outlet		
Adiabatic	5	q_w = 0
Symmetry		
Adiabatic	5	q_w = 0

- Constant Temperature

This option is for a constant surface temperature. The temperature associated with each surface element, as shown is Fig. 10.3, is set initially and remains unchanged throughout the calculation. While the temperature remains fixed, the surface element heat flux is calculated using the relation

$$\dot{q} = UA \left(T_w - T_f \right) . \qquad (10.7)$$

Here

$$U = \frac{1}{\frac{1}{h} + \frac{\Delta L}{2\lambda_w}} , \qquad (10.8)$$

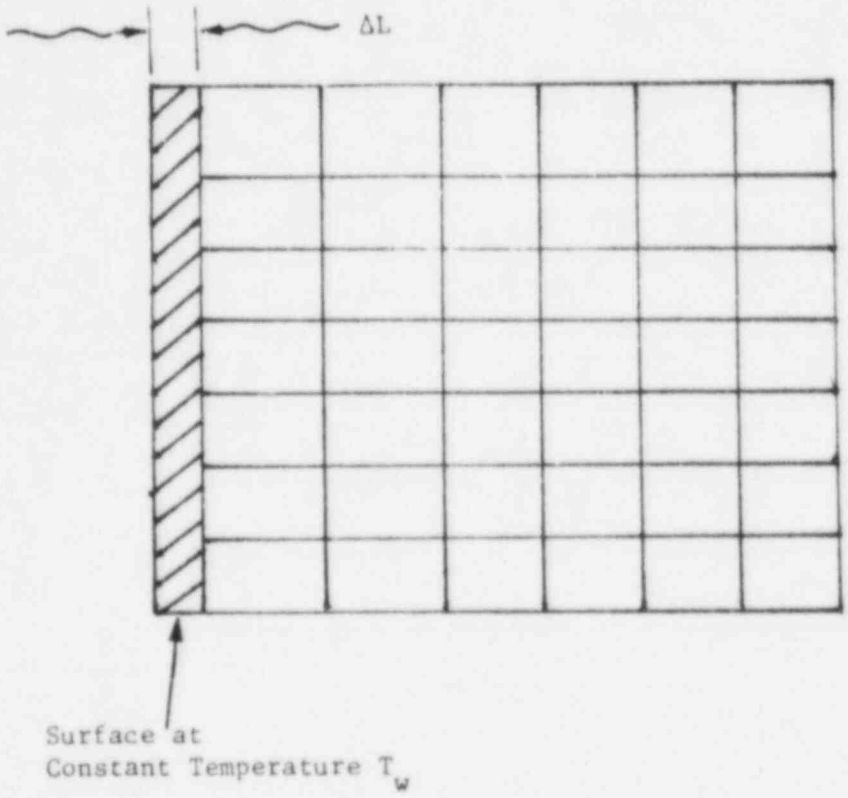

Fig. 10.3 Constant-Temperature Boundary

where h is the heat transfer coefficient, λ is the conductivity of the wall material, and ΔL is the wall thickness. The subscripts w and f refer to the surface element and boundary fluid cell, respectively. For calculation of the overall heat transfer coefficient U, we need to provide wall thickness, suitable correlation for h, and material properties for λ.

If the wall is very thin, as shown in Fig. 10.4, then we do not have to specify wall thickness and material properties. The overall heat transfer U is then equal to h.

If a constant temperature is associated with, say an inlet surface as shown in Fig. 10.5, then we do not have to specify even the heat transfer correlation. The surface heat flux is then calculated from the Fourier relation

$$\dot{q} = \frac{\lambda_{eff} A \left(T_w - T_f \right)}{\frac{\Delta x_f}{2}} \, . \tag{10.9}$$

Here, λ_{eff} is the effective thermal conductivity of the fluid in the adjacent internal cell, Δx_f is the distance between the surface and the boundary cell center, and the subscripts w and f stand for wall (surface element) and adjacent internal cell, respectively.

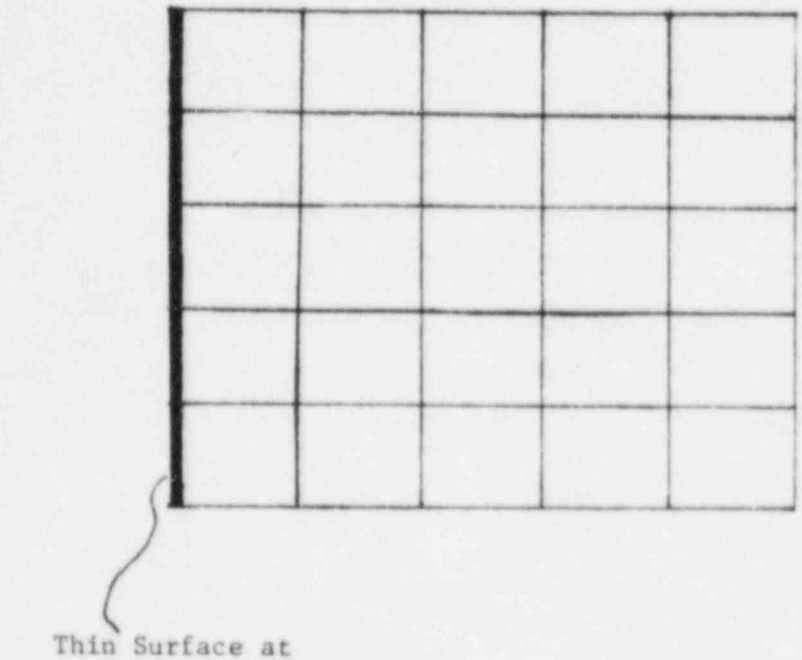

Fig. 10.4 Thin-Wall Constant-Temperature Boundary

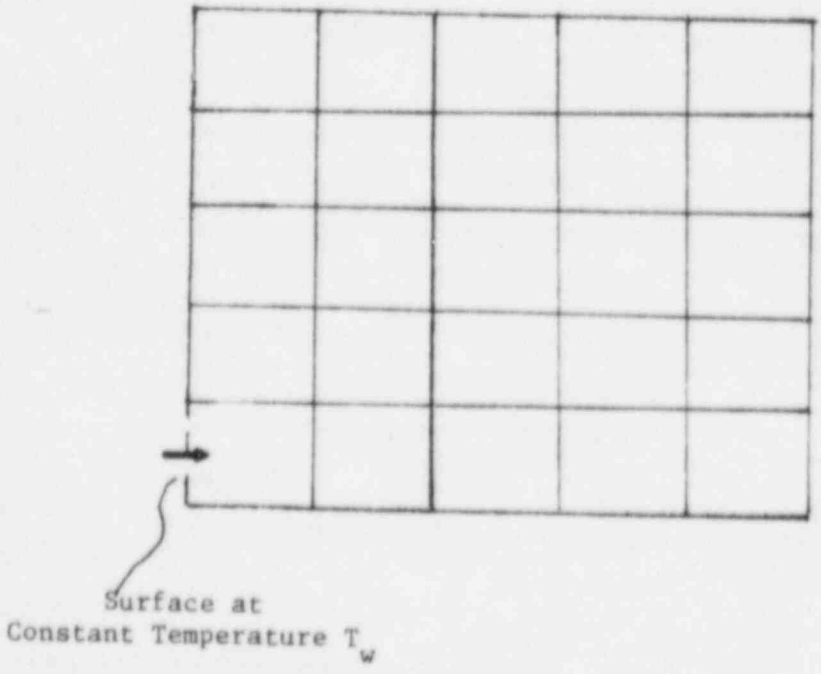

Fig. 10.5 Nonconvective Constant-Temperature Boundary

- Transient Temperature

This option is for a surface whose temperature varies with time, e.g.,

$$T_w = T_0 \, f(t) \ , \tag{10.10}$$

where

T_w = surface temperature at time t ,

T_0 = surface temperature at time = 0 ,

and

f(t) = transient function .

We calculate the surface-element heat flux using the same procedure described for the constant-temperature boundary option.

- Constant Heat Flux

When we have a surface with constant heat flux, then we use this option. The heat flux associated with each surface element is set initially and remains unchanged throughout the calculation. Although the surface heat flux remains fixed, we now calculate the temperature using Eq. 10.9 based on the effective thermal conductivity of the adjacent internal cell.

- Transient Heat Flux

This option is useful when we have surface heat flux varying with time, e.g.,

$$\dot{q} = \dot{q}_0 \, f(t) \ , \tag{10.11}$$

where

$\dot{q}$: surface heat flux at time t ,

$\dot{q}_0$: surface heat flux at time t = 0 ,

and

f(t) : transient function # nf .

Once the surface heat flux is known for a given time t, the surface temperature can be calculated from Eq. 10.9.

- Adiabatic Surface

The adiabatic boundary condition implies that surface heat flux $\dot{q} = 0$. In this option, the normal heat flux for all surface elements of a surface are initialized to zero and remain zero during calculation. The

surface-element temperature is set equal to the temperature of the neighboring internal cell.

- Duct Wall (KTEMP = 500 + NF)

We have provided the duct wall boundary condition option for a case when we want to consider the transient thermal response of a finite-thickness wall. In COMMIX-1B, this is carried out by solving the energy equation for each wall (surface) element. It is assumed that the element is sufficiently small that we can consider it to have a uniform temperature and can apply the lumped-heat-capacity method.

Figure 10.6 shows a finite-thickness surface element. The energy equation for the element is

$$\rho C_p A \Delta L \frac{\partial T_w}{\partial t} = - h_{wf} A (T_w - T_f) - h_{ws} A (T_w - T_{sink}) + \dot{Q} A \Delta L \ , \qquad (10.12)$$

where T is the temperature, A is the area of a surface element, ΔL is the wall thickness, and h is the heat-transfer coefficient. The subscripts w, f, and sink stand for wall element, fluid in the adjacent cell, and surrounding atmosphere, respectively. The transient volumetric heat source $\dot{Q}$ is given by

$$\dot{Q} = \dot{Q}_0 Q_k Q_{ij} f(t) \ . \qquad (10.13)$$

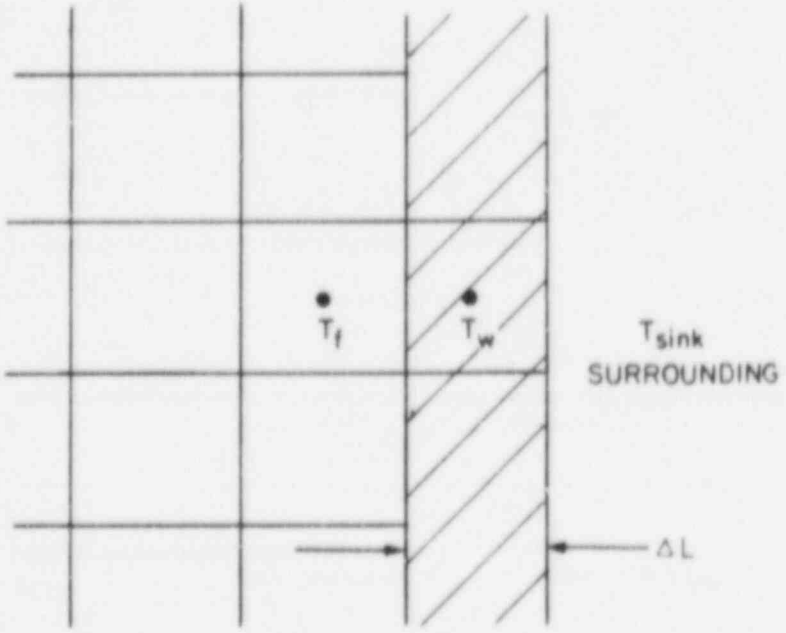

Fig. 10.6 Finite-Thickness Wall Boundary

Here,

$\dot{Q}_0$ = average volumetric heat source at t = 0 ,

Q_k = axial distribution function ,

Q_{ij} = radial distribution function ,

and

f(t) : transient function .

The integration of Eq. 10.12 from time t to time (t + Δt) gives

$$T_w^{t+\Delta t} = T_h + \left(T_w^t - T_h\right)e^{-\alpha\Delta t} , \qquad (10.14)$$

where

$$T_h = \frac{\beta + \alpha_w T_f + \alpha_s T_{sink}}{\alpha_w + \alpha_s} ,$$

$$\alpha_w = \frac{h_{wf}}{\rho C_p \Delta L} ,$$

$$\alpha_s = \frac{h_{ws}}{\rho C_p \Delta L} , \alpha = \alpha_w + \alpha_s ,$$

and

$$\beta = \frac{\dot{Q}}{\rho c_p} .$$

In COMMIX-1B, Eq. 10.14 is used to calculate the advanced time value of the surface-element temperature.

The duct wall boundary condition option requires several input specifications, which are described in Volume II.

10.2.3 **Pressure Boundary Conditions**

Currently, two types of pressure boundary-condition options are provided in COMMIX-1B:

- Constant pressure, and
- Transient pressure.

The pressure boundary is applicable only at the inlet and outlet surfaces. The option is therefore used in conjunction with the continuative mass flow boundary condition.

If an inlet surface has a specified velocity boundary condition, then we do not require a pressure boundary option because surface pressure does not enter into any calculation.

It is important to note here that the pressure boundary condition in COMMIX-1B refers to the pressure of the boundary adjacent fluid cells. It is therefore recommended to model the geometry such that the pressure boundary is applied to

- A surface with one surface element, or
- A surface that is normal to the direction of gravity and has parallel flow

as shown in Fig. 10.7.

When we specify a constant pressure boundary option, the pressures of all internal cells adjacent to a surface are set to prescribed initial value. These values then remain unchanged during the calculation.

For a transient pressure over a surface, the pressure of all internal cells adjacent to that surface are calculated from

$$P_m = P_{m0}\, f(t) \ . \qquad (10.15)$$

Here,

P_m = pressure of the adjacent cell m at time t ,

P_{m0} = pressure of adjacent cell m at time = 0 ,

and

$f(t)$ = transient function .

Volume II explains how to implement these options in the input.

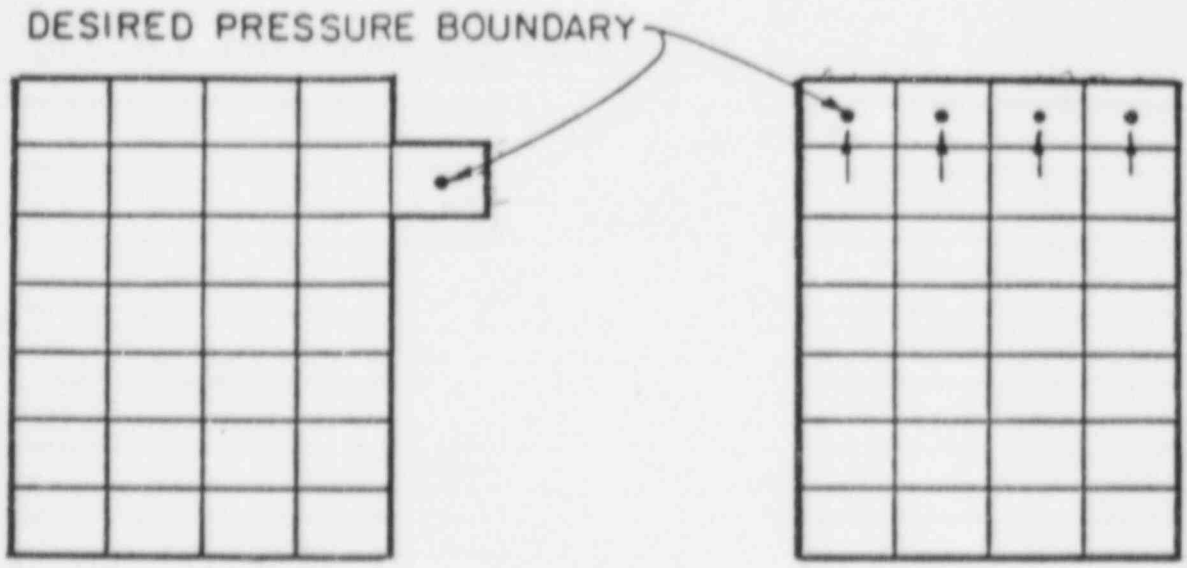

Fig. 10.7 Recommended Surface Arrangements for Pressure Boundary Condition

11. MASS REBALANCING

11.1 INTRODUCTION

All iterative solution procedures provide a solution to a set of algebraic equations of the form of Eq. 4.16. However, it is important to solve them as efficiently as possible to minimize computer running time. A scheme called mass rebalancing has been developed and implemented in COMMIX. The scheme is called mass rebalancing because it uses coarse mesh rebalancing of the pressure equation (the equation of conservation of mass).

After several years of testing, the mass rebalancing scheme has proved to be extremely effective. It significantly reduces the number of iterations required to achieve mass convergence, thus saving computer running time. The description of the scheme and the derivation of the mass rebalancing equations are briefly described here.

11.2 DESCRIPTION

In the mass rebalancing scheme, we form a coarse mesh domain by combining several fine mesh cells, as shown in Fig. 11.1. A coarse mesh containing several computational cells is called a region. For each region, a pressure correction equation is derived by summing up the pressure equations of all cells contained in that region. During summing, we apply the following conditions:

- The pressure corrections for all cells in a region are the same, and
- The pressure correction for each region is determined such that the sum of mass residuals over all cells in that region equals zero.

The pressure corrections obtained from the solution of these equations, when applied to all cells of a flow domain, help in resolving large-scale distributions and hence reduce the number of iterations required for final solution of the pressure equation.

11.3 DERIVATION OF PRESSURE CORRECTION EQUATION

Let us divide the flow domain into, say, N regions, as shown in Fig. 11.1. The regions are chosen such that any region n has neighboring cells contained only in the neighboring regions (n-1) and (n+1). Mass leaving the region n and entering the region (n+1) does so through rebalancing surface n. Mass leaving the last region N goes into the remaining cells, where no rebalancing is performed. Region 1 has neighboring cells only in Region 2.

Let P^* be the pressure distribution, which does not satisfy the continuity equation. The pressure equation for a cell m is

$$a_{m0} P^*_m - \sum_{\ell=1}^{6} a_{m\ell} P^*_\ell - b_{m0} = \delta^*_m , \qquad (11.1)$$

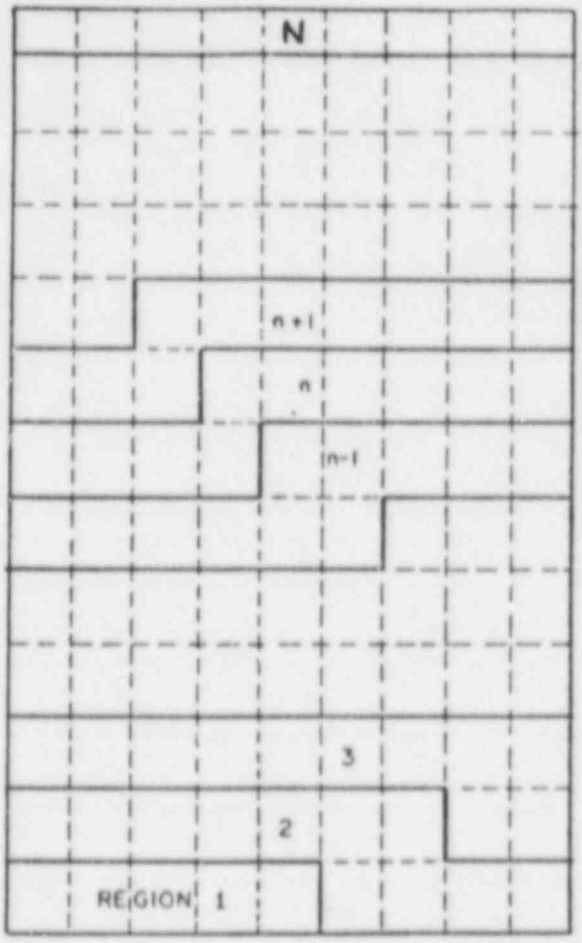

Fig. 11.1 Coarse Mesh Showing Rebalancing Regions

where δ^* is the mass residual, a_m and b_m are the coefficients of the pressure equation, and ℓ indicates the six adjacent cells surrounding cell m. For simplicity in writing, the superscript P is omitted from the coefficients a_m and b_m. We sum the pressure equations for all cells m in the region n. Thus

$$\sum_{m \in n} \left[a_{m0} P^*_m - \sum_{\ell=1}^{6} \left(a_{m\ell} \; P^*_\ell \right) - b_{m0} \right] = \sum_{m \in n} \delta^*_m \, , \tag{11.2}$$

where $\sum_{m \in n}$ indicates the summation over all cells m located in the rebalancing region n,

and

$\sum_{m \in n} \delta^*_m$ is the net mass nonconservation for the region n.

Let ΔP_1, ΔP_2, ... ΔP_n ... ΔP_N be the pressure corrections for the rebalancing regions 1 to N. The new pressure distribution P can be written as

$$P_m = P_m^* + \Delta P_n \quad ; \quad m \in n \ . \tag{11.3}$$

If we substitute the new pressure field in Eq. 11.1, we obtain, for each region, N equations of the form

$$\sum_{m \in n} \left(a_{m0} P_m - \sum_{\ell=1}^{6} a_{m\ell} P_\ell - b_{m0} \right) = \sum_{m \in n} \delta_m \ . \tag{11.4}$$

We want to rebalance all N regions such that the new pressure field achieves net mass conservation. In other words,

$$\sum_{m \in n} \delta_m = 0 \ . \qquad (n = 1 \cdots\cdots N) \ . \tag{11.5}$$

Substitution of Eq. 11.3 into Eq. 11.4, with the constraint of Eq. 11.5, and after some rearrangement, gives us

$$\sum_{m \in n} \left(a_{m0} P_m^* - \sum_{\ell=1}^{6} a_{m\ell} P_\ell^* - b_{m0} \right) + \Delta P_n \left[\sum_{m \in n} \left(a_{m0} - \sum_{\ell \in n} a_{m\ell} \right) \right]$$

$$- \Delta P_{n-1} \left[\sum_{m \in n} \left(\sum_{\ell \in (n-1)} a_{m\ell} \right) \right] - \Delta P_{n+1} \left[\sum_{m \in n} \left(\sum_{\ell \in (n+1)} a_{m\ell} \right) \right] = 0 \ ,$$

$$(n = 1, \cdots\cdots N). \tag{11.6}$$

In the set of equations (Eq. 11.6), we do not have ΔP_{n-1} term for n = 1 and ΔP_{n+1} term for n = N. We rewrite these equations as

$$A_0^n \Delta P_n - A_1^n \Delta P_{n-1} - A_2^n \Delta P_{n+1} - B^n = 0 \ , \tag{11.7}$$

where

$$A_1^n = \sum_{m \in n} \sum_{\ell \in (n-1)} a_{m\ell} = A_2^{n-1} \ , \tag{11.8a}$$

$$A_2^n = \sum_{m \in n} \sum_{\ell \in (n+1)} a_{m\ell} \ , \tag{11.8b}$$

$$A_0^n = A_1^n + A_2^n \ , \tag{11.8c}$$

and

$$B^n = \sum_{m \in n} \delta_m^* \ . \tag{11.8d}$$

In deriving Eqs. 11.8c and 11.8d, we have made use of the relation

$$a_0^P = \sum_{\ell=1}^{6} a_\ell^P \tag{11.9}$$

and Eq. 11.1. For the first rebalancing region (region 1), the coefficients

$$A_1^1 = 0$$

and

$$A_0^1 = A_2^1 .$$

For the last rebalancing region, no pressure correction is desired in the neighboring cells. In this case,

$$\Delta P_{N+1} = 0$$

and A_2^N can be evaluated from the relation in Eq. 11.8.

We now have N equations of the same form as Eq. 11.7 for N rebalancing regions. These equations can be solved for pressure corrections ΔP by any Gaussian elimination-type procedure. In COMMIX we are using the tridiagonal matrix algorithm to solve these equations.

11.4 REMARKS ON REBALANCING

It is important to note that the pressure field P obtained here, after the addition of corrections ΔP to P^*, is not the final solution, because the pressure field obtained with mass rebalancing satisfies only the mass conservation of rebalanced regions, and not of all fluid cells. Rebalancing makes only large-scale corrections. To satisfy the mass convergence of all fluid cells, we must solve a pressure equation for each cell. As rebalancing makes the large-scale final corrections rapidly by direct solution, it reduces the number of iterations required for the solution of the pressure equation.

12. SOLUTION PROCEDURES

12.1 INTRODUCTION

COMMIX performs thermal-hydraulic calculations by marching in time. The values of the dependent variables at a given time step, say n, are known and the values of the dependent variables at time step n+1 are calculated. By repeating this procedure, we determine thermal-hydraulic conditions for the desired time span. The overall flow chart of the program is shown in Fig. 12.1.

For steady-state calculation, the same procedure is followed. We start with an initial guess and continue the marching-in-time process until the values of all dependent variables stop varying with time. The time step size for the implicit steady-state calculation can be many times as large as the Courant time step criterion.

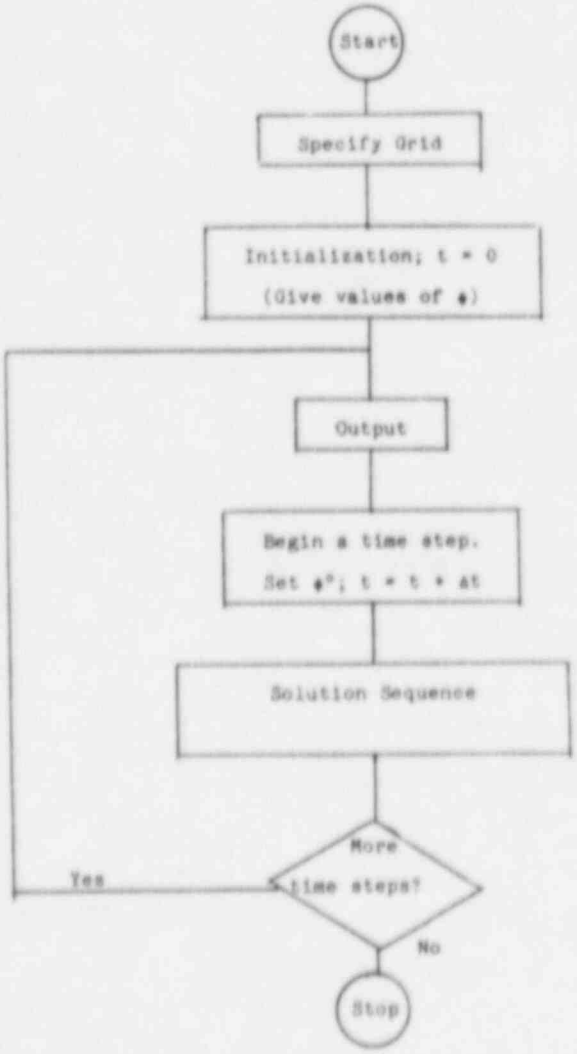

Fig. 12.1 COMMIX-1B Flow Chart

In COMMIX, we have provided two options for the time-step size.

- The user-desired time step size (the details of this input are given in the Input Description in Volume II), and
- The automatic time step option.

In the automatic time-step option, the time step size is evaluated based on the Courant condition:

$$\Delta t = C_1 \Delta t_C \ , \tag{12.1}$$

where C_1 is the user-prescribed coefficient and Δt_C is the time step size evaluated from the Courant condition. The Courant time step size is defined as the minimum time required for fluid to be convected through a cell. In COMMIX, each computational cell is examined with respect to all three component directions to calculate the Courant time step size.

In COMMIX, we have two distinct solution sequences--the semi-implicit and the fully implicit. However, the solution procedure option has been implemented in such a way that a user can switch from one solution scheme to another at any time during the transient simulation of a problem.

Both the solution-sequence options are combined into one formulation through an implicit parameter α. The solution procedure option becomes semi-implicit when $\alpha = 0$ and fully implicit when $\alpha = 1$. Therefore, in principle, we can say that the formulation covers a full range from semi-implicit ($\alpha = 0$) to fully implicit ($\alpha = 1$). But as we have not performed enough testing at this time, we do not recommend any intermediate value of α--only $\alpha = 0$ and $\alpha = 1$.

12.2 SEMI-IMPLICIT SOLUTION SEQUENCE ($\alpha = 0$)

The semi-implicit solution sequence ($\alpha = 0$) used in the original version of COMMIX-1 is based on a modification of the ICE procedure developed at Los Alamos. The solution sequence is called semi-implicit because the old time values of some variables and parameters are assumed to prevail throughout the time-step period.

Because of the semi-implicit nature of the formulation, we are required to limit the size of the time step to obtain a stable solution. The time step size has to satisfy the Courant condition, and must be less than the time sizes associated with all explicitly formulated terms. Thus

$$\Delta t < \Delta t_{Courant} \sim \left(\frac{\Delta x_i}{u_i} \right)_{min} \ , \tag{12.2}$$

$$\Delta t < \Delta t_{vis} \sim C \left(\frac{\rho \Delta x_i^2}{\mu} \right)_{min} \ , \tag{12.3}$$

$$\Delta t < \Delta t_{cond} \sim C \left(\rho \frac{\Delta x_i^2}{\Gamma_h} \right)_{min} , \qquad (12.4)$$

etc. Here, subscripts "Courant", "vis", and "cond" refer to time scales associated with Courant condition, viscous diffusion, and thermal diffusion, respectively, and subscript i refers to the three coordinate directions. The coefficient C has a value between 1/6 and 1/2. In most cases, the Courant limitation is the determining factor; Δt_{vis} and Δt_{cond} are usually much larger. The viscous-diffusion and thermal-diffusion time scales may require consideration only in the case of highly turbulent flow.

Although the semi-implicit scheme has time step limitations, the solution of the equations requires less computer running time per time step. So for fast transients, where the interest is in obtaining information at small time intervals, the semi-implicit sequence works very well.

The details of the semi-implicit solution sequence are shown in Table 12.1.

12.3 FULLY IMPLICIT (SIMPLEST-ANL) SOLUTION SEQUENCE (α = 1)

For long and slowly varying transients, it was found that the semi-implicit procedure, because of its time step size limitation, required a great deal of computer running time. To eliminate this restriction, we have developed and implemented an alternative, a new fully implicit solution option.

The fully implicit solution sequence, named SIMPLEST-ANL, is based on a modification to the SIMPLE/SIMPLER procedures developed at the Imperial College in England. SIMPLEST-ANL requires less computer storage than SIMPLER and still has comparable or better computing efficiency. Because this procedure relieves many of the time step size limitations and permits use of larger time step sizes, it is most suitable for steady-state and slowly varying transient calculations. Rapid-transient situations still are most efficiently calculated using the semi-implicit formulation.

The procedure is called fully implicit because the new-time values of all variables are assumed to prevail during the time step. We therefore need an iterative procedure. Each outer* iteration loop yields a better estimate of the advanced-time values of all variables. When the change in all variable values becomes small from one outer iteration to the next, the iterative process is considered converged and the last outer iterate values are used for the advanced time variable values. The solution sequence for the fully implicit formulation is a seven step iterative process, as shown in Table 12.2.

---

*Here, outer iteration loop is used to distinguish it from the inner iterative loops used for the solution of a specific variable equation, e.g., the iterative loop (successive overrelaxation procedure) used for the solution of pressure equations is considered as an inner iterative loop.

Table 12.1 Algorithm of the Semi-Implicit (Modified ICE) Solution Scheme ($\alpha = 0$)

1. Calculate momentum coefficients using old-time step values of u, v, and w:

$$\hat{\phi},\ d^{\phi}\ ;\ (\phi = u,\ v,\ w)\ .$$

2. Calculate pressure equation coefficients using $\hat{\phi}$, d^{ϕ}:

$$a_0^P,\ a_\ell^P,\ b_0^P\ .$$

3. Solve pressure equation for new-time pressure P^{n+1}:

$$a_0^P P_0 - \sum a_\ell^P P_\ell - b_0^P = 0\ .$$

4. Calculate new-time velocities using

$$\phi = \hat{\phi} - d^{\phi}\,\Delta P\ ;\ (\phi = u,\ v,\ w)$$

and new-time values of pressure.

5. Calculate energy equation coefficient using new-time values of velocities:

$$a_0^h,\ a_\ell^h,\ b_0^h$$

6. Calculate new-time enthalpy h^{n+1}:

$$h_0 = \sum a_\ell^h h_\ell^n + b_0^h\ /a_0^h\ .$$

Table 12.2 Fully Implicit (SIMPLEST-ANL) Solution Sequence ($\alpha = 1$)

1. Calculate velocity-pressure relation coefficients from the previous iterate values of u, v, and w:

   $\hat{\phi}$, d^{ϕ}; (ϕ = u, v, w).

2. Calculate pressure equation coefficients using $\hat{\phi}$, d^{ϕ}:

   a_0^P, a_ℓ^P, b_0^P .

3. Solve pressure equation for new-time, new-iterate pressure P:

   $$a_0^P P_0 = \sum a_\ell^P P_\ell + b_0^P$$

4. Calculate new-time, new iterate velocities u, v, w from velocity-pressure relations:

   $$\phi = \hat{\phi} - d^{\phi} \Delta P \; ; \; (\phi = u, v, w)$$

5. Calculate energy equation coefficients using new-time, new-iterate velocities:

   a_0^h, a_ℓ^h, b_0^h .

6. Solve energy equation for new-time, new-iterate enthalpy h:

   $$a_0^h h_0 = \sum a_\ell^h h_\ell + b_0^h \; .$$

7. Check for convergence of u, v, w, h; if not converged, return to Step 1.

The major differences between the semi-implicit and fully implicit solutions are discussed in Section 13.

12.4 SUCCESSIVE OVERRELAXATION (SOR) ITERATIVE SOLUTION

Both solution procedures, semi-implicit and fully implicit, require solving a set of algebraic equations. In COMMIX-1B, the solution of the equations is achieved by the successive overrelaxation procedure.

The successive overrelaxation (SOR) type iteration scheme uses one pass through the computational cell domain. As each cell is visited, the residual of the ϕ-equation to be solved is computed, using the most recent values of the surrounding ϕ's. In this way, an updated value of ϕ is used if the neighboring cell has been visited earlier in the pass, and a previous iterate value of ϕ is used if the neighboring cell is to be visited later. Immediately after the residual of the ϕ equation for a cell under consideration is computed, the ϕ is adjusted in that cell before the computation proceeds to the next cell in the pass.

After all cells have been visited, the convergence is checked and if it has been achieved, then the iterative process terminates; if convergence has not been achieved, another single-pass iteration is performed.

The SOR scheme requires the relaxation parameter ω to be between 0 and 2. Generally, convergence can be achieved in fewer iterations than for the Jacobi scheme. Because ω can have values greater than 1.0, it is termed overrelaxation. The optimum value of the relaxation parameter is generally geometry- and problem-dependent; usually, it is between 1.4 and 1.8.

12.5 MASS CONVERGENCE CRITERION

In theory, the pressure equation (Eq. 5.5) is considered solved when mass residue δ is equal to 0 for all cells. Because Eq. 5.5 is solved iteratively, this will, in general, never be true. Instead, a nonzero mass residual δ is computed for every cell and a maximum is determined as $|\delta|_{max}$. The iterative process continues until either a maximum specified number of iterations have been performed or the maximum mass residual falls below the convergence criterion.

$$|\delta|_{max} < \text{convergence criterion.} \tag{12.5}$$

The mass convergence criterion is calculated using the relation

$$\text{Convergence criterion} = \varepsilon_1 * \left[\left(\frac{\rho \gamma_i u_i}{\gamma_v \Delta x_i}\right)_{max}\right] + \varepsilon_2 \quad , \tag{12.6}$$

where ε_1 and ε_2 are the input convergence constants and subscript i stands for three coordinates.

12.6 ITERATION CRITERIA

The seventh step in the fully implicit scheme is to check for convergence. Here, the changes from one iteration to the next, in all ϕ's, are

checked against the convergence criteria. The mass convergence criterion is discussed in Sec. 12.5. The iteration criteria are satisfied when

$$\frac{|\phi^{new} - \phi^{old}|_{max}}{\phi^{old}} < \varepsilon_3 ,$$

$$\frac{|u^{new} - u^{old}|_{max}}{V_{max}} < \varepsilon_3 ,$$

$$\frac{|v^{new} - v^{old}|_{max}}{V_{max}} < \varepsilon_3 , \text{ and}$$

$$\frac{|w^{new} - w^{old}|_{max}}{V_{max}} < \varepsilon_3 \qquad (12.7)$$

simultaneously. Here, V_{max} is the maximum velocity magnitude, ε_3 is the user input convergence parameter, and the superscripts new and old refer to current and previous iterate values. If any one of these convergence criteria is not met, the sequence is repeated from Step 1. The solution proceeds through the sequence until it converges or the specified maximum number of iterations have been performed.

13. MAJOR DIFFERENCES BETWEEN SOLUTION PROCEDURES

13.1 FULLY IMPLICIT SIMPLEST-ANL AND SIMPLE/SIMPLER

Although the fully implicit procedure is derived from the SIMPLE/ SIMPLER procedure, there are some major differences in the solution algorithms. To illustrate the major differences we are presenting the solution algorithms of SIMPLE and SIMPLER procedures in Tables 13.1 and 13.2 If we compare these algorithms with that of our fully implicit scheme (SIMPLEST-ANL, Table 12.2), we see that in our SIMPLEST-ANL scheme

- The pressure correction equation is not used, and
- The velocity field is obtained from the momentum equation in the form

$$\phi = \hat{\phi} - d^{\phi} \Delta P; \quad (\phi = u, v, w) \tag{13.1}$$

instead of the momentum equation being solved in the form

$$a_0^{\phi}\phi_0 = \sum_{\ell} a_{\ell}^{\phi}\phi_{\ell} + b_0^{\phi} - a_0 d^{\phi} \Delta p. \tag{13.2}$$

Because of these two major differences, SIMPLEST-ANL requires less computer storage while still maintaining comparable or better computational efficiency. This is illustrated in Table 13.3.

13.2 FULLY IMPLICIT SIMPLEST-ANL ($\alpha = 1$) AND SEMI-IMPLICIT ($\alpha = 0$)

The major differences between the semi-implicit (Table 12.1) and fully implicit SIMPLEST-ANL (Table 12.2) procedures are presented in Table 13.4.

We can see from this table that the fully implicit scheme is preferable for the solution of

- Steady-state, and
- Slow-transient cases.

The semi-implicit solution procedure, due to its simplicity, is beneficial when we are simulating fast transients.

Although we are comparing here semi-implicit and fully implicit procedures, it should be noted that both these procedures are combined into one formulation in COMMIX-1B. It is the value of the implicitness parameter in the formulation that determines whether the procedure to be used is semi-implicit, fully implicit, or between the two.

Table 13.1 Algorithm of the SIMPLE Solution Scheme

1. Calculate coefficients in the momentum equations using previous iterate values of u, v, w:

$$a_0^\phi,\ a_\ell^\phi,\ b_0^\phi,\ d^\phi;\ (\ell = 1, \cdots 6;\ \phi = u, v, w).$$

2. Solve for velocities using these coefficients and pressure field P:

$$a_0^\phi \phi_0 - \sum_\ell a_\ell^\phi \phi_\ell - b_0^\phi + a_0^\phi d^\phi \Delta P = 0;\ (\phi = u, v, w).$$

3. Calculate coefficients in the pressure correction (P') equation:

$$a_0^{P'},\ a_\ell^{P'},\ b_0^{P'}\ .$$

4. Solve for pressure correction field P':

$$a_0^{P'} P_0' - \sum_\ell a_\ell^{P'} P_\ell' - b_0^{P'} = 0\ .$$

5. Update pressure and velocity fields:

$$P = P + P'\ .$$

$$\phi = \phi - d^\phi \Delta P;\quad (\phi = u, v, w).$$

6. Calculate coefficients in the energy equation:

$$a_0^h,\ a_\ell^h,\ b_0^h\ .$$

7. Solve for h:

$$a_0^h h_0 - \sum_\ell a_\ell^h h_\ell - b_0^h = 0.$$

8. Check velocities u, v, w, and energy h for convergence; if not converged, return to Step 1.

Table 13.2 Algorithm of the SIMPLER Solution Scheme

1. Calculate momentum coefficients in using previous iterate values of u, v, w:

$$a_0^\phi,\ a_\ell^\phi,\ b_0^\phi,\ d^\phi;\ (\ell = 1, \cdots 6;\ \phi = u, v, w).$$

2. Calculate coefficients in the pressure:

$$a_0^P,\ a_\ell^P,\ b_0^P\ .$$

3. Solve pressure correction for P:

$$a_0^P P_0 - \sum_\ell a_\ell^P P_\ell - b_0^P = 0\ .$$

4. Using this pressure and the momentum coefficients, solve the momentum equation for u, v, w:

$$a_0^\phi \phi_0 - \sum_\ell a_\ell^\phi \phi_\ell - b_0^\phi + a_0^\phi d^\phi\ \Delta P = 0;\ (\phi = u, v, w).$$

5. Calculate the $b_0^{P'}$ coefficients in the pressure correction equation.

6. Using the a_0^P and a_ℓ^P coefficients of the pressure equation $a_0^{P'} = a_0^P$; $a_\ell^{P'} = a_\ell^P$ and $b_0^{P'}$, solve for the pressure correction P':

$$a_0^{P'} P_0' - \sum_\ell a_\ell^{P'} P_\ell' - b_0^{P'} = 0\ .$$

7. Updated velocities:

$$\phi = \phi - d^\phi\ \Delta P;\quad (\phi = u, v, w).$$

8. Calculate energy equation coefficients:

$$a_0^h,\ a_\ell^h,\ b_0^h\ .$$

9. Solve for h:

$$a_0^h h_0 - \sum_\ell a_\ell^h h_\ell - b_0^h = 0.$$

10. Check for convergence of u, v, w, h; if not converged, return to Step 1.

Table 13.3 Comparison of Computer Storage Requirements

Scheme	Minimum Number of Matrix Coefficients Required per Cell	Number of Matrix Inversions	Coefficient Storage for 2000 Cell Problem Assuming 8 Byte Variables
SIMPLE	14	5 I*	224K
SIMPLER	38	6 I	608K
Fully Implicit (SIMPLEST-ANL)	14	2 I	224K
Semi-Implicit (Modified ICE)	14	1	224K

*I = Number of outer iterations.

13.3 CONCLUDING REMARKS

The fully implicit scheme (SIMPLEST-ANL) is similar to the SIMPLE/SIMPLER procedures but requires less computer storage than SIMPLER with comparable or better computing efficiency. The semi-implicit and fully implicit (SIMPLEST-ANL) schemes of COMMIX-1B both have advantages and limitations.

- The semi-implicit scheme:
  - requires less computer time per time step,
  - has time step size limitations, and
  - is advantageous for simulations of fast transients.
- The fully implicit (SIMPLEST-ANL) scheme:
  - requires more computer time per time step,
  - has no time step size limitaions, and
  - is advantageous for simulations of steady-state and slow transients.

In COMMIX-1B, we have provided an implicitness parameter that permits use of desired implicitness; from semi-implicit to fully implicit. Further, the option has been implemented in such a manner that a user can switch from one implicitness to another at the completion of any time-step during simulations.

Table 13.4 Major Differences between Semi-Implicit and Fully Implicit Procedures

Equation	Semi-Implicit	Fully Implicit (SIMPLEST-ANL)
Conservation of mass	$a_0^P P_0 = \sum_\ell a_\ell^P P_\ell^n + b_0^P$	$a_0^P P_0 = \sum_\ell a_\ell^P P_\ell + b_0^P$
	Coefficients are calculated from previous time-step values.	Coefficients are calculated from previous iterate values.
Conservation of momentum (ϕ = u, v, w)	$a_0^\phi \phi = \sum_\ell a_\ell^\phi \phi_\ell^n + b_0^\phi - d^\phi \Delta P$	$a_0^\phi \phi = \sum_\ell a_\ell^\phi \phi_\ell + b_0^\phi - d^\phi \Delta P$
	Neighboring velocities are at old-time values.	Coefficients and neighboring velocities at previous iterate values.
	Uses new-time values of pressure obtained from conservation of mass.	Direct calculation of ϕ after solution of pressure equation.
Conservation of energy	$a_0^h h = \sum_\ell a_\ell^h h_\ell^n + b_0^h$	$a_0^h h_0 = \sum_\ell a_\ell^h h_\ell + b_0^h$
	Explicitly calculated coefficients have new-time values of velocity. Neighboring enthalpies are at old-time vaues.	Coefficients use current iterate values of velocities. Neighboring enthalpies are at previous iterate values.
		Iteration continued until all mass, momentum, and energy equations are conserved.
Time-step limitation	Yes; unstable for large time-step size.	No; quite stable for large time step size.

Although, as mentioned above, both the semi-implicit and fully implicit schemes have advantages and limitations, we advocate the use of the fully implicit scheme for the following reasons:

- In most simulations, either a transient itself is slowly varying, or a major part of the transient is slowly varying.
- We have found significant savings in computer running time during many of our simulations with the fully implicit scheme. To illustrate this, we present the results of three problems in Table 13.5.

Table 13.5 Comparison of Computer Running Times

Problem	Computer Running Time	
	Semi-Implicit	Fully-Implicit (SIMPLEST-ANL)
German 7-pin hexagonal fuel assembly		
Steady-state	70 sec	31 sec
9-sec transient	56 min, 11 sec	2 min, 48 sec
CRBR upper plenum		
Steady-state	6 min, 3 sec	1 min, 40 sec
Blockage in hexagonal fuel assembly		
Steady-state	3000 min	10 min, 35 sec

14. DISCUSSION

14.1 UNIQUE FEATURES OF COMMIX

All the important features of COMMIX-1B are briefly mentioned or described in detail in the text, . There are several features that are unique and distinct from other computer codes. These features significantly expand the capabilities of COMMIX. Five of these features are discussed here. They are:

- Geometry-modeling,
- New porous-medium formulation,
- Turbulence modeling,
- Volume-weighted skew-upwind differencing, and
- Two solution options.

14.1.1 Geometry Modeling

Unique features related to geometry modeling are the following:

- **Identification of a computational cell by a cell number instead of its (i,j,k) location:** All "do loops" are performed with the cell number as an index instead of with the conventional directional indices i,j,k. Consequently, the storage requirement depends on the total number of computational cells and not on the dimension of IMAX * JMAX * KMAX. This is illustrated through a simple example in Fig. 14.1.

- **Use of surface arrays to store boundary values at the boundary surface:** We do not use fictitious boundary cells to store boundary values.

- **Extra surface to model irregular geometry:** An irregular surface is defined as a surface that is at an angle to a grid plane. An irregular surface is an additional surface to the six normal surfaces (parallel to grid planes) of a computational cell. We also account for heat transfer in the energy equation and shear stress in the momentum equation from this seventh irregular surface, in addition to those from the six normal surfaces. This treatment of an irregular surface as an additional surface facilitates true and proper modeling of a complex irregular geometry.

14.1.2 New Porous-Medium Formulation

In COMMIX, we use four parameters (volume porosity, directional surface porosity, distributed resistance, and distributed heat source) to model a flow domain with solid objects. The inclusion of the parameter directional surface porosity is new. This inclusion has greatly facilitated the modeling of flow and heat transfer in an anisotropic medium and has improved the resolution and accuracy of numerical modeling.

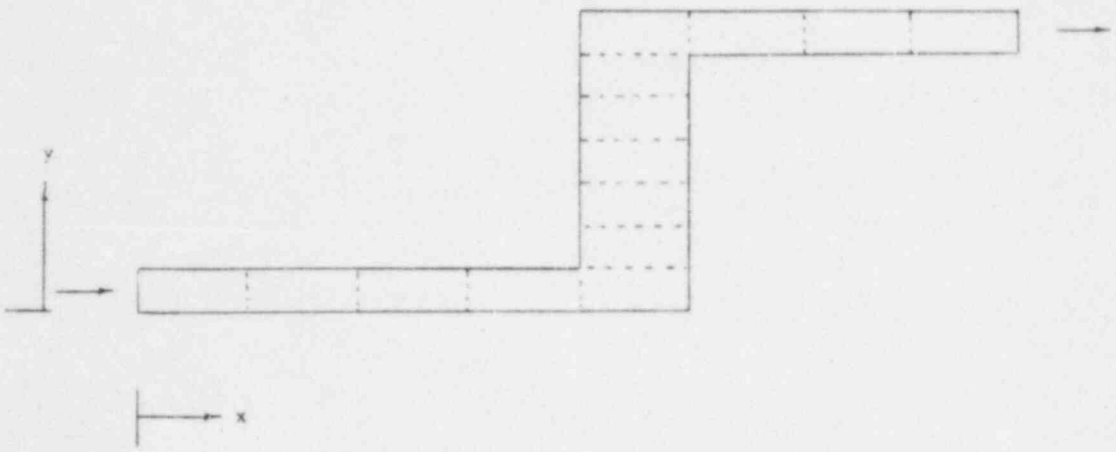

IMAX = 8

JMAX = 7

Total number of cells = 14

Conventional storage requirements = 8 x 7 = 56

Storage requirement in COMMIX-1A = 14

Fig. 14.1 Grid Arrangement in a Two-Dimensional Piping System to Illustrate Storage Requirements in COMMIX-1B

The new porous-medium formulation has been rigorously derived[40,47] from the governing partial differential conservation equation. The derivations use the local volume averaging procedure. The resulting equations are more general. If we substitute directional surface porosity equal to the volume porosity in the formulation, the equations simplify to the same as for the conventional porous-medium formulation. Furthermore, if we set volume porosities and directional surface porosities to unity, and distributed resistances and heat sources to zero, then the new porous-medium formulation simplifies to the same as for the continuum formulation. We can therefore say that the continuum formulation is a subset of the conventional porous-medium formulation, which is a further subset of the new porous-medium formulation.

It is worth stressing here that the porous-medium formulation has provided a wide range of applicability to the COMMIX code. We can now analyze

- A single-component system, such as
  - A fuel assembly,
  - Reactor plenum, and
  - Piping system,

as well as

- A multicomponent system, such as
  - Vessel,
  - Downcomer and lower plenum, and
  - Cold leg, high-pressure injection system, downcomer

in sufficient detail.

14.1.3 Turbulence Modeling

Almost all flows in an engineering system are turbulent. For a computer code to realistically simulate a flow process, the code must account for the effects of turbulence. COMMIX-1B accounts for the effects of turbulence through

- Distributed resistance modeling and
- Turbulence modeling.

For many geometries and flow conditions, the experimentally verified resistance correlations, which include the effects of turbulence, are available in the literature, e.g., flow in a tube, flow normal to a rod bundle, flow through an orifice, etc. For such regions of a system, we employ appropriate correlations through distributed resistance modeling and can provide a realistic account of turbulence.

For geometries where correlations are not available, we have provided the following turbulence models as available options in COMMIX-1B:

- Constant turbulent diffusivity model,
- Zero-equation model,
- One-equation (k) models, and
- Two-equation (k-ϵ) model.

With several turbulence model options and the distributed resistance model, one can perform a very realistic simulation of turbulent flow in any flow geometry system.

14.1.4 Options for Reducing Numerical Diffusion

In the finite-difference formulation, the even derivative terms of the truncation error have a general tendency to reduce the gradients, producing what is known as numerical diffusion. For high Peclet number flows and for flow parallel to grid lines, numerical diffusion is generally small. However, for multidimensional flow oblique to grid lines, the numerical diffusion can be high.

To provide a more realistic and accurate solution, we have provided two options:

- Skew-upwind differencing, and

- Volume-weighted skew-upwind differencing

that reduce numerical diffusion for flows inclined to grid lines.

With these options, COMMIX-1B has the unique capability of performing multidimensional flow simulation with reduced numerical diffusion.

14.1.5 Two Solution Option

In COMMIX, we have two solution options

- Semi-implicit solution algorithm, and

- Fully implicit solution algorithm.

The semi-implicit solution scheme, based on the ICE technique, is ideally suitable for fast transients where our interest is in examining flow and temperature distributions at small time intervals.

The fully implicit scheme, based on the SIMPLE algorithm, on the other hand, is ideally suitable for slow transients and steady-state problems. Here, we can use larger time step sizes without affecting stability and thus save computer running time.

Both solution options have been implemented in such a way that a user can switch from one scheme to another during any part of the transient simulation.

14.2 CODE APPLICATION AND VALIDATION

The COMMIX-1B code has been tested and applied to a variety of problems. Detailed descriptions and numerical results of problems that we have analyzed are published as ANL technical reports or papers in technical journals. We have also compared numerical results with available experimental measurements. References for some major applications and validations are given below.

- **Piping System**

  Thermal-hydraulic transient in a pipe [2,15,17].

- **Fuel Assemblies**

  19-pin fuel assembly with power skew [2,5].
  19-pin fuel assembly with planar blockage [6,7].
  Loss of piping integrity transients in an LMFBR fuel assembly [9].
  Pretest prediction of the W-1 SLSF experiment [10].
  Flow-rundown transient in a 7-pin bundle [11,13].
  6MW P2 transient free-convection test [14].

- **Reactor Upper Plenum**

  CRBR upper plenum under thermal stratification condition [16].

- **Reactor Downcomer and Lower Plenum**

  Thermal-hydraulic mixing in the downcomer and lower plenum due to temperature and flow imbalances between the cold legs [8].

- **Cold-leg High-pressure Injection System and Downcomer**

  B&W/EPRI thermal mixing experiments for OCONEE1 PWR [22].

  Thermal and fluid mixing during high-pressure coolant injection [25].

  Thermal and fluid mixing for Creare scaled experiments and generic full-scale PWRs [34].

- **Reactor Vessel**

  Steady-state/transient in-vessel analysis of FFTF [23,24,26].
  Steady-state/transient in-vessel analysis of EBR-II [28,29].
  LMFBR decay heat removal system [27].

- **Other Areas**

  Heat loss modeling for the ANL solar pond [81].

  Cross-flow between parallel channels connected by a narrow lateral slot [19].

  Atmospheric fluidized bed mixing analysis.

We can see from this list of applications that COMMIX-1B has a wide range of applicability.

Our future plan for COMMIX-1B is to continue to perform representative analyses, validate the models, improve the code, and augment its capabilities.

14.3 FUTURE DEVELOPMENTS

Numerical simulation programming is a very active and developing field. New physical models and better solution procedures are expected to emerge. Like all other computer codes, COMMIX will, therefore, remain a dynamic code. Here we are listing the possible developments that, if incorporated, will further augment the capabilities of COMMIX.

14.3.1 Single-phase Development

New single-phase capabilities that are desirable for future implementation are:

Free-Surface Boundary Condition: Currently, COMMIX-1B does not have a free-surface boundary condition option. With implementation of this additional capability, one could apply the COMMIX computer code to the analysis of free-surface problems, e.g., pool-type reactors.

Regionwise Coordinate System: Although the porous-medium formulation of COMMIX-1B permits modeling of any complex geometry, there are instances in which it appears that a geometry could be

modeled better if COMMIX had a regionwise coordinate system option. We define the regionwise coordinate system as a capability wherein one can use different coordinate systems for different regions of a system. For example, a rectangular duct connected to a cylindrical vessel can be better modeled using a Cartesian coordinate system for the duct and a cylindrical coordinate system for the vessel. So a possible future plan could be to develop and implement a regionwise coordinate system capability in COMMIX.

Transient Three-dimensional Heat Conduction Equation for Solid Structures: At present in COMMIX-1B, we solve the one-dimensional transient heat conduction equation to account for thermal inertia of submerged solid structures. We are therefore assuming that heat conduction in an axial direction is negligible. In most analysis, this assumption is a valid assumption. But to extend the range of applicability, one must implement an option that will permit use of a 3-D heat conduction equation for structures where axial heat conduction is not negligible.

Marching Solution for Partially/Fully Parabolic Flow: In the case of partially/fully parabolic flow, many variables (e.g., temperature) are governed only by the upstream conditions. For such cases, only a two-dimensional array is required. One can also employ a marching solution procedure, which is simpler and faster in computer running time than any conventional solution procedure for elliptic flows. Therefore, a savings in computer storage and running time would be possible if an option (capability) of the marching solution technique were available in COMMIX for partially/fully parabolic flows.

Vectorizing for Supercomputers: Recently there has been a significant development in the area of vectorizing and parallel processing. These developments have increased the speed of computing by several orders of magnitude. Vectorizing COMMIX for adaptation to recent supercomputers will enhance the speed of COMMIX simulations.

Input/Output Processing: COMMIX is a very large computer code with a wide range of generalities and applicabilities. Consequently, input preparation and output processing many times become very tedious tasks. Further developments and efforts need to be made to make COMMIX a more user friendly computer program.

14.3.2 Two-Phase Development

Concurrent with the development of the COMMIX-1B code, efforts have been made to develop a two-phase code (COMMIX-2)[82,83], using a two-fluid model and a homogeneous equilibrium model to analyze two-phase flows. The structure of COMMIX-2 is similar to that of COMMIX-1B with some additions or modifications pertinent to two-phase flow.

We have been successful in applying COMMIX-2 to several two-phase simulations.[84-88] However, more representative analyses and further development work are needed to ensure that

- The solution algorithm is stable for the whole range of applications,
- The convergence rate is sufficient to make numerical simulation favorable, and
- The computer storage requirement is reasonable.

Accordingly, the future plans in two-phase-development work will be to

- Perform more analysis,
- Improve the solution procedure, and
- Implement improved physical models

if development efforts are continued.

ACKNOWLEDGEMENTS

Developing an operational code with such a wide range of applicability requires several years of cooperative effort, and the technical and moral support of many individuals.

We are indebted to all COMMIX users for whom this document is written. Their questions, suggestions, and criticisms have served in making COMMIX-1B a user-oriented computer code.

We acknowledge our special thanks to all our colleagues in the Analytical Thermal Hydraulic Research Program and specifically to Drs. B. C-J. Chen, H-N. Chi, and R. W. Lyczkowski for their contributions in the development, model improvement, and analysis work. We also acknowledge our thanks to Drs. W. L. Baumann and M. Bottoni of KfK-Germany, Drs. B. C. Cha, E. Gelbard, and G. K. Leaf of ANL, and to Profs. B. T. Chao and S. L. Soo of the University of Illinois-Urbana, and to Prof. A. Schor of MIT, for their stimulating discussions and for their constructive comments; and to Mrs. S. A. Moll for her patience, attention to detail, and typing of all reports, including this one.

The development of a code is never complete without validation. Here, we would like to express our sincere thanks to Drs. J. Chao, J. Kim, W. Loewenstein, and B. Sehgal of EPRI, and to H. Alter of the U. S. Department of Energy for providing support, guidance, and encouragement in the validation work.

Finally, COMMIX-1B would never have been developed without the guidance, faith, and support of Drs. R. T. Curtis and C. N. Kelber, and Mr. P. M. Wood, of the United States Nuclear Regulatory Commission.

REFERENCES

1. H. M. Domanus, R. C. Schmitt, W. T. Sha, and V. L. Shah, "COMMIX-1A: A Three-Dimensional Transient Single-Phase Computer Program for Thermal Hydraulic Analysis of Single and Multicomponents Systems: Vol. I User's Manual, and Vol. II Assessment and Verification," NUREG/CR-2896, ANL-82-25 (Dec. 1983).

2. W. T. Sha, H. M. Domanus, R. C. Schmitt, J. J. Oras, and E. I. H. Lin, "COMMIX-1: A Three-Dimensional Transient Single-Phase Component Computer Program for Thermal-Hydraulic Analysis," NUREG/CR-0785, ANL-77-96 (Sept. 1978).

3. W. T. Sha, H. M. Domanus, R. C. Schmitt, and K. Chen, "Three-Dimensional Numerical Simulation of LMFBR Outlet Plenum Mixing," Trans. Am. Nucl. Soc., 26, pp 434-435 (June 1977).

4. H. M. Domanus, R. C. Schmitt, and W. T. Sha, "Numerical Results obtained from the Three-Dimensional Transient Single Phase Version of the COMMIX Computer Code," NUREG-0355, ANL-CT-78-3 (Oct. 1977).

5. H. M. Domanus, R. C. Schmitt, and W. T. Sha, "Three-Dimensional Numerical Simulation of a 19-Pin LMFBR Fuel Assembly in a Hexagonal Duct," Trans. Am. Nucl. Soc. 28, pp. 540-543 (June 1978).

6. H. M. Domanus and W. T. Sha, "Numerical Results for a Hexagonal Fuel Assembly with a Planar Blockage using the COMMIX-1A Computer Code," NUREG-CR-0483, ANL-CT-79-8 (Sept. 1978).

7. H. M. Domanus and W. T. Sha, "Three-Dimensional Numerical Simulation of Flow Blockage in a 19-Pin LMFBR Fuel Assembly," Trans. Am. Nucl. Soc. 30, pp. 534-535 (Nov. 1978).

8. W. T. Sha, H. M. Domanus, and R. C. Schmitt, "Some Numerical Results obtained from the Single-Phase Version of the COMMIX Code," Proc. of IAEA Specialists' Meeting on Thermodynamics of FBR Fuel Assemblies under Nominal and Non-Nominal Operating Conditions, held in Karlsruhe, West Germany (Feb. 2-7, 1979).

9. H. M. Domanus, M. J. Chen, and W. T. Sha, "Analysis of a Loss-of-Piping Integrity Transient in an LMFBR Fuel Assembly," Trans. Am. Nucl. Soc., 32, pp. 827-829 (June 1979).

10. H. M. Domanus, M. J. Chen, and W. T. Sha, "Pretest Prediction of the W-1 SLSF Experiment using the COMMIX-1A Computer Code," NUREG/CR-0816, ANL-CT-79-33 (May 1979).

11. H. M. Domanus, M. J. Chen, and W. T. Sha, "Simulation of a 7-Pin Bundle during a Flow-rundown Transient," Trans. Am. Nucl. Soc., 33, pp. 630-632 (Nov. 1979).

12. W. T. Sha, H. M. Domanus, R. C. Schmitt, J. J. Oras, and E. I. H. Lin, "A New Approach for Rod-Bundle Thermal-Hydraulic Analyses," Proc. of International Meeting on Nuclear Power Reactor Safety, Brussels, Belgium, October 16-19, 1978, Nuclear Technology, 46, pp. 268-280 (Dec. 1979).

13. H. M. Domanus, M. J. Chen, and W. T. Sha, "Computational Results for a 7-Pin Hexagonal Fuel Assembly during a Flow Rundown Transient using the COMMIX-1A Computer Code," NUREG/CR-1285, ANL-CT-80-10 (Jan. 1980).

14. H. M. Domanus, M. J. Chen, T. M. Kuzay, and W. T. Sha, "Numerical Simulation of the 6MW P2 Transient Free Convection Test using the COMMIX-1A Computer Code," Proc. of the Specialists' Meeting on Decay Heat Removal and Natural Convection in FBRs (Feb. 1980).

15. M. J. Chen, H. M. Domanus, and W. T. Sha, "Simulation of a Thermohydraulic Transient in a Pipe using the COMMIX-1A Computer Code," NUREG/CR-1323, ANL-CT-80-15 (Feb. 1980).

16. H. M. Domanus and W. T. Sha, "Simulation of the CRBR Upper Plenum under Thermal Stratification Conditions," Trans. Am. Nucl. Soc. 34, pp. 884-887 (June 1980).

17. M. J. Chen, H. M. Domanus, and W. T. Sha, "Numerical Thermal Hydraulic Simulation of an LMFBR Pipe during a Flow Coastdown," Trans. Am. Nucl. Soc. 35, pp. 673-674 (Nov. 1980).

18. H. M. Domanus, V. L. Shah, and W. T. Sha, "Applications of the COMMIX Code using the Porous Medium Formulation," Nucl. Engr. & Des. (Special Issue on LMFBR Single-Phase Rod Bundle Thermal Hydraulics) (Dec. 1980).

19. H. P. Fohs, R. W. Lyczkoswki, and W. T. Sha, "A Three-Dimensional Simulation of Diversion Cross-Flow between Two Parallel Channels Connected by a Narrow Lateral Slot using the COMMIX-1A Computer Program," ANL-CT-81-34 (Oct. 1981).

20. H. M. Domanus and W. T. Sha, "Numerical Simulation of Combined Natural and Forced Convection during Thermal Hydraulic Transients," Proc. of the 74th Annual Meeting of the AIChE (Nov. 1981).

21. R. W. Lyczkowski, H. M. Domanus, R. C. Schmitt, W. T. Sha, J. H. Kim, and K. H. Sun, "Prediction of Thermal Stratification in the Cold Leg of a PWR during a LOCA," Trans. Am. Nucl. Soc. 39, pp. 1057-1058 (Nov. 1981).

22. R. W. Lyczkowski, W. L. Baumann, H. M. Domanus, W. T. Sha, and J. H. Kim, "Analysis of B&W/EPRI Thermal Mixing Experiments for OCONEE1 PWR using COMMIX-1A," Trans. Am. Nucl. Soc. 39, pp. 1062-1063 (Nov. 1981).

23. S. P. Vanka, H. M. Domanus, and W. T. Sha, "COMMIX-1A Three-Dimensional In-Vessel Simulation of the FFTF Thermal Hydraulics," NUREG/CR-2535, ANL-CT-82-1 (Jan. 1981).

24. S. P. Vanka, H. M. Domanus, and W. T. Sha, "COMMIX-1A Three-Dimensional In-Vessel Simulation of the FFTF Transient Thermal Hydraulics," NUREG/CR-2773, ANL-CT-82-14 (July 1982).

25. R. W. Lyczkowski, J. R. Hull, C. C. Miao, H. M. Domanus, R. C. Schmitt, and W. T. Sha, "Three-Dimensional Modeling of Thermal and Fluid Mixing in PWR's during High Pressure Coolant Injection," Trans. Am. Nucl. Soc. 41, pp. 261-263 (June 1982).

26. S. P. Vanka, H. M. Domanus, and W. T. Sha, "Steady State Simulation of the FFTF In-Vessel Thermal Hydraulics," Trans. Am. Nucl. Soc. 41, pp. 703-706 (June 1982).

27. W. T. Sha, A. Amorosi, S. S. Borys, P. R. Huebotter, J. R. Hull, and R. M. Singer, "Three-Dimensional Analysis of LMFBR Decay Heat Removal System," Proc. of the Int. Topical Meeting on LMFBR Safety and Related Design and Operational Aspects, Lyon-Ecully, France (July 1982).

28. W. L. Baumann, H. M. Domanus, D. Mohr, W. T. Sha, R. C. Schmitt, and J. E. Sullivan, "EBR-II In-Vessel Natural-Circulation Analysis," NURFG/CR-2821, ANL-CT-82-19 (July 1982).

29. W. L. Baumann, H. M. Domanus, and W. T. Sha, "EBR-II In-Vessel Thermal-Hydraulic Transient Simulation using COMMIX-1A Computer Code," Trans. Am. Nucl. Soc. 43, pp. 499-501 (Nov. 1982).

30. W. T. Sha, W. L. Baumann, H. M. Domanus, R. C. Schmitt, and J. E. Sullivan, "In-Vessel Thermal Hydraulic Analysis," Proc. of IAHR Specialists Mtg. on Liquid Metal Thermal Hydraulics in Plena and Pipes, Sunnyvale, California (Jan. 1983).

31. W. T. Sha, "A Unified Approach for Thermal Hydraulic Numerical Simulation," Proc. of ASME Intl. Mtg. on Modeling and Simulation, Bermuda (Mar. 1983).

32. B. C-J. Chen, B. K. Cha, C. C. Miao, W. T. Sha, J. H. Kim, and B. K. H. Sun, "COMMIX-1A Analysis of Fluid and Thermal Mixing in a Model Cold Leg and Downcomer of a PWR," Submitted to Canadian Nuclear Society Numerical Methods in Nuclear Engineering Conference, Montreal Canada, September 6-9, 1983.

33. F. F. Chen, H. M. Domanus, and W. T. Sha, "Turbulence Modeling of Thermal and Fluid Mixing in PWRs during High Pressure Coolant Injection using COMMIX-1B," Submitted to Canadian Nuclear Society Numerical Methods in Nuclear Engineering Conference, Montreal Canada, September 6-9, 1983.

34. R. W. Lyczkowski, C. C. Miao, J. R. Hull, H. M. Domanus, R. C. Schmitt, and W. T. Sha, "Three-Dimensional Analysis of Thermal and Fluid Mixing for Creare Scaled Experiments and Generic Full-Scale PWR's," EPRI Interim Report RP-1749-2 (Sept. 1983).

35. F. F. Chen, H. M. Domanus, W. T. Sha, and V. L. Shah, "Turbulence Modeling in the COMMIX Computer Code," ANL-83-65 (March 1984).

36. C. C. Miao, R. W. Lyczkowski, G. K. Leaf, F. F. Chen, B. C. Cha, B. C-J. Chen, H. M. Domanus, W. T. Sha, and V. L. Shah, "A Volume-Weighted Skew-Upwind Difference Scheme in COMMIX," NUREG/CR-3505, EPRI NP-3547, ANL-83-66 (March 1984).

37. R. W. Lyczkowski, C. C. Miao, H. M. Domanus, J. R. Hull, W. T. Sha, and R. C. Schmitt, "Three-Dimensional Analysis of Thermal and Fluid Mixing in Cold Leg and Downcomer of PWR Geometries," EPRI NP-3321 (Dec. 1983).

38. W. T. Sha, H. M. Domanus, R. C. Schmitt, J. J. Oras, and E. I. H. Lin, "A New Approach for Rod-Bundle Thermal-Hydraulic Analysis," Proc. of the Int. Meeting on Nuclear Power Reactor Safety, Brussels, Belgium (Oct. 1978), Nuclear Technology, 46, pp. 268-290 (Dec. 1979).

39. W. T. Sha and B. T. Chao, "Conservation Equations for Finite Control Volume Containing Single-Phase Fluid with Fixed, Dispersed, and Heat Generating (or Absorbing) Solids," ANL-CT-79-42, NUREG/CR-0945 (July 1979).

40. W. T. Sha and J. C. Slattery, "Local Volume-Time Averaged Equations of Motion for Dispersed, Turbulent, Multiphase Flows," NUREG/CR-1491, ANL-80-51 (Nov. 1980).

41. W. T. Sha and B. T. Chao, "Local Volume-Averaged Transport Equations for Single-Phase Flow in Regions Containing Fixed, Dispersed Heat-Generating (or Absorbing) Solids," NUREG-CR-1969, ANL-80-124 (Apr. 1981).

42. W. T. Sha, "A New Porous Media Approach for Thermal Hydraulic Analysis," Trans. Am. Nucl. Soc. 39, pp. 510-512 (Nov. 1981).

43. W. T. Sha, B. T. Chao, and S. L. Soo, "Local Volume-Averaged Transport Equations for Multiphase Flow in Regions Containing Distributed Solid Structures," NUREG/CR-2354, ANL-81-69 (Dec. 1981).

44. W. T. Sha, B. T. Chao, and S. L. Soo, "Time Averaging of Local Volume-Averaged Conservation Equations of Multiphase Flow," ANL-83-49, NUREG/CR-3434 (July 1983).

45. W. T. Sha, B. T. Chao, and S. L. Soo, "Time-Averaging of Local Volume-Averaged Conservation Equations of Multiphase Flow," Proc. AIChE/ASME National Heat Transfer Conference, Seattle, Washington July 25-29, 1983.

46. W. T. Sha, B. T. Chao, and S. L. Soo, "Porous Media Formulation for Multiphase Flow with Heat Transfer," to be published in Nuclear Engineering and Design (Special Issue on LMFBR Two-Phase Rod Bundle Thermal Hydraulics - in Press) (1983).

47. W. T. Sha, B. T. Chao, and S. L. Soo, "Time- and Volume-Averaged Conservation Equations for Multiphase Flow, Part One: System without Internal Solid Structures," NUREG/CR-3989, ANL-84-66 (Dec. 1984).

48. F. H. Harlow and A. A. Amsden, "A Numerical Fluid Dynamics Calculation Method for All Flow Speeds," J. Computational Phys. 8, p. 197 (1971).

49. F. H. Harlow and A. A. Amsden, "Numerical Calculation of Multiphase Fluid Flow," J. Comp. Phys. 17, pp. 19-52 (1975).

50. F. H. Harlow and A. A. Amsden, "Flow of Interpenetrating Material Phases, J. Comp. Phys. 18, pp. 440-464 (1975).

51. S. V. Patankar, "Numerical Heat Transfer and Fluid Flow," Numerical Heat Transfer, Vol. 2, McGraw-Hill, New York (1979).

52. G. D. Raithby, "A Critical Evaluation of Upstream Differencing Applied to Problems Involving Fluid Flow," Comp. Methods Appl. Mech. Eng., Vol. 9, pp. 75-103 (1976).

53. L. Prandtl, "Bericht uber Untersuchungen zer ansgebil-derter Turbulenz," ZAMM, Vol. 5, pp. 136-139 (1925).

54. L. Prandtl, Nach. Akad. Wiss. Goett. Math-Phys. Kl. (1945). translated as Jet Propul. Lab Publication 13 (1952).

55. P. Bradshaw, D. H. Ferris, and N. P. Atwell, "Calculation of Boundary Layer Development using the Turbulent Energy Equation," J. Fluid Mech., Vol. 28, p. 593 (1967).

56. V. W. Nee and L. S. G. Kovasznay, "The Calculation of the Incompressible Turbulent Boundary Layer by a Simple Theory," Physics of Fluids, Vol. 12, p. 473 (1969).

57. F. H. Harlow and P. I. Nakayama, "Transport of Turbulence Energy Decay," Los Alamos Scientific Lab. Report LA-3854/UC-34 physics/TID-4500 (1968).

58. W. P. Jones and B. E. Launder, "The Prediction of Laminarization with a 2-equation Model of Turbulence," Int. J. Heat Mass Trans., Vol. 15, pp. 301-313 (1982).

59. P. Y. Chou, "On Velocity Correlation and Solution of the Equations of Turbulent Fluctations," Q. J. Mech. Appl. Math., Vol. 3, pp. 38-54 (1945).

60. K. Hanjalic and B. E. Launder, "A Reynolds-Stress Model of Turbulence and its Application to Asymmetric Shear Flows," J. Fluid Mech., Vol. 52, pp. 609-638 (1972).

61. B. E. Launder, G. J. Reese, and W. Rodi, "Progress in the Development of a Reynolds-Stress Turbulent Closure," J. Fluid Mech., Vol. 68, pp. 537-566 (1975).

62. W. T. Sha and B. E. Launder, personal communication (1979).

63. R. Nijsing and W. Eifler, "Temperature Fields in Liquid Metal Cooled Assemblies," Prog. Heat Mass Transfer 7, p. 115 (1973).

64. B. J. Daley and F. H. Harlow, "Transport Equations in Turbulence," Physics of Fluids, Vol. 13, pp. 2634-2649 (1970).

65. J. J. Lumley and B. J. Khajeh-Nouri, "Computational Modeling of Turbulent Transport," Adv. Geophysics, Vol. 18A, p. 169-192 (1974).

66. B. E. Launder, A. Morse, W. Rodi, and D. B. Spalding, "The Prediction of Free Shear Flows--A Comparison of the Performance of Six Turbulent Models," Proc. of NASA Conference on Free Shear Flows, Langbery (1972).

67. W. P. Jones and B. E. Launder, "The Calculation of Low-Reynolds-Number Phenomena with a Two-Equation Model of Turbulence," Int. J. Heat Mass Trans., Vol. 16, pp. 1119-1130 (1973).

68. G. D. Raithby, "Skew Upstream Differencing Schemes for Problems involving Fluid Flow, "Comp. Methods Appl. Mech. Eng., Vol. 9, pp. 153-164 (1976).

69. S. V. Patankar, Numerical Heat Transfer and Fluid Flow, Hemisphere Publ. Corp. (1980).

70. M. A. Leschziner, "Practical Evaluation of Three Finite Difference Schemes for the Computation of Steady-State Recirculatory Flows," Comp. Methods Appl. Mech. Eng., Vol. 23, pp. 293-312 (1980).

71. W. C. Rivard, O. A Farmer, T. D. Butler, and P. J. O'Rourke, "A Method for Increased Accuracy in Eulerian Fluid Dynamic Calculations," Los Alamos Report LA-5426-MS (Oct. 1973).

72. J. P. Boris and D. L. Book, "Flux-Corrected Transport. III. Minimal-Error FCT Algorithms," J. Comp. Phys., Vol. 20, pp. 397-431 (1976).

73. S. T. Zalesak, "Fully Multidimensional Flux-Corrected Transport Algorithms for Fluids," J. Comp. Phys. Vol. 31, pp. 335-362 (1979).

74. P. Romstedt and W. Werner, "Efficient High-Order Method for the Solution of Fluid Dynamics Equations, " Nucl. Sci. and Engr., Vol. 64 (1977).

75. R. G. Steinke, "Triangular Geometry Fluid Dynamics with Reduced Artificial Diffusion," ANS Trans., Vol. 34, pp. 310-311 (1980).

76. M. J. Chapman, "FRAM - Nonlinear Dumping Algorithms for the Continuity Equation," J. Comp. Phys., Vol. 44, pp. 84-103 (1981).

77. W. P. Crowley, "Second-Order Numerical Advection," J. Comp. Phys., Vol. 1, pp. 471-484 (1967).

78. W. P. Crowley, "PUFL: An Almost Lagrangian Gasdynamic Calculation for Pipe Flows with Mass Entrainment," J. Comp. Phys., Vol. 2, pp. 61-86 (1967).

79. J. N. Lillington, "A Vector Upstream Differencing Scheme for Problems in Fluid Flow involving Significant Source Terms in Steady-State Linear Systems," Int. J. For Numer. Methods Fluids, Vol. 1, pp. 3-16 (1981).

80. W. T. Sha and V. L. Shah, "Some Resistance Correlations for COMMIX Users," Analytical Thermal Hydraulic Research Program, Report # ATHRP-13 (April 1983).

81. H. M. Domanus, W. T. Sha, V. L. Shah, J. G. Bartzis, J. L. Krazinski, C. C. Miao, and R. C. Schmitt, "COMMIX-2: A Steady/Unsteady, Single-Phase/Two-Phase Three-Dimensional Computer Program for Thermal Hydraulic Analysis of Reactor Components," ANL-81-10, NUREG/CR-1807 (Oct 1980).

82. J. G. Bartzis, H. M. Domanus, J. L. Krazinski, C. C. Miao, W. T. Sha, and V. L. Shah, "COMMIX-2: Steady/Unsteady, Three-Dimensional Two-Phase Thermal Hydraulics Computer Code," ANS Trans., Vol. 35, pp. 259-261 (Nov. 1980).

83. M. Bottoni, H. N. Chi, T. H. Chien, H. M. Domanus, R. W. Lyczkowski, W. T. Sha, and V. L. Shah, "COMMIX-2: A Three-Dimensional Transient Computer Program for Thermal-Hydraulic Analysis of Two-Phase Flows based on Slip Model (SM) and Separated Phases Model (SPM)," NUREG/CR-4371, ANL-85-47 (Sept. 1985).

84. J. G. Bartzis, J. L. Krazinski, V. L. Shah, and W. T. Sha, "Comparison of the COMMIX-2 Two-Phase Flow Model with Experimental Data," ANS Trans., Vol. 35, pp. 669-671 (Nov. 1980).

85. H. M. Domanus, R. C. Schmitt, W. T. Sha, and V. L. Shah, "Two-Phase Simulation of a 7-Pin Bundle during a Flow-Rundown Transient," ANS Trans., Vol. 38, pp. 757-758 (June 1981).

86. C. C. Miao, W. T. Sha, H. M. Domanus, V. L. Shah, and R. C. Schmitt, "An Improved Iteration Scheme for a Two-Fluid Model in COMMIX-2," Trans. Am. Nucl. Soc., Vol. 39, pp. 508-509 (Nov. 1981).

87. C. C. Miao, W. L. Baumann, V. L. Shah, and W. T. Sha, "COMMIX-2 Simulation of FEBA Experiment," Proc. AIChE 1982 Annual Meeting, Los Angeles, California, November 14-19, 1982.

88. C. C. Miao, W. L. Baumann, H. M. Domanus, V. L. Shah, and W. T. Sha, "Two-Phase Thermal-Hydraulic Simulations with COMMIX-2," To be published in Nuclear Engineering and Design (Special Issue on LMFBR Two-Phase Rod Bundle Thermal Hydraulics) 1983.

89. G. H. Golden and J. V. Tokar, "Thermophysical Properties of Sodium", ANL-7323 (Aug. 1967).

APPENDIX A. ACCURACY AND STABILITY ANALYSIS OF THE VOLUME-WEIGHTED SKEW-UPWIND DIFFERENCING SCHEME

Our discussion of the volume-weighted skew-upwind differencing scheme is limited to two dimensions; however, the results can be readily extended to three dimensions. The weighting scheme is shown in Fig. A.1 for the north and east faces. Two flows are shown, one at 30° and the other at 60°. The situations on the south and west faces follow from this figure. In this discussion we shall assume that u and v velocities are positive and uniform with Courant numbers α and β defined as $\alpha = u\delta t/\delta x$ and $\beta = v\delta t/\delta y$, where δx and δy are the cell sizes in the x and y direction, respectively. The scheme uses volume weighting to determine the value of ϕ at the calculational faces. That is, the scheme is like Raithby's but uses volume weighting rather than linear interpolation. Our first task is to write expressions for the volumes in terms of the Courant numbers.

- East and West Face

$$A_0 = \begin{cases} \frac{1}{2}\delta x\delta y\left(1 - \beta/4\alpha\right) & \text{when } \beta/2 < \alpha \\ \frac{1}{2}\delta x\delta y\,\alpha/\beta & \text{when } \alpha < \beta/2 \end{cases} \tag{A.1a}$$

$$A_1 = \begin{cases} \frac{1}{4}\delta x\delta y\,\beta/2\alpha & \text{when } \beta < \alpha \\ \frac{1}{4}\delta x\delta y\left(1 - \alpha/2\beta\right) & \text{when } \alpha < \beta \end{cases} \tag{A.1b}$$

- North and South Face

$$A_0 = \begin{cases} \frac{1}{2}\delta x\delta y\left(1 - \alpha/4\beta\right) & \text{when } \beta > \alpha/2 \\ \frac{1}{2}\delta x\delta y\,\beta/\alpha & \text{when } \beta < \alpha/2 \end{cases} \tag{A.2a}$$

$$A_1 = \begin{cases} \frac{1}{8}\delta x\delta y\,\alpha/\beta) & \text{when } \beta > \alpha/2 \\ \frac{1}{2}\delta x\delta y\left(1 - \beta/2\alpha\right) & \text{when } \beta < \alpha/2 \end{cases} \tag{A.2b}$$

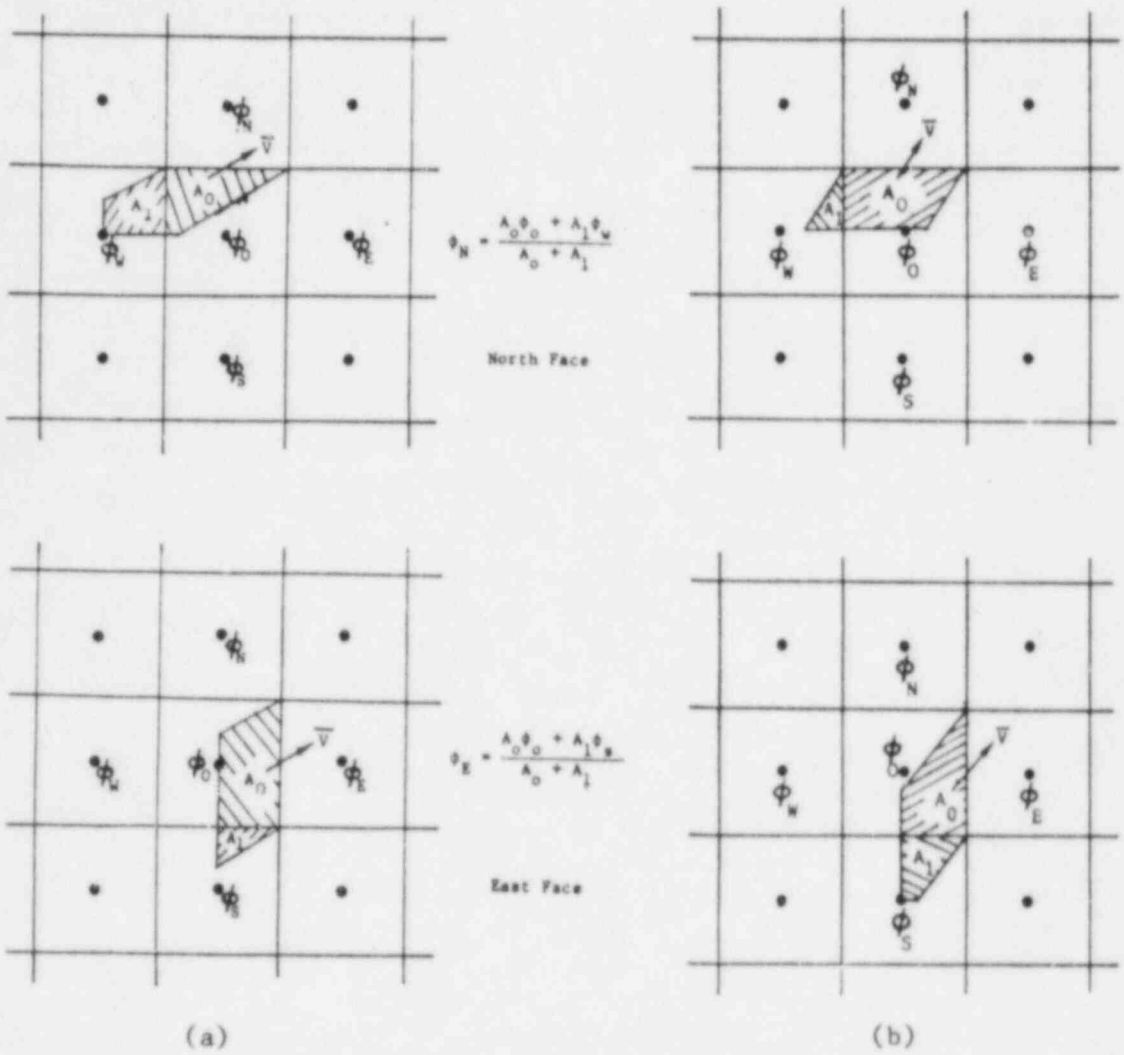

Fig. A.1 Volume-Weighted Skew-Upwind Scheme for North and East Faces at (a) 30° Angle and (b) 60° Angle

Having found the areas, we can approximate ϕ_e, ϕ_w, ϕ_n, and ϕ_s just as in Raithby's scheme. Thus, we have

$$\phi_{ij}^{n+1} = \phi_{ij}^{n} - \frac{\delta t}{\delta x \delta y}\left(F_e - F_w + F_n - F_s\right) , \qquad (A.3)$$

where we approximate the fluxes as

$$F_e \doteq u\delta y \phi_e^{*}, \; F_w \doteq u\delta y \phi_w^{*}, \; F_n \doteq v\delta x \phi_n^{*}, \; F_s \doteq v\delta x \phi_s^{*} .$$

In the VWSUD scheme, we use (u, v > 0):

$$\phi_e^* = \frac{A_0\phi_0 + A_1\phi_S}{A_0 + A_1},$$

$$\phi_w^* = \frac{A_0\phi_W + A_1\phi_{SW}}{A_0 + A_1},$$

$$\phi_n^* = \frac{A_0\phi_0 + A_1\phi_W}{A_0 + A_1},$$

and

$$\phi_s^* = \frac{A_0\phi_S + A_1\phi_{SW}}{A_0 + A_1}, \tag{A.4}$$

Here it is understood that A_0 and A_1 are calculated in accordance with Eq. A.1 for the appropriate face.

Using Eq. A.1 with Eq. A.4, setting $\omega = \beta/\alpha$, and

$$\phi_0 = \phi^n_{ij},\ \phi_S = \phi^n_{ij-1},\ \phi_W = \phi^n_{i-1,j},\ \phi_{Sw} = \phi^n_{i-1,j-1},$$

we find that

$$\phi_e^* = \begin{cases} 1 - \frac{\omega}{4}\ \phi_0 + \frac{\omega}{4}\phi_S & \text{for } 0 < \omega < 1 \\ \dfrac{1 - \frac{\omega}{4}\ \phi_0 + \frac{1}{2}\ 1 - \frac{1}{2\omega}\ \phi_S}{\frac{3}{2} - \frac{\omega}{4} - \frac{1}{4\omega}} & \text{for } 1 < \omega < 2 \\ \dfrac{\frac{1}{\omega}\phi_0 + \frac{1}{2}\ 1 - \frac{1}{2\omega}\ \phi_S}{\frac{1}{2} + \frac{3}{4\omega}} & \text{for } 2 < \omega \end{cases} \tag{A.5}$$

$$\phi_w^* = \begin{cases} 1 - \frac{\omega}{4}\ \phi_W + \frac{\omega}{4}\phi_{SW} & \text{for } 0 < \omega < 1 \\ \dfrac{1 - \frac{\omega}{4}\ \phi_W + \frac{1}{2}\ 1 - \frac{1}{2\omega}\ \phi_{SW}}{\frac{3}{2} - \frac{\omega}{4} - \frac{1}{4\omega}} & \text{for } 1 < \omega < 2 \\ \dfrac{\frac{1}{\omega}\phi_W + \frac{1}{2}\ 1 - \frac{1}{2\omega}\ \phi_{SW}}{\frac{1}{2} + \frac{3}{4\omega}} & \text{for } 2 < \omega \end{cases} \tag{A.6}$$

$$\phi_n^* = \begin{cases} \dfrac{\omega\phi_o + \frac{1}{2}\left(1 - \frac{\omega}{2}\right)\phi_W}{\frac{1}{2} + \frac{3}{4}\omega} & \text{for } 0 < \omega < \frac{1}{2} \\ \dfrac{\left(1 - \frac{1}{4\omega}\right)\phi_0 + \frac{1}{2}\left(1 - \frac{\omega}{2}\right)\phi_W}{\frac{3}{2} - \frac{1}{4\omega} - \frac{\omega}{4}} & \text{for } \frac{1}{2} < \omega < 1 \\ \left(1 - \frac{1}{4\omega}\right)\phi_0 + \frac{1}{4\omega}\phi_W & \text{for } 1 < \omega \end{cases} \qquad (A.7)$$

$$\phi_s^* = \begin{cases} \dfrac{\omega\phi_S + \frac{1}{2}\left(1 - \frac{\omega}{2}\right)\phi_{SW}}{\frac{1}{2} + \frac{3}{4}\omega} & \text{for } 0 < \omega < 1 \\ \dfrac{\left(1 - \frac{1}{4\omega}\right)\phi_0 + \frac{1}{2}\left(1 - \frac{\omega}{2}\right)\phi_{SW}}{\frac{3}{2} - \frac{1}{4\omega} - \frac{\omega}{4}} & \text{for } \frac{1}{2} < \omega < 1 \\ \left(1 - \frac{1}{4\omega}\right)\phi_s + \frac{1}{4\omega}\phi_{SW} & \text{for } 1 < \omega \ . \end{cases} \qquad (A.8)$$

Just as in Raithby's scheme, we use the approximation

$$\frac{\delta t}{\delta x \delta y} F_e \doteq \alpha\phi_e^*, \ \frac{\delta t}{\delta x \delta y} F_w \doteq \alpha\phi_w^*, \ \frac{\delta t}{\delta x \delta y} F_n \doteq \beta\phi_n^*, \ \frac{\delta t}{\delta x \delta y} F_s \doteq \beta\phi_s^* \qquad (A.9)$$

to obtain

$$\phi_{ij}^{n+1} = \phi_{ij}^n - \left\{\alpha\phi_e^* - \alpha\phi_w^* + \beta\phi_n^* - \beta\phi_s^*\right\} , \qquad (A.10)$$

which can be written for each of the four cases

$$0 < \omega \leq \frac{1}{2} \ , \ \frac{1}{2} < \omega \leq 1 \ , \ 1 < \omega \leq 2 \ , \ 2 < \omega \ .$$

- Case I: $0 < \omega < \frac{1}{2} \quad (\omega = \beta/\alpha)$

$$\phi_{ij}^{n+1} = \left(1 - \alpha + \frac{\beta}{4} - \frac{\beta^2/\alpha}{\frac{1}{2} + \frac{3}{4}\frac{\beta}{\alpha}}\right)\phi_{ij}^n + \left(-\frac{\beta}{4} + \frac{\beta^2/\alpha}{\frac{1}{2} + \frac{3}{4}\frac{\beta}{\alpha}}\right)\phi_{i,j-1}^n$$

$$+\left[\alpha-\frac{\beta}{4}-\frac{\frac{\beta}{2}\left(1-\frac{\beta}{2\alpha}\right)}{\frac{1}{2}+\frac{3}{4}\frac{\beta}{\alpha}}\right]\phi^{n}_{i-1,j}+\left[\frac{\beta}{4}+\frac{\frac{\beta}{2}\left(1-\frac{\beta}{2\alpha}\right)}{\frac{1}{2}+\frac{3}{4}\frac{\beta}{\alpha}}\right]\phi^{n}_{i-1,j-1} \qquad (A.11)$$

- Case II: $\frac{1}{2}<\omega<1$

$$\phi^{n+1}_{ij}=\left[1-\alpha+\frac{\beta}{4}-\frac{\beta\left(1-\frac{\alpha}{4\beta}\right)}{\frac{3}{2}-\frac{\alpha}{4\beta}-\frac{\beta}{4\alpha}}\right]\phi^{n}_{ij}+\left[-\frac{\beta}{4}+\frac{\beta\left(1-\frac{\alpha}{4\beta}\right)}{\frac{3}{2}-\frac{\alpha}{4\beta}-\frac{\beta}{4\alpha}}\right]\phi^{n}_{i,j-1}$$

$$+\alpha\left[-\frac{\beta}{4}-\frac{\frac{\beta}{2}\left(1-\frac{\beta}{2\alpha}\right)}{\frac{3}{2}-\frac{\alpha}{4\beta}-\frac{\beta}{4\alpha}}\right]\phi^{n}_{i-1,j}+\left[\frac{\beta}{4}+\frac{\frac{\beta}{2}\left(1-\frac{\beta}{2\alpha}\right)}{\frac{3}{2}-\frac{\alpha}{4\beta}-\frac{\beta}{4\alpha}}\right]\phi^{n}_{i-1,j-1} \qquad (A.12)$$

- Case III: $1<\omega<2$

$$\phi^{n+1}_{ij}=\left[1-\beta+\frac{\alpha}{4}-\frac{\alpha\left(a-\frac{\beta}{4\alpha}\right)}{\frac{3}{2}-\frac{\beta}{4\alpha}-\frac{\alpha}{4\beta}}\right]\phi^{n}_{ij}+\left[\beta-\frac{\alpha}{4}-\frac{\frac{\alpha}{2}\left(1-\frac{\alpha}{2\beta}\right)}{\frac{3}{2}-\frac{\beta}{4\alpha}-\frac{\alpha}{4\beta}}\right]\phi^{n}_{i,j-1}$$

$$+\left[-\frac{\alpha}{4}+\frac{\alpha\left(1-\frac{\beta}{4\alpha}\right)}{\frac{3}{2}-\frac{\beta}{4\alpha}-\frac{\alpha}{4\beta}}\right]\phi^{n}_{i-1,j}+\left[\frac{\alpha}{4}+\frac{\frac{\alpha}{2}\left(1-\frac{\alpha}{2\beta}\right)}{\frac{3}{2}-\frac{\beta}{4\alpha}-\frac{\alpha}{4\beta}}\right]\phi^{n}_{i-1,j-1} \qquad (A.13)$$

- Case IV: $2<\omega$

$$\phi^{n+1}_{ij}=\left(1-\beta+\frac{\alpha}{4}-\frac{\alpha^2/\beta}{\frac{1}{2}+\frac{3}{4}\frac{\alpha}{\beta}}\right)\phi^{n}_{ij}+\left[\beta-\frac{\alpha}{4}-\frac{\frac{\alpha}{2}\left(1-\frac{\alpha}{2\beta}\right)}{\frac{1}{2}+\frac{3}{4}\frac{\alpha}{\beta}}\right]\phi^{n}_{i,j-1}$$

$$+\left(-\frac{\alpha}{4}+\frac{\alpha^2/\beta}{\frac{1}{2}+\frac{3}{4}\frac{\alpha}{\beta}}\right)\phi^{n}_{i-1,j}+\left[\frac{\alpha}{4}+\frac{\frac{\alpha}{2}\left(1-\frac{\alpha}{2\beta}\right)}{\frac{1}{2}+\frac{3}{4}\frac{\alpha}{\beta}}\right]\phi^{n}_{i-1,j-1} \qquad (A.14)$$

Just as for Raithby's scheme, we can interpret this difference scheme as an interpolation scheme. We again recall that the interpolation point in the xy (spatial) plane is R^*: (ξ^*,η^*) where $\xi^*=-\alpha$, $\eta^*=-\beta$. Thus, the right side of Eqs. A.11 through A.14 can be regarded as interpolants of ϕ evaluated at (ξ^*,η^*). We shall call this interpolant $\tilde{\phi}(\xi,\eta)$, but we will not write it

out because the expressions are quite involved. However, one obtains it from Eqs. A.11 through A.14 by replacing α by $-\xi$ and β by $-\eta$. Thus,

$$\phi_{ij}^{n+1} = \tilde{\phi}\,(\xi^*, \eta^*) \quad . \tag{A.15}$$

The interpolation domain is the square shown in Fig. A.2, and this domain is subdivided into four subregions. We note that the VWSUD scheme involves four points whereas the Raithby scheme involved six points. The domain is now divided into four parts, whereas in the Raithby scheme the domain was divided into three parts. The VWSUD scheme is entirely rational; the Raithby scheme was partially polynomial and partially rational.

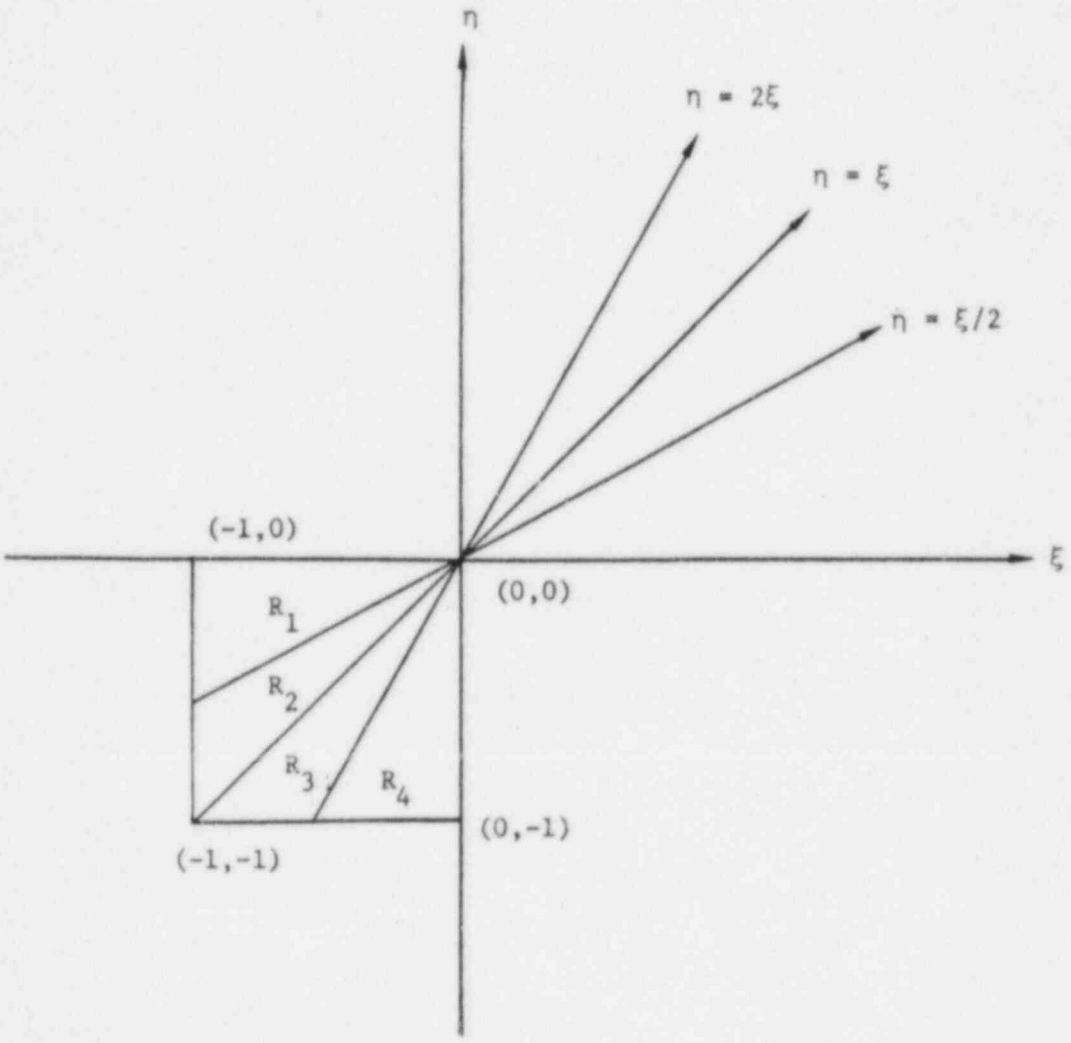

Fig. A.2 Interpolation Domain

On the question of order of accuracy, we see immediately that $\tilde{\phi}$ is a continuous interpolant that will reproduce the set $\begin{matrix} 1 & \xi \\ \eta & \end{matrix}$, but will not reproduce $\xi\eta$. Thus, we are again considering a first-order scheme, just as Raithby's.

We next consider the stability of the VWSUD scheme. (Again, the regions R1 - R4 are in the α,β plane reflected through the origin and we denote the corresponding regions in the α,β plane by $\hat{R}1 - \hat{R}4$.) Consider a Fourier mode $\rho^n_{k\ell} \exp(\hat{i}kx_i + \hat{i}\ell y_j)$ and set $\theta = k\delta x$ and $\phi = \ell\delta y$; then from Eqs. A.11 through A.14, we find the following:

- Case I: $0 < p/k < \frac{1}{2}, \alpha, p > 0$, Region 1 $(\hat{R}1)$

$$\rho_{k,\ell} = 1 - \alpha + \frac{\beta}{4} - \frac{\beta^2/\alpha}{\frac{1}{2} + \frac{3}{4}\frac{\beta}{\alpha}} + \left[\alpha - \frac{\beta}{4} - \frac{\frac{\beta}{2}\left(1 - \frac{\beta}{2\alpha}\right)}{\frac{1}{2} + \frac{3}{4}\frac{\beta}{\alpha}}\right]\cos\theta$$

$$+ \left(-\frac{\beta}{4} + \frac{\beta^2/\alpha}{\frac{1}{2} + \frac{3}{4}\frac{\beta}{\alpha}}\right)\cos\phi + \left[\frac{\beta}{4} + \frac{\frac{\beta}{2}\left(1 - \frac{\beta}{2\alpha}\right)}{\frac{1}{2} + \frac{3}{4}\frac{\beta}{\alpha}}\right]\cos(\theta + \phi)$$

$$- i\left\{\left[\alpha - \frac{\beta}{4} - \frac{\frac{\beta}{2}\left(1 - \frac{\beta}{2\alpha}\right)}{\frac{1}{2} + \frac{3}{4}\frac{\beta}{2\alpha}}\right]\sin\theta + \left[-\frac{\beta}{4} + \frac{\beta^2/\alpha}{\frac{1}{2} + \frac{3}{4}\frac{\beta}{\alpha}}\right]\sin\phi\right.$$

$$\left. + \left[\frac{\beta}{4} + \frac{\frac{\beta}{2}\left(1 - \frac{\beta}{2\alpha}\right)}{\frac{1}{2} + \frac{3}{4}\frac{\beta}{\alpha}}\right]\sin(\theta + \phi)\right\} \qquad \text{(A.16)}$$

- Case II: $\frac{1}{2} < \frac{\beta}{\alpha} < \frac{1}{2}$, $\alpha, \beta > 0$ Region 2$(\hat{R}2)$

$$\rho_{k,\ell} = 1 - \alpha + \frac{\beta}{4} - \frac{\beta\left(1 - \frac{\alpha}{4\beta}\right)}{\frac{3}{2} - \frac{\alpha}{4\beta} - \frac{\alpha}{4\alpha}} + \left[\alpha - \frac{\beta}{4} - \frac{\frac{\beta}{2}\left(1 - \frac{\beta}{2\alpha}\right)}{\frac{3}{2} - \frac{\alpha}{4\beta} - \frac{\beta}{4\alpha}}\right]\cos\theta$$

$$+ \left[-\frac{\beta}{4} + \frac{\beta\left(1 - \frac{\alpha}{4\beta}\right)}{\frac{3}{2} - \frac{\alpha}{4\beta} - \frac{\beta}{4\alpha}}\right]\cos\phi + \left[\frac{\beta}{4} + \frac{\frac{\beta}{2}\left(1 - \frac{\beta}{2\alpha}\right)}{\frac{3}{2} - \frac{\alpha}{4\beta} - \frac{\beta}{4\alpha}}\right]\cos(\theta + \phi)$$

$$- i\left\{\left[\left[\alpha - \frac{\beta}{4} - \frac{\frac{\beta}{2}\left(1 - \frac{\beta}{2\alpha}\right)}{\frac{3}{2} - \frac{\alpha}{4\beta} - \frac{\beta}{4\alpha}}\right]\sin\theta + \left[-\frac{\beta}{4} + \frac{\beta\left(1 - \frac{\alpha}{4\beta}\right)}{\frac{3}{2} - \frac{\alpha}{4\beta} - \frac{\beta}{4\alpha}}\right]\sin\phi\right.\right.$$

$$\left.\left.+\left[\frac{\beta}{4} + \frac{\frac{\beta}{2}\left(1 - \frac{\beta}{2\alpha}\right)}{\frac{3}{2} - \frac{\alpha}{4\beta} - \frac{\beta}{4\alpha}}\right]\sin(\theta + \phi)\right\}\right. \qquad \text{(A.17)}$$

- Case III: $1 < \frac{\beta}{\alpha} < 2$, $\alpha, \beta > 0$, Region 3 $(\hat{R}3)$

$$\rho_{k,\ell} = 1 - \beta + \frac{\alpha}{4} - \frac{\alpha\left(1 - \frac{\beta}{4\alpha}\right)}{\frac{3}{2} - \frac{\beta}{4\alpha} - \frac{\beta}{4\beta}} + \left[-\frac{\alpha}{4} - \frac{\alpha\left(1 - \frac{\beta}{4\alpha}\right)}{\frac{3}{2} - \frac{\beta}{4\alpha} - \frac{\alpha}{4\beta}}\right]\cos\theta$$

$$+\left[\beta - \frac{\alpha}{4} - \frac{\frac{\alpha}{2}\left(1 - \frac{\alpha}{2\beta}\right)}{\frac{3}{2} - \frac{\beta}{4\alpha} - \frac{\alpha}{4\beta}}\right]\cos\phi + \left[\frac{\alpha}{4} + \frac{\frac{\alpha}{2}\left(1 - \frac{\alpha}{2\beta}\right)}{\frac{3}{2} - \frac{\beta}{4\alpha} - \frac{\alpha}{4\beta}}\right]\cos(\theta + \phi)$$

$$- i\left\{\left[+\frac{\alpha}{4} - \frac{\alpha\left(1 - \frac{\beta}{4\alpha}\right)}{\frac{3}{2} - \frac{\beta}{4\alpha} - \frac{\alpha}{4\beta}}\right]\sin\theta + \left[\beta - \frac{\alpha}{4} - \frac{\frac{\alpha}{2}\left(1 - \frac{\alpha}{2\beta}\right)}{\frac{3}{2} - \frac{\beta}{4\alpha} - \frac{\alpha}{4\beta}}\right]\sin\phi\right.$$

$$\left.+\left[\frac{\alpha}{4} + \frac{\frac{\alpha}{2}\left(1 - \frac{\alpha}{2\beta}\right)}{\frac{3}{2} - \frac{\beta}{4\alpha} - \frac{\alpha}{4\beta}}\right]\sin(\theta + \phi)\right\} \qquad \text{(A.18)}$$

- Case IV: $2 < \frac{\beta}{\alpha}$, $\alpha, \beta > 0$, Region 4 $(\hat{R}4)$

$$\rho_{k,\ell} = 1 - \beta + \frac{\alpha}{4} - \frac{\alpha^2/\beta}{\frac{1}{2} + \frac{3}{4}\frac{\alpha}{\beta}} + \left(-\frac{\alpha}{4} + \frac{\alpha^2/\beta}{\frac{1}{2} + \frac{3}{4}\frac{\alpha}{\beta}}\right)\cos\theta$$

$$+\left[\beta - \frac{\alpha}{4} + \frac{\frac{\alpha}{2}\left(1 - \frac{\alpha}{2\beta}\right)}{\frac{1}{2} + \frac{3}{4}\frac{\alpha}{\beta}}\right]\cos\phi + \left[\frac{\alpha}{4} + \frac{\frac{\alpha}{2}\left(1 - \frac{\alpha}{2\beta}\right)}{\frac{1}{2} + \frac{3}{4}\frac{\alpha}{\beta}}\right]\cos(\theta + \phi)$$

$$- i\left\{\left(-\frac{\alpha}{4} + \frac{\alpha^2/\beta}{\frac{1}{2} + \frac{3}{4}\frac{\alpha}{\beta}}\right)\sin\theta + \left[\beta - \frac{\alpha}{4} - \frac{\frac{\alpha}{2}\left(1 - \frac{\alpha}{2\beta}\right)}{\frac{1}{2} + \frac{3}{4}\frac{\alpha}{\beta}}\right]\sin\phi\right.$$

$$+\left[\frac{\frac{\alpha}{4}+\frac{\frac{\alpha}{2}\left(1-\frac{\alpha}{2\beta}\right)}{\frac{1}{2}+\frac{3}{4}\frac{\alpha}{\beta}}}{}\right]\sin(\theta+\phi)\Bigg\} \qquad \text{(A.19)}$$

In the α,β plane we have four regions defined, as shown in Fig. A.3. For each region, $\rho_{k,\ell}$ has the form

$$\rho_{k,\ell} = A_m + B_m e^{-i\phi} + C_m e^{-i\theta} + D_m e^{-i\theta} e^{-i\phi} \quad , \quad m = 1,2,3,4 \ , \qquad \text{(A-20)}$$

where A_m, B_m, C_m, D_m can be read from Eqs. A.16 through A.19. Consider any one of the four regions and drop the subscript m for now. Because this interpolation procedure reproduces the set of monomials $\begin{Bmatrix}1\\ \xi\\ \eta\end{Bmatrix}$ and because $\xi^* = -\alpha$ and $\eta^* = -\beta$, we have the following relations:

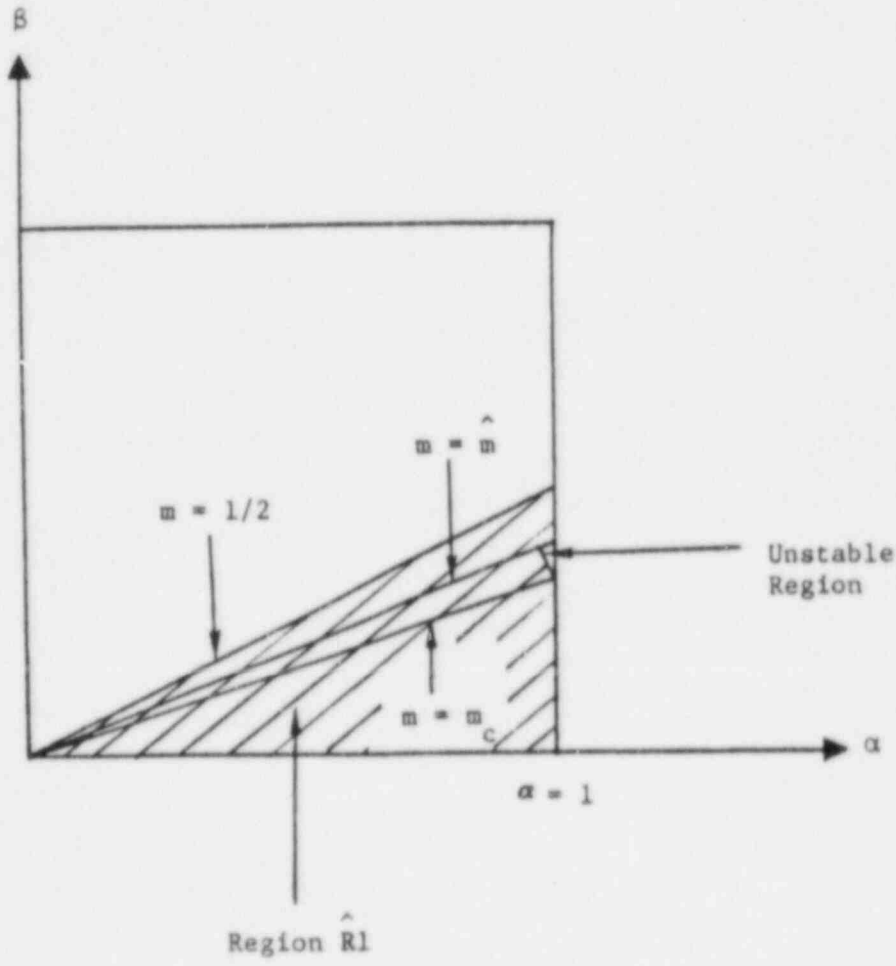

Fig. A.3 Domain Showing Unstable Region for Case $\theta = \phi$ in $\hat{R}1$

$$A + B + C + D = 1,$$

$$C + D = \alpha, \text{ and}$$

$$B + D = \beta. \tag{A.21}$$

Thus, we can write any ρ in Eq. A.20 as

$$\rho = 1 - \alpha - \beta + D + (\alpha - D)e^{-i\theta} + (\beta - D)e^{-i\phi} + De^{-i\theta}e^{-i\phi} . \tag{A.22}$$

Set

$$C(\theta) = 1 - \cos\theta = 2 \sin \frac{\theta}{2} ;$$

then from Eq. A.22, we find

$$\begin{aligned} |\rho|^2 = {} & 1 - 2\alpha C(\theta) + 2\alpha^2 C(\theta) - 2\beta C(\phi) + 2\beta^2 C(\phi) \\ & + 2\alpha\beta \, [C(\theta) + C(\phi) - C(\theta - \phi)] \\ & + 2D \, [C(\theta) + C(\phi) - C(\theta + \phi)] , \end{aligned} \tag{A.23}$$

i.e.,

$$\begin{aligned} |\rho|^2 = {} & 1 - 2[(\alpha - \alpha^2 - \alpha\beta) \, C(\theta) - DC(\theta) + D(\alpha + \beta - D)C(\theta)C(\phi) \\ & + (\beta - \beta^2 - \alpha\beta) \, C(\phi) - DC(\phi) + D(\alpha + \beta - D) \, C(\theta) \, C(\phi) \\ & + \alpha\beta \, C(\theta - \phi) + DC(\theta + \phi)] . \end{aligned} \tag{A.24}$$

We are going to rewrite this expression in a form more convenient for checking stability. Before doing this, we note that any four parameter interpolating scheme that reproduces the set of monomials $1, \xi, \eta$ will produce Eqs. A.21 through A.23. In particular, a bilinear donor cell scheme corresponds to setting $D = \alpha\beta$. A linear donor cell scheme corresponds to the choice $D \equiv 0$. So at this point we are looking at the question of stability for general four point schemes. Raithby's skew-upwind scheme, as we have seen, is a six point scheme rather than a four point scheme, so it does not fit this discussion. The form in Eq. A.24 is convenient when $D = 0$, because in this case one can see that

$$|\rho|^2 = 1 - 2f , \tag{A.25}$$

where

$$f = \alpha(1 - \alpha - \beta) \, C(\theta) + \beta \, (1 - \alpha - \beta) \, C(\phi) + \alpha\beta \, C(\theta - \phi) , \tag{A.26}$$

and one sees that a sufficient condition for $f \geq 0$ (i.e., the linear donor cell scheme is stable) is that

$$0 \leq \alpha,\ 0 \leq \beta,\ \alpha + \beta \leq 1 \ . \tag{A.27}$$

However, Eq. A.24 is not convenient when $D = \alpha\beta$ (bilinear donor cell scheme) and we do not think this form would be convenient for the D's associated with the VWSUD scheme. For this reason, we will rewrite Eq. A.24. We start with the identity

$$\begin{aligned}
&[1 - 2(\alpha - \alpha^2 + D - \alpha\beta)\, C(\theta)]\ [1 - 2(\beta - \beta^2 + D - \alpha\beta)\, C(\phi)] \\
&\equiv [\text{fac}\,\alpha]\ [\text{fac}\,\beta] \\
&= 1 - 2(\alpha - \alpha^2)\, C(\theta) - 2(\beta - \beta^2)\, C(\phi) \\
&\quad + 4(\alpha - \alpha^2)(\beta - \beta^2)\, C(\theta)\, C(\phi) \\
&\quad - 2(D - \alpha\beta)\, C(\theta)\, [1 - 2(\beta - \beta^2)\, C(\phi)] \\
&\quad - 2(D - \alpha\beta)\, C(\phi)\, [1 - 2(\alpha - \alpha^2)\, C(\theta)] \\
&\quad + 4(D - \alpha\beta)^2\, C(\theta)\, C(\phi)
\end{aligned} \tag{A.28}$$

and use Eq. A.38 in Eq. A.23 to obtain

$$\begin{aligned}
|\rho|^2 &= [\text{fac}\,\alpha]\ [\text{fac}\,\beta] - 2\alpha\beta\, C(\theta - \phi) - 2DC(\theta + \phi) + 4DC(\theta) + 4DC(\phi) \\
&\quad + C(\theta)\, C(\phi)\, [-4(\alpha - \alpha^2)(\beta - \beta^2) - 4(D - \alpha\beta)(\beta - \beta^2) \\
&\quad - 4(D - \alpha\beta)(\alpha - \alpha^2) - 4(D - \alpha\beta)^2 - 4\alpha D - 4\beta D + 4D^2] \ .
\end{aligned} \tag{A-29}$$

Next we use the relation

$$C(\theta + \phi) + C(\theta - \phi) = 2C(\theta) + 2C(\phi) - 2C(\theta)\, C(\phi) \ . \tag{A-30}$$

Then after some algebra, we find that

$$|\rho|^2 = 1 - 2f \ , \tag{A-31}$$

where

$$\begin{aligned}
f &= [\alpha(1 - \alpha) + D - \alpha\beta]\ \{1 - [\beta(1 - \beta) + D - \alpha\beta]\, C(\phi)\}\, C(\theta) \\
&\quad + [\beta(1 - \beta) + D - \alpha\beta]\ \{1 - [\alpha(1 - \alpha) + D - \alpha\beta]\, C(\theta)\}\, C(\phi) \\
&\quad + (\alpha\beta - D)\, C(\theta - \phi) \ .
\end{aligned} \tag{A-32}$$

The form in Eq. A.32 is very convenient for the bilinear donor scheme where $D = \alpha\beta$. In this case, it is easily shown that $f \geq 0$ if and only if $0 \leq \alpha \leq 1$, and $0 \leq \beta \leq 1$. When considering stability for the VWSUD scheme, we shall use Eq. A.32. For the VWSUD scheme we shall consider $(\alpha,\beta) \in \hat{R1} = \{(\alpha,\beta):\ 0 \leq \alpha/\beta \leq 1/2,\ \beta \geq 0,\ 0 \leq \alpha \leq 1\}$. In this case, D is defined from Eq. A.11; that is,

$$D(\alpha,\beta) = \frac{\beta}{4} + \frac{\frac{\beta}{2}\left(1 - \frac{\beta}{2\alpha}\right)}{\frac{1}{2} + \frac{3}{4}\frac{\beta}{\alpha}} = \frac{\beta}{4}\left(\frac{10 - \beta/\alpha}{2 + 3\beta/\alpha}\right) . \tag{A.33}$$

To investigate stability, we use this expression for D in Eq. A.32 and ask whether f is greater than or less than 0 for $(\alpha\beta)\epsilon\hat{R}1$ and $0 \leq \theta \leq \pi$, $0 \leq \phi \leq \pi$. The most obvious approach would be to look at sufficiency conditions for $f > 0$. For example, a set of sufficient conditions for $f > 0$ would be

$$\begin{aligned} &0 \leq \alpha(1 - \alpha) + D - \alpha\beta \leq 1/2 \qquad \text{for } (\alpha,\beta)\epsilon\hat{R}1 \\ &0 \leq \beta(1 - \beta) + D - \alpha\beta \leq 1/2 \\ &0 \leq \alpha\beta - D , \end{aligned} \tag{A.34}$$

where D is defined by Eq. A.33. Unfortunately, these conditions define a small domain $D_1 \wedge \hat{R}1 \epsilon \hat{R}1$ that is too small to be useful. If $D_1 \wedge \hat{R}1$ denotes the set $(\alpha,\beta)\epsilon\hat{R}1$ where $f \geq 0$, then we shall call $D \wedge \hat{R}1$ the stability domain. The problem is that conditions in Eq. A.34 define a domain $D_1 \subset D_1$, where D_1 is too small to be able to use as an indication of stability.

Set

$$\beta = m\alpha , \quad 0 \leq \alpha \leq 1, \quad 0 \leq m \leq 1/2$$

$$\begin{aligned} a_1(\alpha;m) &= \alpha \tilde{a}_1(\alpha;m) = \alpha\left[\frac{8 + 22m - m^2}{8 + 12m} - (1 + m)\alpha\right] \\ a_2(\alpha;m) &= \alpha \tilde{a}_2(\alpha;m) = m\alpha\left[\frac{18 + 11m}{8 + 12m} - (1 + m)\alpha\right] \\ a_3(\alpha;m) &= \alpha \tilde{a}_3(\alpha;m) = m\alpha\left(\alpha - \frac{10 - m}{8 + 12m}\right) . \end{aligned} \tag{A.35}$$

Then Eq. A.32 can be written

$$\begin{aligned} f = \alpha h = \alpha\{ &\tilde{a}_1\left[1 - \alpha\tilde{a}_2\, C(\phi)\right] C(\theta) + \tilde{a}_2\left[1 - \alpha\tilde{a}_1\, C(\theta)\right] C(\phi) \\ &+ \tilde{a}_3\, C(\theta - \phi)\} . \end{aligned} \tag{A.36}$$

The central question is whether $h(\alpha;m;\theta,\phi)$, defined in Eq. A.36, is positive for $0 \leq \alpha \leq 1$, $0 \leq \theta, \phi \leq \pi$, and $0 \leq m \leq 1/2$. Consider a special case when $\theta = \phi$. Setting $x = C(\theta)$, we have

$$h(\alpha;m;\theta) = \tilde{a}_1(\alpha;m)\left[1 - \alpha\tilde{a}_2(\alpha;m)\, X\right] X + \tilde{a}_2(\alpha;m)\left[1 - \alpha\tilde{a}_1(\alpha;m)\, X\right] X$$

$$= X\{[\tilde{a}_1(\alpha;m) + \tilde{a}_2(\alpha;m)] - 2\alpha x\tilde{a}_1(\alpha;m)\,\tilde{a}_2(\alpha;m)\}$$

$$= X[g_1(\alpha;m) - 2\alpha x g_2(\alpha;m)]\ , \qquad (A.37)$$

where

$$g_1(\alpha;m) = \frac{8 + 40m + 10m^2}{8 + 12m} - (1 + m)^2\alpha \qquad (A.38)$$

and

$$g_2(\alpha;m) = \frac{(8 + 22m - m^2)(18m + 11m^2)}{(8 + 12m)^2}$$

$$- \frac{m(m+1)}{8 + 12m}(26 + 33m - m^2)\alpha + m(1 + m)^2\alpha^2\ ,$$

$$= \frac{m(144 + 4m + 224m^2 - 11m^3)}{(8 + 12m)^2}$$

$$- \frac{m}{8 + 12m}(1 + m)(26 + 33m - m^2)\alpha + m(1 + m)^2\alpha^2\ . \qquad (A.39)$$

The function $g_1(\alpha;m)$ is a straight line $m\alpha$ with a negative slope:

$$g_1(0;m) > 0,\ 0 < m < 1/2$$

$$g_1(1;m) = \frac{m(6 - 11m - 6m^2)}{4 + 6m}\ .$$

We observe that

$$g_1(1;m) > 0 \text{ when } 0 < m < m_c \doteq 0.43990171634$$

$$g_1(1;m) < 0 \text{ when } m_c < m < 1/2. \qquad (A.40)$$

Hence, when $0 < m < m_c$, $g_1(\alpha;m) < 0$ for $0 \leq \alpha \leq 1$. When $m_c < m < 1$, then $g_1[\alpha;m]$ has a root in $[0,1]$. The root is

$$\alpha_{11} = \frac{8 + 40m + 10m^2}{(8 + 12m)(1 + m)^2} = \frac{4 + 20m + 5m^2}{4 + 14m + 16m^2 + 6m^3} \qquad (A.41)$$

and when $m_c < m < 1$, then

$$g_1(\alpha;m) > 0 \text{ for } 0 < \alpha < \alpha_{11}$$

$$g_1(\alpha;m) < 0 \text{ for } \alpha_{11} < \alpha < 1. \tag{A.42}$$

Note $\alpha_{11}(m_c) = 1$, $\alpha_{11}(1/2) = 0.968253968$.

Next we consider the nature of $g_2(\alpha;m)$. Because

$$g_2(\alpha;m) = \tilde{a}_1(\alpha;m)\, \tilde{a}_2(\alpha;m) , \tag{A.43}$$

we can gain some information from the properties of $\tilde{a}_1$ and $\tilde{a}_2$.

Consider $\tilde{a}_2$, from Eq. A.35; we have

$$\tilde{a}_2(0;m) = \frac{18m + 11m^2}{8 + 12m}$$

$$\tilde{a}_2(1;m) = \frac{m(10 - 9m - 12m^2}{8 + 12m} \geq 0 \text{ for all } 0 \leq m \leq 1/2 .$$

Hence, the sign of $g_2(\alpha;m)$ is determined by the sign $\tilde{a}_1$.

From Eq. A.35, we have

$$\tilde{a}_1(0;m) = \frac{8 + 22m - m^2}{8 + 12m} > 0 \text{ for } 0 < m < 1/2$$

$$\tilde{a}_1(1;m) = \frac{m\,(2 - 13m)}{8 + 12m}$$

Hence, when $0 < m < 2/13 \triangleq 0.15385$, then

$$\tilde{a}_1(\alpha;m) < 0 \text{ for } 0 \leq \alpha \leq 1 . \tag{A.44}$$

And when $2/13 < m < 1/2$, then $\tilde{a}_1(\alpha;m)$ changes sign in $[0,1]$.

$$\tilde{a}_1(\alpha;m) > 0 \text{ when } 0 < \alpha < \alpha_{01}$$

$$\tilde{a}_1(\alpha;m) < 0 \text{ when } \alpha_{01} < \alpha < 1 , \tag{A.45}$$

where

$$\alpha_{01} = \frac{8 + 22m - m^2}{8 + 20m + 12m^2} . \tag{A.46}$$

Now the sign of $g_1(\alpha;m)$ is the same as the sign of $\tilde{a}_1$. Thus, when $0 < m \leq 2/13$, then

$$g_2(\alpha;m) > 0 \text{ for } 0 \leq \alpha \leq 1 . \tag{A.47}$$

When $2/13 < m \leq 1/2$, then

$$g_2(\alpha;m) > 0 \text{ when } 0 < \alpha < \alpha_{01}$$

$$g_2(\alpha;m) < 0 \text{ when } \alpha_{01} < \alpha < 1 \ . \tag{A.48}$$

Table A.1 combines this information. (Note that $\alpha_{01} < \alpha_{11}$ when $m_c < m < 1/2$.)

From Table A.1, we see that our task is to check whether $g_1 - 4g_2 > 0$ for various ranges of m and α. If necessary, we look at $g_1 - 4\alpha g_2$, which is greater than $g_1 - 4g_2$. However, we note from Case III that when $m_c < m < 1/2$ and $\alpha_{11} < \alpha < 1$, then the quantity of interest is

$$\hat{H}(\alpha;m;x) = - \left|g_1(\alpha;m)\right| + 2\alpha x \left|g_2(\alpha;m)\right| \ .$$

Clearly for a given m, $m_c < m < 1/2$, and a given α, $\alpha_{11} < \alpha < 1$, there is a value of x such that $\hat{H}(\alpha;m;x) < 0$. The question is whether this value of x satisfies $0 < x \leq 2$; i.e., whether $\left|g_1(\alpha;m)\right| < 4\alpha \left|g_2(\alpha;m)\right|$ for some $\alpha_{11} < \alpha < 1$, $m_c < m < 1/2$. In any event, it is clear that we have to investigate the functions

$$H(\alpha;m) = g_1(\alpha;m) - 4\alpha g_2(\alpha;m) \tag{A.49}$$

and/or

$$H_1(\alpha;m;) = g_1(\alpha;m) - 4g_2(\alpha;m) \ . \tag{A.50}$$

$H(\alpha;m)$ provides a stronger estimate and is cubic in α, whereas $H_1(\alpha;m)$ provides a weaker estimate and is quadratic in α.

$$H(\alpha;m) = C_4(m) - C_3(m)\alpha + C_2(m)\alpha^2 - C_1(m)\alpha^3 \ , \tag{A.51}$$

where

$$C_4(m) = \frac{8 + 40m + 10m^2}{8 + 12m} \ ,$$

$$C_3(m) = \frac{\left(16 + 224m + 632m^2 + 344m^3 + 25m^4\right)}{4\left(2 + 3m\right)^2} \ ,$$

$$C_2(m) = \frac{4m(1 + m)\ (26\ + 33m - m^2)}{8 + 12m} = \frac{m(1 + m)\left(26 + 33m - m^2\right)}{2 + 3m} \ ,$$

$$C_1(m) = 4m(1 + m)^2 \ ,$$

and

$$H_1(\alpha;m) = D_3(m) + D_2(m)\alpha - D_1(m)\alpha^2 \ ,$$

Table A.1 Sign Properties of the Function H

Case	m Range	Properties g_1, g_2	Question of Sign
I	$0 < m < 2/13$	$g_1 > 0,\ g_2 > 0,\ \alpha$	$g_1 - 2\alpha x g_2 > g_1 - 4g_2 > 0?,\ 0 \leq \alpha \leq 1$
II	$2/13 < m < m_c$	$g_1 > 0,\ \alpha$	$g_1 - 2\alpha x g_2 > g_1 - 4g_2 > 0?,\ 0 < \alpha < \alpha_{01}$
		$g_2 \gtrless 0$, root α_{01}	$g_1 - 2\alpha x g_2 = g_1 + 2\alpha x \lvert g_2 \rvert > 0,\ \alpha_{01} < \alpha < 1$
III	$m_c < m < 1/2$	$g_1 \gtrless 0$, root α_{11}	$g_1 - 2\alpha x g_2 > g_1 - 4g_2 > 0?,\ 0 < \alpha < \alpha_{01}$
		$g_2 \gtrless 0$, root α_{01}	$g_1 - 2\alpha x g_2 = g_1 + 2\alpha x \lvert g_2 \rvert > 0,\ \alpha_{01} < \alpha < \alpha_{11}$
			$g_1 - 2\alpha x g_2 = -\lvert g_1 \rvert + 2\alpha x \lvert g_2 \rvert,\ \alpha_{11} < \alpha < 1$

where

$$D_3(m) = \frac{4}{(8 + 12m)^2}\left(16 - 40m - 344m^2 - 194m^3 + 11m^4\right),$$

$$D_2(m) = \frac{\left(-2 + 19m + 51m^2 + 29m^3 - m^4\right)}{2 + 3m}, \text{ and}$$

$$D_1(m) = 4m(1 + m)^2 .$$

Now, whenever $g_1 > 0$, $g_2 > 0$, then $H > H_1$; so if we can show $H_1 > 0$, we have established stability for these values of α, m. From Table A.1, we see that $g_1 > 0$, $g_2 > 0$ in all cases of interest except the last subcase for Case III. However, the coefficient $D_3(m)$ changes sign in the interval $[0,1/2]$, so we find it more convenient to work with the cubic function $H(\alpha m)$. When $0 \leq m \leq 1/2$, this cubic has exactly **one** real positive root $\alpha_{00}(m)$. Moreover, for

$$0 \leq m < 0.490250 , \tag{A.52}$$

the root $\alpha_{00}(m)$ satisfies

$$1 < \alpha_{00}(m).$$

Thus, referring to Table A.1, we see that $g_1 - 2\alpha x g_2 > 0$ in every case except possibly the last subcase of Case III. Consider $m_c < m < 1/2$ and $\alpha_{11}(m) < \alpha < 1$. Thus we have $g_1(\alpha;m) < 0$ and $g_2(\alpha;m) < 0$. Thus, the equation

$$g_1 - 2\alpha x g_2 = -|g_1| + 2\alpha x|g_2| = 0 \tag{A.54}$$

has the solution

$$x = \frac{|g_1|}{2\alpha|g_2|} = \frac{-g_1}{-2\alpha g_2} . \tag{A.55}$$

Now we must have $0 < x < 2$; therefore, we must have

$$x = \frac{|g_1|}{2\alpha|g_2|} < 2, \text{ for } \alpha_{11} < \alpha < 1$$

or $|g_1| < 4\alpha|g_2| \Rightarrow -g_1 < -4\alpha g_2 \Rightarrow g_1 > 4\alpha g_2$,

i.e., $H(\alpha;m) = g_1 - 4\alpha g_2 > 0$.

Now we have $H(\alpha;m) > 0$ on $0 < \alpha < 1$ for $m < 0.49025 = \hat{m}$. Thus, if $m_c = 0.4399017 < m < \hat{m} = 0.49025$ and $\alpha_{11} < \alpha < 1$, then $H(\alpha;m) > 0$ for $\alpha_{11} < \alpha < 1$.

Therefore, $x = \dfrac{|g_1|}{2\alpha|g_1|} < 2$, and we see that for each $m_c < m < \hat{m}$, and each $\alpha_{11} < \alpha < 1$, there is an $x = x(\alpha;m)$ such that

$$0 < x < 2$$

and

$$g_1(\alpha;m) - 2\alpha x g_2(\alpha;m) < 0. \tag{A.56}$$

Moreover, the values of $x = x(\alpha;m)$ defined by Eq. A.55 range over the full interval $[0,2]$. To see this, we recall that $\alpha_{11}(m)$ is a root of $g_1(\alpha;m)$ and $g_2(\alpha;m) \neq 0$ for $\alpha_{11} < \alpha < 1$. Thus, if we set

$(g_2)_{min} = \min\{|g_2(\alpha;m)| : \alpha_{11}(m) \leq \alpha \leq 1\}$, then

$$x(\alpha;m) = \frac{|g_1(\alpha;m)|}{2\alpha|g_2(\alpha;m)|} \leq \frac{|g_1(\alpha;m)|}{2\alpha_{11}(g_2)_{min}}$$

and the right side goes to zero as $\alpha \to \alpha_{11}$. Thus, when $\theta = \phi$, there are values $(\alpha,\beta) \in \hat{R1}$ when h as defined in Eq. A.37 is negative; hence, for these values $(\alpha,\beta) \in \hat{R1}$, the VWSUD scheme is unstable. It is worth noting that these points $(\alpha,\beta) \in \hat{R1}$ occur in a small region, as shown in Fig. A.3. (Note that $\alpha_{11}(\hat{m}) = 0.97345$). The figure has exaggerated the values of $m_c, \hat{m}$ to illustrate the shaded region. Our conclusion is that the VWSUD scheme is essentially stable in $\hat{R1}$ when $\theta = \phi$.

APPENDIX B. THERMODYNAMIC AND TRANSPORT PROPERTIES

Thermodynamic and transport properties of sodium were obtained from Golden and Tokar[89], and those of water are from Brookhaven National Laboratory.

B.1 SODIUM/LIQUID PROPERTIES

Density (kg/m^3)

$$\rho(T) = 9.50076E2 + T[-2.2976E-1 + T(-1.46049E-5 + 5.63788E-9\ T)]. \quad (B.1)$$

Viscosity (pascal-second) or (Pa• s)

$$\mu(T) = 3.2419E-3 \exp[5.0807E2/(T + 273.15) - 0.4925\ \ell n(T + 273.15)]. \quad (B.2)$$

Specific Heat (J/kg• K)

$$c_p(T) = 1.43605E3 + T(-5.802E-1 + 4.62506E-4\ T). \quad (B.3)$$

Conductivity (W/m• K)

$$k(T) = 92.948 - 5.809E-2\ T + 1.1727E-5\ T^2. \quad (B.4)$$

In the above, T is the temperature in degrees Celsius.

Enthalpy (J/kg)

The enthalpy of liquid H(P,T) is calculated from the enthalpy of saturated liquid and the enthalpy change relation

$$dH = \frac{K}{\rho_\ell}\left[\left(1 + \frac{T_K}{\rho_\ell}\right)\frac{\partial \rho_\ell}{\partial T_K}\right]_p dp\ , \quad (B.5)$$

where K is the ratio of gas constants in joules/pascal• m^3, and T_K is the temperature in Kelvin.

Temperature (°C)

The temperature of sodium liquid T(H,P,T) is calculated using an iterative procedure. Initially the liquid temperature T* is assumed, and then the enthalpy H*(T*,P) is calculated. If the enthalpy H* does not agree with the specified enthalpy H, then T* is modified. The procedure is repeated until H*(T,P) is in close agreement with the prescribed enthalpy.

Saturation Pressure (pascals)

$$P_{sat}(T) = 1.01325E5 \frac{3.03266E6}{T_R} e^{-2.30733E4/T_R} \quad (\text{for } T_R \leq 2059.7) . \quad (B.6)$$

$$P_{sat}(T) = 1.01325E5 \frac{6.8817602E6}{(T_R)^{0.61344}} e^{-22981.96/T_R} \quad (\text{for } T_R > 2059.7) . \quad (B.7)$$

Here, T_R is the temperature in degrees Rankine.

Saturation Enthalpy (J/kg)

$$H_{sat}(T) = 2.32444E3\{-29.02 + \{T_R[0.389352 + T_R(-0.5529955E-4 + 0.113726E-7\ T_R)]\}\} . \quad (B.8)$$

Saturation Temperature (°C)

The saturation temperature $T_{sat}(p)$ is obtained by iterative solution of Eqs. B.6 and B.7.

B.2 WATER/LIQUID PROPERTIES

Density

$$\rho(P,H) = 16.018436 \left(a_1 + a_2 H_R^2 + a_3 H_R^4\right) \quad (H \leq 6.4477E5) . \quad (B.9)$$

$$\rho(P,H) = 16.018463 \left[\left(a_1 + a_2 H_R^2 + a_3 H_R^4\right) f(y) + [1 - f(y)] \left(b_1 + \frac{b_2}{H_R - b_3}\right)\right]$$

$$(6.4477E5 < H \leq 6.57793E5) . \quad (B.10)$$

$$\rho(P,H) = 16.018436 \left(b_1 + \frac{b_2}{H_R - b_3}\right) \quad (H > 6.57793E5) . \quad (B.11)$$

Here,

$$a_1 = 62.4 + 2.14E-4\ P_R, \quad (B.12)$$

$$a_2 = -8.73E-5 + 1.438E-9\ P_R, \quad (B.13)$$

$$a_3 = 2.32E-10 - 6.20E-15\ P_R, \quad (B.14)$$

$$b_1 = 92.924 + 5.761E-4\ P_R, \quad (B.15)$$

$$b_2 = 3.94402E4 + 1.6386\ P_R \tag{B.16}$$

$$b_3 = 1.37735E3 + 3.5704E\text{-}2\ P_R\ , \tag{B.17}$$

$$y = \frac{H_R - 280}{2.8}\ , \tag{B.18}$$

$$f(y) = \frac{1}{16}\left(8 - 15y + 10y^3 - 3y^5\right)\ , \tag{B.19}$$

$$H_R = 4.299226E\text{-}4\ H, \text{ and} \tag{B.20}$$

$$P_R = 1.4503774E\text{-}4\ P, \tag{B.21}$$

where H is the enthalpy in J/kg, and P is the pressure in pascals.

Viscosity (Pa• sec)

$$\mu(P,H) = \left[\left(a_1 + a_2x + a_3x^2 + a_4x^3 + a_5x^4\right) - \left(b_1 + b_2\,\eta + b_3\eta^2 + b_4\eta^3\right)\right]\left(P - 6.8945753E5\right)$$

$$(H \geq 2.765E5)\ . \tag{B.22}$$

$$\mu(P,H) = \left[\left(e_1 + e_2H + e_3H^2 + e_4H^3\right) + \left(f_1 + f_2H + f_3H^2 + f_4H^3\right)\right]\left(P - 6.8945753E5\right)$$

$$(2.76E5 < H \leq 3.94E5)\ . \tag{B.23}$$

$$\mu(P,H) = \left(d_1 + d_2y + d_3y^2 + d_4y^3 + d_5y^5\right) \quad (H > 3.94E5). \tag{B.24}$$

Here,

$a_1 = 1.29947E\text{-}3$, $a_2 = -9.2640321E\text{-}4$,

$a_3 = 3.8104706E\text{-}4$, $a_4 = -8.2194445E\text{-}5$,

$a_5 = 7.022438E\text{-}6$, $b_1 = -6.5959E\text{-}12$,

$b_2 = 6.763E\text{-}12$, $b_3 = 2.88825E\text{-}12$,

$b_4 = 4.4525E\text{-}13$, $d_1 = 3.0260323E\text{-}4$,

$d_2 = -1.8366069E\text{-}4$, $d_3 = 7.5670758E\text{-}5$,

$$d_4 = -1.6478789E\text{-}5, \qquad d_5 = 1.4164576E\text{-}6,$$

$$e_1 = 1.4526053E\text{-}3, \qquad e_2 = -6.9880085E\text{-}9,$$

$$e_3 = 1.5210230E\text{-}14, \qquad e_4 = -1.2303195E\text{-}20,$$

$$f_1 = -3.8063508E\text{-}11, \qquad f_2 = 3.9285208E\text{-}16,$$

$$f_3 = -1.2585799E\text{-}21, \qquad f_4 = 1.2860181E\text{-}27, \tag{B.26}$$

$$x = \frac{H - 42658.84}{116532.6}, \tag{B.27}$$

$$\eta = \frac{H - 55358.8}{154213.8}, \tag{B.28}$$

and

$$y = \frac{H - 401467.6}{256953.22}. \tag{B.29}$$

Specific Heat (J/kg• K)

$$c_p(P,H) = \left(x_1 - \frac{x_2}{(H - 1.7556418E6)^2}\right)^{-1} \qquad (H \leq 8.12E5) \tag{B.30}$$

$$c_p(P,H) = \left(x_1 - \frac{x_2}{(H - 1.7556418E6)^2}\right)^{-1} \quad f(y)$$

$$+ \left(Z_1 + Z_2 H + Z_3 H^2\right)^{-1} \quad [1 - f(y)] .$$

$$(8.12E5 < H \leq 8.16E5) \tag{B.31}$$

$$c_p(P,H) = \left(Z_1 + Z_2 H + Z_3 H^2\right)^{-1} \qquad (H > 8.16E5) . \tag{B.32}$$

Here,

$$x_1 = 2.4688303E\text{-}4 + 1.24419E\text{-}13\ P,$$

$$x_2 = 1.8790464E7 - 5.634438E\text{-}2\ P,$$

$$Z_1 = 1.1964506E\text{-}5 + 6.291758E\text{-}12\ P,$$

$$Z_2 = 4.58929E\text{-}10 - 1.1980206E\text{-}17\ P,$$

$$Z_3 = -2.576343E\text{-}16 + 6.046356E\text{-}24\ P, \tag{B.33}$$

$$f(y) = \frac{1}{16}\left(8 - 15y + 10y^3 - 3y^5\right), \tag{B.34}$$

and

$$y = \frac{H - 8.14E4}{2000} . \tag{B.35}$$

Conductivity (W/m K)

$$k(H) = a_1 + a_2x + a_3x^2 + a_4x^3. \tag{B.36}$$

Here,

$$a_1 = 0.57373862, \qquad a_2 = 0.25361036,$$

$$a_3 = -0.14546827, \qquad a_4 = 0.013874725,$$

and

$$x = H/5.815E5. \tag{B.37}$$

Enthalpy (J/kg)

The enthalpy H(P,T) is calculated iteratively. We start with an assumed value of enthalpy. Liquid temperature is calculated. If the calculated liquid temperature does not agree with the prescribed temperature, then enthalpy is modified. The modification is continued until the agreement in temperatures is achieved.

Temperature (°C)

$$T(P,H) = \left(x_1 + x_2H + \frac{x_3}{H - 1.7556418E6}\right) - 273.15 \quad (H < 8.12E5) . \tag{B.38}$$

$$T(P,H) = \left(x_1 + x_2H + \frac{x_3}{H - 1.7556418E6}\right) f(y) + \left(Z_1 + Z_2H + Z_3H^2 + Z_4H^3\right)[1 - f(y)] - 273.15$$

$$(8.12E5 < H \leq 8.16E5) . \tag{B.39}$$

$$T(P,H) = \left(Z_1 + Z_2H + Z_3H^2 + Z_4H^3\right) - 273.15 \qquad (H > 8.16E5). \tag{B.40}$$

Here,

$$x_1 = 2.8378E2 - 2.752333E\text{-}7\ P,$$

$$x_2 = 2.4688303E\text{-}4 + 1.24419E\text{-}13\ P,$$

$$x_3 = 1.8790464E7 - 5.634438E\text{-}2\ P,$$

$$Z_1 = 3.49661E2 - 2.364921E\text{-}6\ P,$$

$$Z_2 = 1.1964506E\text{-}5 + 6.291758E\text{-}12\ P,$$

$$Z_3 = 2.294645E\text{-}10 - 5.990103E\text{-}18\ P,$$

$$Z_4 = -8.587812E\text{-}17 + 2.015452E\text{-}24\ P, \qquad (B.41)$$

and y and f(y) are given by Eqs. B.34 and B.35 respectively.

Saturation Temperature (°C)

$$T_{sat}(P) = \frac{1}{1.8}\left(C_1 + C_2P_R + C_3P_R^2 - \frac{226805}{P_R + 768.85}\right),$$

$$(P_R > 1090.8). \qquad (B.42)$$

$$T_{sat}(P) = \frac{1}{1.8}\left(\frac{a_1}{a_2 - x} + a_3 + a_4x\right),$$

$$(P_R \leq 43.4302). \qquad (B.43)$$

$$T_{sat}(P) = \left[\frac{1}{1.8}\left(\frac{a_1}{a_2 - x} + a_3 + a_4x\right) + 273.15\right] f(y)$$

$$+ \left[\frac{1}{1.8}\left(b_1 + b_2x + b_3x^2 + b_4x^3 + b_5x^4\right)\right.$$

$$\left. + 273.15\right] [1 - (y)] - 273.15$$

$$(43.4302 < P_R \leq 45.4298). \qquad (B.44)$$

$$T_{sat}(P) = \frac{1}{1.8}\left(b_1 + b_2x + b_3x^2 + b_4x^3 + b_5x^4\right)$$

$$(P_R \leq 1069.2). \qquad (B.45)$$

$$T_{sat}(P) = \left[\frac{1}{1.8}\left(b_1 + b_2x + b_3x^2 + b_4x^3 + b_5x^4\right) + 273.15\right] f(y_1)$$

$$+ \left(\frac{1}{1.8}c_1 + c_2P_R + c_3P_R^2 - \frac{226805}{P_R + 768.85}\right.$$

$$\left. + 273.15\right) [1 - f(y_1)] - 273.15$$

$$(1069.2 < P_R \leq 1090.8). \tag{B.46}$$

Here,

$$c_1 = 588.994, \qquad c_2 = 0.055386,$$

$$c_3 = -3.516E\text{-}6, \qquad a_1 = 2634.7,$$

$$a_2 = 6.026, \qquad a_3 = -367.486,$$

$$a_4 = 4.484, \qquad b_1 = 73.802,$$

$$b_2 = 65.14, \qquad b_3 = 24.859,$$

$$b_4 = -4.3391, \qquad b_5 = 1.6889, \tag{B.47}$$

$$P_R = 1.4503774E\text{-}4\ P, \tag{B.48}$$

$$y = \frac{P_R - 44.98}{0.4498}, \tag{B.49}$$

$$y_1 = \frac{P_R - 1080}{10.80}, \tag{B.50}$$

$$x = \mathrm{Log}_{10}\left(P_R\right), \tag{B.51}$$

and

f(y) is given by Eq. B.34.

Distribution for NUREG/CR-4348 Vol. I (ANL-85-42 Vol. I)

Internal:

C. E. Till
R. S. Zeno
F. F. Chen
H. M. Domanus
G. K. Leaf
R. C. Schmitt
W. T. Sha (5)
V. L. Shah (231)
S. K. Zussman
ANL Patent Dept.
ANL Contract File
ANL Libraries (2)
TIS Files (3)

External:

USNRC, Washington, for distribution per R7 (250)
DOE-TIC (2)
Manager, Chicago Operations Office, DOE
Components Technology Division Review Committee:
P. Alexander, Flopetrol Johnston Schlumberger, Houston, Texas 77236
D. J. Anthony, General Electric Company, San Jose, California 95125
A. A. Bishop, U. Pittsburgh, 1249 Benedum Hall, Pittsburgh, Pa 15261
B. A. Boley, Northwestern University, Evanston, Illinois 60201
R. N. Christensen, Ohio State University, Columbus, Ohio 43210
R. Cohen, Purdue University, West Lafayette, Indiana 47907
R. E. Scholl, URS, 150 Fourth Street, San Francisco, California 94103
J. Weisman, U. of Cincinnati, Cincinnati, Ohio 45221

NRC FORM 335 (2-84) NRCM 1102 3201 3202

U.S. NUCLEAR REGULATORY COMMISSION

BIBLIOGRAPHIC DATA SHEET

SEE INSTRUCTIONS ON THE REVERSE

1. REPORT NUMBER (Assigned by TIDC, add Vol. No., if any)

NUREG/CR-4348, Vol. I
ANL-85-42, Vol. I

2. TITLE AND SUBTITLE

COMMIX-1B: A THREE-DIMENSIONAL TRANSIENT SINGLE-PHASE COMPUTER PROGRAM FOR THERMAL HYDRAULIC ANALYSIS OF SINGLE AND MULTICOMPONENT SYSTEMS, VOL. I: EQUATIONS AND NUMERICS

3. LEAVE BLANK

4. DATE REPORT COMPLETED

MONTH	YEAR
September	1985

5. AUTHOR(S)

Analytical Thermal Hydraulic Research Program

6. DATE REPORT ISSUED

MONTH	YEAR
September	1985

7. PERFORMING ORGANIZATION NAME AND MAILING ADDRESS (Include Zip Code)

Argonne National Laboratory
9700 South Cass Avenue
Argonne, Illinois 60439

8. PROJECT/TASK/WORK UNIT NUMBER

9. FIN OR GRANT NUMBER

A2045

10. SPONSORING ORGANIZATION NAME AND MAILING ADDRESS (Include Zip Code)

Containment Research Systems Branch
Division of Accident Evaluation
Office of Nuclear Regulatory Research
U. S. Nuclear Regulatory Commission
Washington, D.C. 20555

11a. TYPE OF REPORT

Technical

b. PERIOD COVERED (Inclusive dates)

1/1/83 - 9/31/85

12. SUPPLEMENTARY NOTES

13. ABSTRACT (200 words or less)

The COMMIX-1B computer program, an extended version of COMMIX-1A, is designed to analyze steady-state/transient, single-phase, three-dimensional fluid flow with heat transfer in reactor components and multicomponent systems. The concepts of volume porosity, directional surface permeability, distributed resistance, and distributed heat source or sink is used to model a flow domain with stationary structures. The new porous-medium formulation permits simulation of either a single component or a multicomponent system. The conservation equations of mass, momentum, and energy based on the new porous-medium formulation are solved as a boundary-value problem in space and an initial-value problem in time.

Volume I of this report, entitled "Equations and Numerics," describes in detail, the basic equations, formulations, solution procedures, rebalancing scheme for faster convergence, models to describe the auxiliary phenomena, etc. Volume II, entitled "Users Manual," describes in detail, flow chart, available options, input instructions, sample problems, etc.

14. DOCUMENT ANALYSIS - a. KEYWORDS/DESCRIPTORS

Thermal Hydraulics
Numerical Analysis
Finite-Difference Procedures
Computer Codes

b. IDENTIFIERS/OPEN-ENDED TERMS

15. AVAILABILITY STATEMENT

Unlimited

16. SECURITY CLASSIFICATION

(This page)
Unclassified

(This report)
Unclassified

17. NUMBER OF PAGES

170

18. PRICE